

Detection and Classification of Partial Discharge Sources under Variable Frequency and Air pressure

by

Ali Nasr Esfahani

A thesis submitted to the Faculty of Graduate Studies of
The University of Manitoba
in partial fulfilment of the requirements of the degree of

Master of Science

Department of Electrical and Computer Engineering
University of Manitoba
Winnipeg, Canada

Copyright © 2018 Ali Nasr Esfahani

Examining Committee

This thesis was examined and approved by the following examining committee on December 14, 2018:

- **Prof. B. Kordi** (advisor)
Department of Electrical & Computer Engineering
University of Manitoba
- **Prof. A. Major**
Department of Electrical & Computer Engineering
University of Manitoba
- **Prof. P. Ferguson**
Department of Mechanical Engineering
University of Manitoba

Abstract

With the development of electrical apparatus in more-electric aircraft (MEA), demand for higher electric power is increasing rapidly. In turn, this requires a higher voltage level in the power generation system of aircraft which increases the electric stress on the insulation systems. At higher voltages, the insulation systems of more-electric aircraft are prone to partial discharge (PDs) initiation under the operating condition.

The objective of this thesis is to perform a comprehensive study on developing diagnostic methods for the insulation condition monitoring and PD source identification. An algorithm is developed based on the combination of wavelet and energy techniques to detect the PD pulses from the measured noisy PD signals. In addition, based on the statistical distributions of PD pulse waveform characteristics, a classification and separation algorithm is developed for the identification of multi-source PDs using kernel support vector machine (KSVM) as the classifier. The experimental results show that the proposed algorithms show a high performance and accuracy for PD source detection and recognition.

Acknowledgments

In conducting this research there are far more people I ought to thank than I can identify. First and foremost, I would like to express my deep and sincere gratitude to my supervisor, Prof. Behzad Kordi, who was abundantly supportive and offered invaluable assistance and much-needed guidance. He was always available for my trivial questions and showed me the keys to understanding. With his patience and encouragement reaching the end of this thesis became possible.

I would like to express many thanks to my examining committee, Dr. Arkady Major and Dr. Philip Ferguson for their comments and suggestions to enhance my thesis. I am also grateful to Saeed Shahabi and Daryl Hamelin for their invaluable suggestions and professional advice on conducting this research. Their insightful comments and beneficial feedback and support guided me a lot throughout the process of this study.

Financial support from Natural Sciences and Engineering Research Council of Canada (NSERC) and University of Manitoba Graduate Enhancement of Tri-Council Stipends (GETS) is greatly appreciated.

I extend my most heartfelt thanks to my beloved parents who taught me how to love unconditionally, to forgive and to forget always. They provided me with pencil for the first time, and their patience, tenacity and cooperation lightened up my way and directed me to the pursuit of knowledge in the first place. It is also worthwhile to thank my dear sister for her continuous encouragement and support of this endeavor from the beginning.

Table of Contents

Examining Committee	ii
Abstract	iii
Acknowledgements	iv
List of Figures	vii
List of Tables	xii
1 Introduction	1
1.1 Motivation	1
1.2 Research Objectives and Contributions	4
1.3 Thesis Outline	6
2 Background and Literature Review	7
2.1 Partial Discharge	8
2.2 Definition of Gas Discharge	10
2.3 Gas Discharge Mechanism	11
2.4 Investigation of PD activity	12
2.5 Partial Discharge Detection Methods	21
2.5.1 Electrical Method	22
2.5.2 RF Method	24
2.5.3 EMI Method	24
3 PRPD Pattern Recognition	26
3.1 The Description of Experimental Setup	26
3.1.1 Test Cells	28
3.1.2 PD Measurement Setup	30
3.2 PD Detection Method	30
3.3 Effect of Air Pressure and Frequency on PDIV	36

3.4	Corona Discharge PRPD Pattern	40
3.5	Multiple PD Sources PRPD Pattern	47
3.6	Summary	52
4	Classification of Concurrent PD Sources	53
4.1	PD Pulse Waveform Analysis	55
4.1.1	PD Pulse Waveform Measurement	56
4.2	Probabilistic Analysis	59
4.3	Support Vector Machine	60
4.4	The Algorithm of Concurrent Multiple PD Source Classification	61
4.5	Results and Discussions	64
4.5.1	Detailed Characteristics of PD Pulse Waveforms	64
4.5.2	Separation and Classification of Multiple Concurrent PD Sources	71
4.6	Summary	87
5	Conclusions	88
5.1	Future Work	90
	References	92
	Appendix A First Appendix	100
A.1	Single Source PRPD Patterns	100
A.2	Multi Sources PRPD Patterns	101
	Appendix B Second Appendix	111
B.1	Separation and Probabilistic analysis	111

List of Figures

2.1	Air Pressure as a function of altitude	8
2.2	Paschen curve for uniform electric field at different pressure and constant gap spacing (gap length= 2 mm)	9
2.3	Test circuits for PD measurement: (a) Coupling device in series with coupling capacitor (b) Coupling device on the ground side of the test object	23
3.1	Experimental setup of two-source PDs consists of an HV source, a coupling capacitor, two PD source cells, a measuring device, and an oscilloscope. (a) Test circuit for partial discharge measurement. (b) Photo of the experimental setup.	27
3.2	PD source test cells, each cell consists of a pressure gauge and Perspex tube and is able to withstand vacuum pressure. (a) Needle-plane electrode configuration. (b) Twisted-pair of magnet wires.	29
3.3	Measured PD signals under sine wave applied voltage with the frequency of 1 kHz.	32
3.4	Proposed algorithm for PD detection.	33
3.5	PD signals under sine wave voltage after using wavelet transform.	33
3.6	Differential energy of signal in reference to phase angle under sine wave voltage	35
3.7	Mean of Differential Energies (MDE) of signal in reference to phase angle under sine wave voltage	36
3.8	Cumulative Distribution of MDE in reference to phase angle under sine wave voltage.	37
3.9	PDIV measurement, obtained from conducting PD test on each test cell separately at different level of air pressure and applied frequency. (a) PDIV as function of frequency and pressure for needle-plane electrode. (b) PDIV as function of frequency and pressure for twisted-pair of magnet wires.	39

3.10	Obtained MDE and CD patterns for corona discharge under frequency of 50 Hz and sub-atmospheric pressure (33 kPa). (a) MDE pattern. (b) CD pattern.	42
3.11	Obtained MDE and CD patterns for corona discharge under frequency of 50 Hz and atmospheric pressure (101 kPa). (a) MDE pattern. (b) CD pattern.	43
3.12	Obtained MDE and CD patterns for corona discharge under frequency of 2000 Hz and sub-atmospheric pressure (33 kPa). (a) MDE pattern. (b) CD pattern.	44
3.13	Obtained MDE and CD patterns for corona discharge under frequency of 2000 Hz and atmospheric pressure (101 kPa). (a) MDE pattern. (b) CD pattern.	45
3.14	Cumulative Distribution of MDE in reference to phase angle of measured signal with PD pulses generated by two PD sources under applied frequency of 1 kHz. (a) PRPD pattern generated by PD pulses from twisted-pair wires. (b) PRPD pattern generated by both of PD pulses sources.	49
3.15	Cumulative Distribution of MDE in reference to the phase angle of the measured signal. (a) Without any PD pulses. (b) PD pulses generated by twisted-pair wires.	50
3.16	Cumulative Distribution of MDE in reference to the phase angle of the measured signal in the presence of two activated PD sources . (a) PD signals after using wavelet transform (both PD sources are activated). (b) PD pulses generated by both PD sources.	51
4.1	PD signal shape, recorded from PD measurement on needle-plane electrode under voltage applied frequency of 500 Hz and atmospheric pressure. (a) Measured signal by oscilloscope (b) Definition of time-domain parameters.	57
4.2	Flowchart of the proposed algorithm.	63
4.3	The separation map of PD sources under the applied frequency of 500 Hz and sub-atmospheric pressure of 67 kPa. (a) (RT, FT, PW) (b) (RT, FT, SR)	72
4.4	The separation map of PD sources under the applied frequency of 1000 Hz and sub-atmospheric pressure of 33 kPa. (a) (PW, FT, SR) (b) (FT,PW) .	74
4.5	Weibull and Normal distribution of rise time for applied frequency of 500 Hz and air pressure level of 67 kPa. (a) Weibull distribution. (b) Normal distribution.	76

4.6	Weibull and Normal distribution of rise time for applied frequency of 1000 Hz and air pressure level of 33 kPa. (a) Weibull distribution (b) Normal distribution	77
4.7	Weibull and Normal distribution of slew rate for applied frequency of 500 Hz and under air pressure level of 67 kPa. (a) Weibull distribution. (b) Normal distribution.	78
4.8	Weibull and Normal distribution of slew rate for applied frequency of 1000 Hz and under air pressure level of 33 kPa. (a) Weibull distribution. (b) Normal distribution.	79
4.9	Weibull and Normal distribution of pulse width for applied frequency of 500 Hz and air pressure level of 67 kPa. (a) Weibull distribution. (b) Normal distribution.	81
4.10	Weibull and Normal distribution of pulse width for applied frequency of 1000 Hz and air pressure level of 33 kPa. (a) Weibull distribution. (b) Normal distribution.	82
4.11	Weibull and Normal distribution of fall time for applied frequency of 500 Hz and air pressure level of 67 kPa. (a) Weibull distribution. (b) Normal distribution	83
4.12	Weibull and Normal distribution of fall time for applied frequency of 1000 Hz and air pressure level of 33 kPa. (a) Weibull distribution. (b) Normal distribution.	84
A.1	Differential Energy (DE) pattern for corona in air generated by needle-plane electrode under AC applied voltage frequency of 1kHz and air pressure levels of (a) 33 kPa (b) 67 kPa (c) 101 kPa.	102
A.2	Differential Energy (DE) pattern generated by twisted-pair wires under AC applied voltage frequency of 1kHz and air pressure levels of (a) 33 kPa (b) 67 kPa (c) 101 kPa.	103
A.3	MDE pattern for corona in air generated by needle-plane electrode under AC applied voltage frequency of 1kHz and air pressure levels of (a) 33 kPa (b) 67 kPa (c) 101 kPa.	104
A.4	MDE pattern generated by twisted-pair wires under AC applied voltage frequency of 1kHz and air pressure levels of (a) 33 kPa (b) 67 kPa (c) 101 kPa.	105

A.5	CD pattern for corona in air generated by needle-plane electrode under AC applied voltage frequency of 1kHz and air pressure levels of (a) 33 kPa (b) 67 kPa (c) 101 kPa.	106
A.6	CD pattern generated by twisted-pair wires under AC applied voltage frequency of 1kHz and air pressure levels of (a) 33 kPa (b) 67 kPa (c) 101 kPa.	107
A.7	DE pattern generated by two simultaneously activated PD sources under AC applied voltage frequency of 500 Hz and air pressure levels of (a) 33 kPa (b) 67 kPa (c) 101 kPa.	108
A.8	MDE pattern generated by two simultaneously activated PD sources under AC applied voltage frequency of 500 Hz and air pressure levels of (a) 33 kPa (b) 67 kPa (c) 101 kPa.	109
A.9	CD pattern generated by two simultaneously activated PD sources under AC applied voltage frequency of 500 Hz and air pressure levels of (a) 33 kPa (b) 67 kPa (c) 101 kPa.	110
B.1	The separation map of PD sources under the applied frequency of 500 Hz and sub-atmospheric pressure of 33 kPa (a) (SR, FT,RT) (b) (PW, FT, RT)	112
B.2	The separation map of PD sources under the applied frequency of 500 Hz and sub-atmospheric pressure of 33 kPa (a) (PW, SR, RT) (b) (PW, SR, FT)	113
B.3	Weibull and Normal distribution of fall time for applied frequency of 500 Hz and air pressure level of 33 kPa (a) Weibull distribution (b) Normal distribution.	114
B.4	Weibull and Normal distribution of pulse width for applied frequency of 500 Hz and air pressure level of 33 kPa (a) Weibull distribution (b) Normal distribution.	115
B.5	Weibull and Normal distribution of rise time for applied frequency of 500 Hz and air pressure level of 33 kPa (a) Weibull distribution (b) Normal distribution.	116
B.6	Weibull and Normal distribution of slew rate for applied frequency of 500 Hz and air pressure level of 33 kPa (a) Weibull distribution (b) Normal distribution.	117
B.7	The separation map of PD sources under the applied frequency of 500 Hz and atmospheric pressure of 101 kPa (a) (SR, FT, RT) (b) (PW, FT, RT) .	118
B.8	The separation map of PD sources under the applied frequency of 500 Hz and atmospheric pressure of 101 kPa (a) (PW, SR, RT) (b) (PW, SR, FT)	119

B.9 Weibull and Normal distribution of fall time for applied frequency of 500 Hz and air pressure level of 101 kPa (a) Weibull distribution (b) Normal distribution.	120
B.10 Weibull and Normal distribution of pulse width for applied frequency of 500 Hz and air pressure level of 101 kPa (a) Weibull distribution (b) Normal distribution.	121
B.11 Weibull and Normal distribution of rise time for applied frequency of 500 Hz and air pressure level of 101 kPa (a) Weibull distribution (b) Normal distribution.	122
B.12 Weibull and Normal distribution of slew rate for applied frequency of 500 Hz and air pressure level of 101 kPa (a) Weibull distribution (b) Normal distribution.	123

List of Tables

- 4.1 PD pulse rise time occurred at positive and negative half voltage cycles for needle-plane electrode (corona discharge). 64
- 4.2 PD pulse rise time occurred at positive and negative half cycles of AC applied voltage for twisted-pair of magnet wires. 65
- 4.3 PD signal pulse width occurred at positive and negative half voltage cycles for corona discharge 66
- 4.4 PD signal pulse width occurred at positive and negative half voltage cycles for twisted-pair of magnet wires 67
- 4.5 PD pulse slew rate occurred at positive and negative half voltage cycles for corona discharge 68
- 4.6 PD pulse slew rate occurred at positive and negative half voltage cycles for twisted-pair of magnet wires 68
- 4.7 PD pulse fall time occurred at positive and negative half voltage cycles for corona discharge 69
- 4.8 PD pulse fall time occurred at positive and negative half voltage cycles for twisted-pair of magnet wires 69
- 4.9 The Statistical Moments of Feature Distribution associated with different sources of pulses 85
- 4.10 The Classification Error Rate for Each of PD Measurements Using the Proposed Algorithm 86

Chapter 1

Introduction

1.1 Motivation

Driven by the demand to replace the heavy mechanical, hydraulic and pneumatic based systems by electrical systems, the aircraft manufacturers are moving toward the concept of more electric aircraft (MEA). The MEA concept provides many potential advantages such as higher efficiency of power electrical system, higher reliability, lower weight, and maintenance costs compared to the conventional architecture of the aircraft. The increasing demand for electric power energy puts the generating system design under pressure to step up the operating voltage of the aircraft or to increase the rated current. For a fixed operating voltage, increasing the electric current of aircraft power supply rises the necessity to choose a higher level of current carrying capacity for the feeder cables. This leads to use larger diameter cables to allow more current to be carried with reasonable levels of loss. The drawback of this design is increasing the weight of power system generation and distribution that is not acceptable. Therefore, the focus of electrical system designers, is mainly on rising the voltage of the power supply [1,2]. However, the increase of rated voltage results in high level of electrical stress on the electrical insulation system of aircraft which may cause partial

discharges (PDs) in electrical insulation system [3].

It is well known from Paschen' law that the insulating characteristics of the gaseous media depend on the gas pressure. During cruising altitude of the aircraft, the air pressure drops to as low as 30% of the atmospheric pressure at the sea-level. Hence, the air pressure change with altitude may affect the partial discharge mechanism in the electric power system of the aircraft. Paschen curve has been developed for uniform electric fields such as that of two parallel plates. However, more studies are required to investigate the effect of air pressure on electric discharge under non-uniform electric fields. This is because of using various shape of electrodes in the HV equipment that change the uniformity of electric fields [4, 5].

The growth of electric equipment in MEA has led to an enhancement in aircraft power distribution systems. There are different types of power distribution systems used in MEA. These power distribution systems are low voltage DC system (LVDC), high voltage DC system (HVDC), high voltage AC system (HVAC), variable-speed constant-frequency system (VSCF), and variable-speed variable-frequency (VSVF) [2, 6, 7]. In modern aircraft, the generator used in VSCF system is the main source of HVAC and HVDC systems. The rotor of the synchronous generator is rotated by the aircraft engine. The aircraft engine speed changes during operation, and results in frequency variation of the generator output voltage. A bidirectional back-to-back power converter is used to convert the three-phase variable frequency AC (VFAC) system to the three-phase high voltage AC system (HVAC) with a nominal phase to ground voltage of $115 V_{rms}$ and constant frequency of 400 Hz. The rated voltage of the VFAC system is 115 V phase to ground with a frequency variation between 360 and 900 Hz [7]. Considering the current trend in the development of MEA, it is expected that the voltage of power supply will exceed the Paschen minimum voltage which may cause PD in the electrical insulation system. Also, the existence of voltage harmonics due to power supply converters and the reduction of air pressure at high altitude make the

frequency and air pressure two important factors which must be considered in design of an aircraft electrical insulation system.

Partial Discharge (PD) measurement is a non-destructive and none-invasive method for condition-based assessment of insulation systems [8]. The noise interference from external part affects the measurement of PD signals that reduce the accuracy of the measurements. Repetitive switching noise coming from the switching-type power source and PD occurring in neighboring apparatus are the main external interferences. The power electronic converters that are used in electrical AC power system of MEA are the sources of switching noises. The high frequency switching signals can penetrate to the AC power system and mix with PD signals. The other switching noise sources in MEA are inverter drives that generate Pulse Width Modulation (PWM) voltages.

The performance and reliability of the electrical insulation system of generators and motors in more-electric aircraft is one of the main concerns at cruising altitude. The conventional winding structure for low voltage motors and generators is random wound stator. In this type of winding arrangement, winding turns are very prone to PD occurrence due to air gaps between turns. These air pockets in conjunction with the presence of high enough voltage stress between turns, may result in PD ignition and severe winding insulation deterioration [9]. Several insulation PD-resistant materials and stress-relief coating have been employed to reduce the number of winding insulation attack by PDs. Experience, however, has demonstrated that the lifetime of insulation system may be reduced notably by an increase in PD numbers with time [10]. Therefore, it is significant to monitor the operating condition of winding insulation system especially under harsh environmental condition such as low air pressure in order to stay away from in-service failure.

1.2 Research Objectives and Contributions

The objective of this research thesis is to detect PD at sub-atmospheric pressure under AC applied voltage with variable frequency. Although, the proper operation of aircraft electric power system components can be assured using the PD detection methods under atmospheric pressure, however, these techniques are not reliable at low air pressure condition. The pulse width and rise time of PD pulses under sub-atmospheric pressure is larger compared to sea-level pressure [11]. Hence, PD test procedure, technical specifications and diagnostic equipments recommended in the international PD-testing standard, IEC 60270 [8], may not be beneficial for detecting PD in MEA application [11].

The first task of this research study is to investigate the effect of air pressure and frequency on the partial discharge inception voltage (PDIV) of PD sources, the minimum applied voltage across the air gap at which PDs start to ignite continuously. For this purpose, two test cells were developed to model the artificial single source and multi-source of PDs that may be present in power system of an aircraft. The typical PD defects that are considered for this study are corona discharge and PDs between turns of motors or generators winding. In addition, switching and background noises are the most challenging noises to remove. To overcome this, an algorithm based on the combination of the wavelet and energy techniques is developed to detect PD pulses in a noisy environment under operating air pressure of a typical aircraft. This proposed technique aims at extracting PD pulses from noisy measured PD data and generating phase-resolved PD (PRPD) pattern for single PD sources, as well as multiple concurrent activated PD sources.

The main objective of this research thesis is to detect and classify PD in a variable frequency AC system under sub-atmospheric pressures. For this reason, the pulse PD parameters such as rise time, fall time, pulse width and slew rate are extracted from the time-domain of PD signal. After performing the time-resolved (TRPD) analysis, the statistical operators are employed to characterize the features distributions extracted from TRPD

analysis. To perform PD recognition under TRPD mode based on the generated dataset, support vector machine (SVM) is used for the classification of simultaneously activated PD sources.

The contributions of this thesis are as follows:

- The effect of air pressure and frequency on partial discharge inception voltage (PDIV) for both PD sources, corona discharge and motors winding, are investigated experimentally. The performed experiments are repeated several times due to stochastic nature of PD and the average value of the obtained PDIVs is calculated.
- PD pulse parameters in time-domain, are examined under sub-atmospheric pressure and a wide range of frequency.
- Power converters and drive circuits in the power distribution system of MEA are capable of producing high levels of switching noise. This noise source in combination with the background noise and parasitic impedances will cause amplitude ringing (resonance) in the measured partial discharge signal waveform. An energy based method is developed to detect PDs in such condition.
- This technique is capable of providing PRPD pattern for single sources and multiple activated PD sources. Variation in the PRPD pattern provides means to identify the PD defects in early stages and prevent in-service failure.
- The PD measurements are accomplished on artificial defects that are implemented in laboratory pressure-controllable test cells. A needle-plane electrode and twisted-pair magnet wires are used and placed in the test cells to simulate the corona discharge and PD in motors winding respectively.
- For the classification of concurrent PD sources, PD waveform analysis is performed to extract and calculate time-domain features of PD signals under sub-atmospheric

pressure and different range of frequency. Statistical moments of these feature distributions are calculated to provide fingerprints of PD sources.

- The classification of PD sources is carried out based on the extracted features using KSVM as a classifier. The classification success rate of the applied classifier in different level of air pressure and frequency has been evaluated.

The outcomes of this study have been published in one conference paper and two IEEE Transaction journal papers on Industry Applications and DEIS have been submitted [12].

1.3 Thesis Outline

This thesis is organized into 5 chapters:

Chapter 1: Motivation, research objectives and contributions are presented.

Chapter 2: Background and literature review of the current state of knowledge in the area of PD detection under low air pressure and, the most common PD measurement techniques are presented.

Chapter 3: An algorithm is presented to detect PD pulses in a noisy environment. This method is based on the combination of energy techniques and wavelet transform. The experimental results obtained from PD test under different range of frequency and air pressure are discussed.

Chapter 4: For the separation and classification of simultaneously activated PD sources, a method is developed. This algorithm is based on the statistical moments calculated from probabilistic analysis of PD pulse waveform. Kernel support vector machine (KSVM) is used as the classifier.

Chapter 5: Conclusion of this thesis project and potential future research work are discussed.

Chapter 2

Background and Literature Review

Air is the simplest and most commonly used gaseous insulating media whose dielectric characteristics depends on the density of the gas molecules. Operating air pressure of electric power components of aircraft varies widely during ascending and descending. Typical aircrafts fly at an altitude of 33,000-46,000 feet (10-14 km), where air pressure is only 30% of that at the ground level [1,13]. The air pressure as a function of altitude is depicted in Fig. 2.1. The figure shows that the atmospheric pressure decreases as the altitude increases. The air pressure drops to as low as 20 kPa at an altitude of 12 km. It is well known from Paschen's law that the breakdown voltage of an air gap depends on the product of the gap length d and the air pressure p . The product pd is an indication of the number of collisions that a free electron may have with other gas particles when crossing the air gap [14]. As shown in Fig.2.2 , the dielectric strength of air is reduced as the pressure decreases before reaching a minimum. When the dielectric strength reaches a minimum value and the pressure still keeps on decreasing, the breakdown voltage increases sharply. Under this condition, the electrode materials also have a key role in the breakdown mechanism [15].

There are a number of classification, recognition techniques, as well as detection methods that have been developed for the investigation of the PD phenomena mostly under atmospheric pressure. In this chapter, a summary of the available literature and current

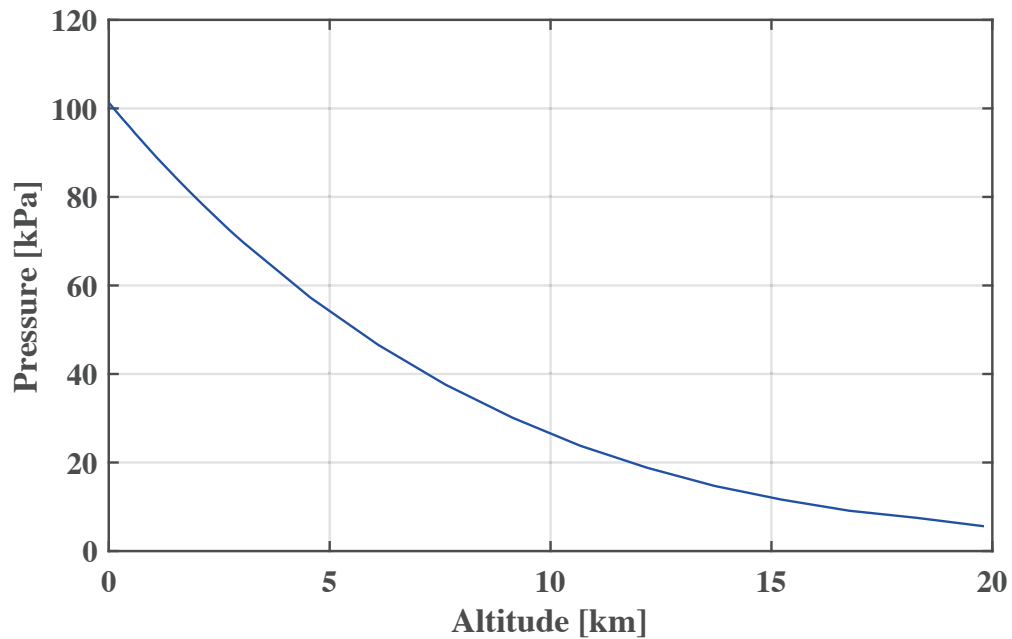


Fig. 2.1: Air Pressure as a function of altitude [14].

state of knowledge in the area of PD investigation is reviewed.

2.1 Partial Discharge

A partial discharge (PD) is defined by IEC60270 standard as

“A localized electrical discharge that only partially bridges the insulation between conductors and which can or cannot occur adjacent to a conductor. Partial discharges are in general a consequence of local electrical stress concentrations in the insulation or on the surface of the insulation. Generally, such discharges appear as pulses having a duration of much less than $1 \mu s$. More continuous forms can, however, occur, such as the so-called pulse less discharges in gaseous dielectrics.” [8].

Insulation failure is one of the foremost problems for the electrical apparatus. Detection of PD and its impact on the condition of insulation system used in the HV equipments

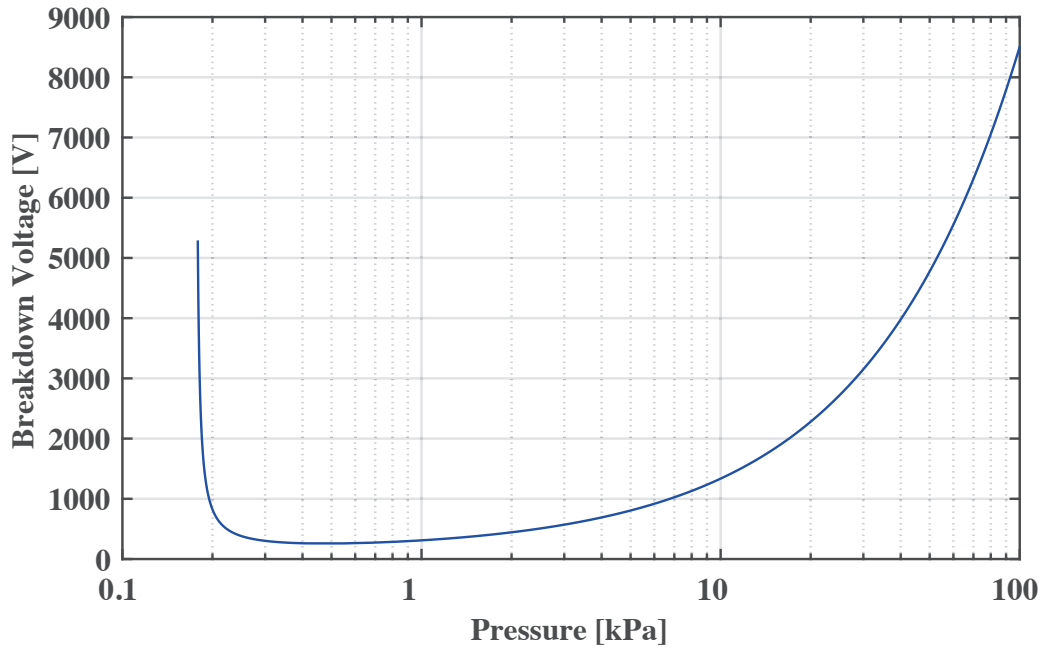


Fig. 2.2: Paschen curve for uniform electric field at different pressure and constant gap spacing (gap length= 2 mm) [14].

during their lifetime is a significant necessity to prevent the electrical power system from a sudden and severe insulation failure. Partial discharge activity inside or on the surface of the insulation depends greatly upon certain factors such as impurities in the insulation, cracking of insulation and HV equipment operating condition that involves temperature, vibration, air pressure, and contamination [5]. The continued existence of PD activity leads to physical or chemical deterioration in the condition of insulation material. Useful information, which is obtained from PD data, can be used to predict the extent of insulation degradation and premature failure.

Partial discharge may take place in a void within a solid or liquid insulating material, as corona discharges, or on the surface of insulation. Corona refers to an external type of partial discharge which occurs around the energized conductors in gaseous media. As stated in [16], the corona discharge (in air) is described as

“A luminous discharge due to ionization of the air surrounding a conductor caused by a voltage gradient exceeding a certain critical value.”

Generally, corona discharge may occur in none-uniform high electric field around a sharp edge, loose wire strands, or transmission line conductor in aircraft power system [17].

The air around HV conductors and equipment functions as an insulating gaseous media that its properties affect the PD characteristics . There are many factors such as electrode shape, gas pressure, humidity, and applied voltage that affect the discharge phenomena in air. Due to the complexity of PD modeling in gas, the study of these factors experimentally plays a huge role in better understanding of phenomenon and contributes to the development of the gas discharge theory. A great deal of information on discharge processes in gas, especially under standard sea-level air pressure, has obtained by many researchers, but more investigation must be pursued to explain this phenomenon from various aspects. In this chapter, a brief overview of the gas discharge is presented.

2.2 Definition of Gas Discharge

Gas discharge refers to different types of current flowing in the gaseous atmosphere. As the gas experiences normal condition and there is no external ionization source, the electrical conduction through gas is very low. In fact, a small amount of charged particles is always found in the air due to cosmic rays and radiation that exists on Earth [4,5]. These charged particles have erratic movements that makes the average current approximately equal to zero. If the gas is subjected to a weak electric field, these movements will be in the direction of electric field which leads to have an extremely small current. When the electric field in the gas becomes strong enough, the current suddenly increases and the gas will not function as insulation anymore. The transition from the state of insulating to the conductive condition is called breakdown. The minimum voltage in the gas that causes to have breakdown in gas is called “breakdown voltage (U_b)” [4].

In the study of the discharge in gases, six particles are considered: electron, photon, ground-state atoms or molecules, excited atoms or molecules, cation and anion [4, 15, 18]. These particles interact with each other via collision which leads to a change in their state. Ions are generated from neutral atoms or molecules via ejection or attachment of an electron. a negative ion is produced through absorption of an electron by a molecule, whereas ejection of an electron from a neutral molecule produce a positive ion. The mass of a molecule in comparison to that of an electron is much higher thus it can be assumed that the mass of a molecule is equal to the corresponding ion. Due to the higher mass, the drift velocity of an ion is much lower whereas a light electron moves with a significant higher drift velocity. Because of this, the ions can be considered stationary from the place at which they are produced. The discharge process therefore is mostly precipitated by generated free electrons [4, 15, 18].

2.3 Gas Discharge Mechanism

Gas discharge phenomena is basically described by two types of mechanisms: non-self sustaining discharge and self-sustaining discharge. An external ionization source is required to generate an ample number of electrons for maintaining discharge phenomenon in non-self sustaining gas discharges. When the applied voltage between conductors reaches a sufficient value, the formation of discharge becomes independent of the external ionization source, which is called the self-sustaining discharge [4, 18].

According to Townsend discharge theory, a rapid change in the number of space charges in the discharge space is resulted by three different processes [4]. Colliding with other particles, the initial free electrons moving towards the energized conductor at positive polarity (anode) result in the generation of a huge number of positive ions and electrons. This ionization process is known as the α process. Positive ions, that are present in the air gap, move toward the electrode at negative polarity (cathode) and make collision with gas

particles. The number of electrons and positive ions that are produced as a result of this process, are negligible compared to the α process. This process is known as the β process and is not considered in the study of gas discharge under normal conditions due to the small probability of obtaining required kinetic energy for positive ions to ionize gas particles. The third ionization process is known as γ process which relates to the emission of secondary electrons when the meta-stable particles such as positive ions strike the cathode surface. It has been shown by experiments that this process depends on the cathode material, gas properties, kinetic energy of positive ions, cleanliness of the cathode surface, etc. The breakdown voltage value is related to this process [4,18].

2.4 Investigation of PD activity

Different types of voltage waveforms with various frequency have been used to detect and analyze PD in different type of insulation under a wide range of atmospheric pressure. For investigating PD characteristics in gaseous media, electronegative gases such as Helium, Argon, as well as air, have been considered as testing media. The PD experiments were mostly performed on different laboratory electrodes geometry under sea-level pressure. Hence, there are a few number of research works that have studied monitoring and recognition of PD at low pressure. Since the main objective of this thesis is to study PD under sub-atmospheric pressure and variable frequency, the available literature pertinent to the focus of this thesis is summarized in this section.

Surface partial discharge was investigated in dry air under power frequency (50 Hz) at pressure ranges from 91.333 down to 0.067 kPa by Husain and Nema [19]. PD tests were performed on Rogowski profile electrodes, which create a uniform electric field in the space between electrodes, with various thickness of solid insulation. It was observed that partial discharges occur in an air gap between the insulation surface and the curved metal part of electrode. It was reported that the PD inception voltage changes with air pressure and

increasing the thickness of dielectric has no significant impact on PDIV at low pressures. However, samples with higher insulation thickness show higher PD inception voltage at near atmospheric pressures. The main observation of this study is that the breakdown voltage of solid-gas insulation system is lower by 20% to 30% compared to Paschen's curve [19].

Okubo *et al.* conducted PD tests over a wide range of pressure from 100 mPa to atmospheric pressure level of 100 kPa in Helium, Argon and air. The reason for selecting Helium and Argon for investigation discharge phenomenon was that these gases are integral elements of the residual gas at high altitude where space shuttles and satellites fly. Partial discharge inception voltage was investigated experimentally under a positive DC ramp voltage at simulated space environment. Various electrode configurations were mounted in a vacuum chamber to create non-uniform electric field. The non-uniformity of electric field distribution along the gap space, was varied from a weakly uniform (sphere-plane electrode) to highly non-uniform (needle-plane electrode). It was concluded that an increase in the pressure of gas leads to an increase in the electric field strength of the gas. The spatial distribution of E/P , where E is the electric field and P is gas pressure, along the electrodes axis was investigated quantitatively to examine the discharge inception mechanism. It was shown that partial discharge occurs in the gap space when the spatial distribution exceed a critical value which is independent of none-uniformity of the electric field [20, 21].

Li *et al.* studied negative corona discharge in air over a pressures range of 20 kPa to 100 kPa under negative DC applied voltage and compared the experimental results with simulations. The electrode shapes were hemispherically-tipped pointed electrode at a negative polarity and a concave hemispherical grounded electrode. Effects of space charge were not considered in the simulation of the negative corona, however, the calculated results were in good agreement with the experimental results. It was concluded that the use of concave hemispherical electrode as the ground electrode is more desirable than point-plane configuration because a spherically-symmetrical system alleviates the burden of simulation

and computation of pre-breakdown phenomena in a highly non-uniform electric field [22].

PD characteristics were investigated in air and Argon under 60 Hz AC energizing voltage waveform by Kasten *et al.* [13, 23]. To generate PD pulses, a needle-plane electrode configuration was placed in a vacuum chamber and the effect of pressure was studied at different pressures from 13.3 Pa up to 101.3 kPa. The typical waveforms of PD pulse current were measured for a 20 mm gap length between the needle tip and the plane electrode with and without a Teflon cap as a dielectric barrier. It was shown that the rise time of negative corona discharge is longer than the rise time of positive corona discharge under the same pressure which indicates that the positive pulses have higher frequency content compared to negative pulses under the same pressure for both gases. It was concluded that the frequency content of the PD current pulses is lower at sub-atmospheric pressures than standard atmospheric pressure. Therefore, PD detection equipment, which is designed to detect the high-frequency content of PD current pulses at atmospheric pressure, are not able to inspect insulation system at low pressures [13, 23]. Hence, it is important to test and validate the HV components at the operational condition.

Tabrizchi *et al.* investigated and compared the effect of pressure and temperature on the ion mobilities for a corona discharge as ionization source. The ion mobility is defined as the ratio of the drift velocity of ions divided by the applied electric field. Dry nitrogen was used as the testing media with a pressure range of the ambient pressure down to 2 kPa. The moisture level of nitrogen gas was controlled to be below 20 ppm (parts per million). The major peak of ion mobility spectra at different pressure and temperature was employed as the evaluation tool. Based on the experimental results, pressure changes the drift time linearly whereas temperature affects it exponentially. The rationale for this different behavior was attributed to the fact that the equilibrium of gas is varied exponentially by temperature whereas the pressure change the equilibrium linearly [24, 25].

Liu *et al.* conducted PD tests in air, Helium, Argon for an AC 60 Hz source and

bipolar DC voltage source under pressures from 0.27 kPa up to 101.3 kPa. A needle-plane electrode with a dielectric barrier and a twisted pair of insulated conductors were used for electrode arrangements. For the purpose of analysis, PD current pulses were measured for both 5% and 20% above the inception voltage under AC 60 Hz energizing voltage. The difference between PD current waveforms under these two level of applied voltage was not significant but the frequency of PD occurrence and maximum amplitude of PD pulses were higher for 20% above inception voltage condition. It was concluded that the PD current waveform characteristics such as rise time, pulse width, fall time and amplitude are pressure dependent for all testing gases. It was reported that the rise time of PD current pulses decreases with increasing the pressure for Helium and air. However, the rise time of PD pulses increases with increasing the pressure for Argon. The average amplitude of PD pulses decreases with decreasing the pressure for air , Helium, and Argon. Trichel pulses were observed in air for a pressures range of 0.27 kPa up to 13.4 kPa. These types of discharge are repetitive series of discharges which are found mostly in electronegative gases for a needle-plane electrode [26,27].

Cecilia and Edin measured PD in disc-shaped cavities in polycarbonate under a frequency range of 100 Hz down to 0.01 Hz. It was shown that PD activity is frequency dependent and the rate of this dependency changes with the magnitude of applied voltage. Statistical time lag was proposed to study the influence of frequency on partial discharge pattern. This parameter was defined as the average pause time for an electron to pop up in the cavity when the applied electric field exceeds the critical field. The role of statistical time lag is to shift forward PDs in phase. It was observed that statistical effect is diminished with decreasing the frequency, due to extending period time, and results in frequency dependency of PDs. In addition, the PD magnitude increases with increasing the frequency while the PDs number increases for cavity discharge. Also, the size and location of the cavity affect the the PD frequency dependence. It was indicated that the PD activity in

the small cavities (diameter less than 1.5 mm) is frequency dependent while the number of PDs increases with increasing the frequency for larger cavities [28, 29].

The positive and negative corona discharges were investigated at various pressure and humidity levels by Bian *et al.* [30, 31]. A mixture of air gases and water vapor was used as the case study in a perspex chamber and a needle-plane electrode arrangement. Linear interpolation of the effective ionization coefficient of dry air and water vapor was used to determine the effective ionization coefficient of the gas mixture. It was shown that this calculated coefficient reduces at higher rate with humidity as the pressure is decreased. Under constant humidity, it was found that this coefficient has an inverse relation with the relative air density. For a constant applied voltage, it was observed that corona current decreased when the air pressure or humidity increased mostly as a consequence of drop in the ion mobility. It was concluded that the PD inception voltage for both of the negative and positive corona discharges decreases with increasing the humidity and decreasing the air pressure [30, 31].

Sattari *et al.* studied the effect of air pressure on Trichel pulse characteristics via three-species 2D numerical model and compared the numerical results with experimental data. Negative and positive oxygen ions, and electrons were considered for simulating Trichel pulses in air. In order to model negative corona discharge, the electric field and charge density distributions were obtained by solving the Poisson's equation and charge transport equations under negative DC applied voltage, respectively. It was reported that the pulse duration of Trichel pulses increases with decreasing the air pressure and the frequency occurrence of pulses has an inverse relation with pressure. Also, it was shown that increasing corona electrode radius expands the ionization region which results in rising the charge value produced per pulse. It was concluded that secondary electron emission coefficient (γ) has a relatively small impact on Trichel pulse characteristics [32, 33].

Shou *et al.* investigated Trichel pulses generated by the needle-plane electrode arrange-

ment in low air pressure (0.134 to 6.67 kPa) under a negative DC voltage . The current-voltage characteristics of negative corona discharge were obtained for different stages of discharge phenomena. Then, the averaged current increases abruptly while the voltage drops and the Trichel pulses are initiated (corona discharge stage). Further increasing the current leads to transition from corona discharge to glow discharge. Within this stage, the voltage is almost unaltered during current raising and pulses disappear suddenly. It was reported that the peak current of PD is greater at higher pressure since more electron avalanches can be produced due to the higher air density [34].

PD experiments were performed on sample tests consisting of a piece of insulated wire wound with a metallic conductor and a pair of twisted insulated wires by Rui and Cotton [1]. The experiments were conducted in air for an AC 50 Hz voltage waveform in a pressure range of 100 kPa down to 10 kPa. It was concluded that the inception voltage decreases while the pressure drops from atmospheric pressure to low pressure. In addition, It was indicated that the magnitude and repetition rate of partial discharge pulses decreases with decreasing the air pressure. The main outcome of this paper is that the PD activity is initiated at lower voltage level in the aircraft insulation system [1].

Partial discharge measurements were carried out on varnished coils (motorettes) for a pressure range of 1.2 kPa to 75 kPa by Cavallini *et al.* [35]. Repetitive square and sinusoidal voltage waveforms were used as the supply voltage frequency at 5 kHz. PD pulses were captured and detected using a ultra wide band (UWB) PD detector with a bandwidth of 50 MHz. The advantage of this measuring device is to provide the means of recording the complete waveform of PD and comparing dependency of PD waveform on the air pressure. A high frequency current transformer (HFCT) was used for detecting PD under sinusoidal voltage waveform. However, the implementation of this sensor is not practical when a square voltage generator is employed to energize the system since the switching noises from the voltage supply will overlap with the PD signal. Hence, a second sensor was introduced by the

authors that works in ultra-high frequency (UHF) with a upper cutoff frequency of 3 GHz to overcome the inverter interference. Under sinusoidal and square voltage waveform, it was reported that partial discharge inception voltage (PDIV) decreases steadily as the altitude increases. The PDIV values obtained for square waveform were lower than sinusoidal voltage waveform. It was shown that the main drawback of using UHF sensor is losing sensitivity since the PD pulses lose frequency content with increasing altitude [35].

Emersic *et al.* studied the effect of temperature and pressure on partial discharge degradation of silicone-coated printed circuit boards using a 50 Hz sinusoidal AC voltage signal. The sample tests were two mirror-curved tracks on a printed circuit board coated with different thickness of silicone layer. The experiments performed at pressures of 11.6 and 50 kPa and room temperature, with two further experiments carried out at temperatures of -55°C and $+70^{\circ}\text{C}$ and atmospheric pressure. It was observed that the surface of the samples are subjected to partial discharge despite the good quality of applied coating. The number of surface cracks on the silicone coating created as the result of partial discharges, were significantly increased by reducing the air pressure specially for coating thicknesses less than $100\ \mu\text{m}$. It was shown that the temperature has a huge impact on growing of surface cracks and damage rate. The main conclusion of this paper is that silicone coating thicknesses greater than $250\ \mu\text{m}$ prevents partial discharge occurrence in the bulk and on the surface of silicon coating during aging process and under environmental condition [36,37].

Abadie *et al.* investigated the impact of pressure on partial discharge spectra for twisted pairs of enamel wires subjected to sinusoidal and repetitive square waveform voltage. Partial discharge measurements were performed at pressure ranges of 10 kPa to 101.3 kPa. As a reference value for the PDIV, a Rogowski coil was employed to detect complete waveform of PD under AC voltage. For detecting PD during rise and fall of a square voltage waveform, different cut-off frequency were used (50, 90 and 200 MHz). The effect of filtering on PD signal and PDIV was studied at 10 kPa pressure with the assumption that the PDIV

value for both of the AC waveform and square waveform is the same. It was noted that a larger PDIV value is obtained for the higher cut-off frequency since a higher voltage is needed to increase the magnitude of the high frequency components of the spectrum for PD detection. Such a behavior was not noticed at the atmospheric pressure indicating that cut-off frequency has no influence on the PDIV. It was concluded that the amplitude of low frequency components of the PD spectrum increases with decreasing the pressure whereas the high frequency ones decrease. Therefore, the bandwidth of the sensors and of the filter must be adopted according to the operational condition and the supply voltage [38].

Li *et al.* studied the impact of air pressure on the detailed characteristics of positive corona current pulses. The PD experiments were performed on a corona point mounted in a coaxial conductor-cylinder electrode arrangement at an air pressure ranging from 60 kPa up to 100 kPa. It was shown that pulse amplitude decreases with decreasing the air pressure whereas rise time, pulse width, duration time, and pulse repetition frequency increases notably under the same ratio of the applied voltage to the PD inception voltage. In this paper, some empirical formulas for PD pulses characteristics are established to consider the influence of air pressure [39].

Billard *et al.* performed partial discharge tests on magnet wires used in electric actuators and feeder cables under DC and AC voltage waveforms. It was reported that the PD inception voltage (PDIV) of typical magnet wires decreases with increasing the altitude. The amplitude analysis of phase resolved partial discharge (PRPD) pattern indicated that the amplitude PD pulse at atmospheric pressure is several times smaller than that at low pressure under the same applied voltage magnitude. It was concluded that the pressure changes the frequency spectra of partial discharge for AC applied voltage while the frequency spectra of PD is not affected by the pressure under DC voltage [3].

Liu *et al.* conducted PD experiments on polyimide films under AC sinusoidal voltage waveform at a frequency range of 5 kHz to 30 kHz, triangle wave, bipolar square wave and

repetitive pulse with a frequency of 1 kHz at atmospheric pressure. Sphere-to-plane electrode configuration was adopted in the chamber with polyimide films as dielectric barrier. For detection of PD pulses, electric current transducer was employed with a bandwidth of 500 kHz to 120 MHz and a minimum sensitivity of 1 mA. It was shown that discharges mostly occur during the falling and rising edges of the applied voltage. With increasing the frequency, the total PD number increases while the maximum of PD discharge magnitude decreases. These two obtained parameter were correlated to the lifetime of the specimen which indicated that the lifetime of insulation system decreases as a higher frequency used for the voltage supply. It was concluded that the sinusoidal and square voltage waveforms with equal applied frequency and peak-to-peak voltage affect the lifetime approximately identical [40,41].

Zhou *et al.* performed PD tests on a tip-plane electrode for a frequency range of 0.1 to 50 Hz. It was reported that the magnitude of corona discharge in negative half cycle is noticeably smaller than that in the positive half cycle. With increasing the frequency, PD is initiated at a lower voltage with a higher discharge magnitude in the positive half cycle and lower magnitude in the negative half cycle. It was shown that the magnitude of discharge in the positive half cycle increases as the applied voltage raises while the discharge magnitude decreases in the negative half cycle. The analysis of phase resolved PD (PRPD) pattern indicated that the characteristic parameters of discharge patterns are frequency dependent and can be used in the recognition of PD under low frequency. Variation in the PRPD pattern was attributed to the fact that the frequency affects the the quantity of residual space charge and discharge time. Under Trichel pulse mode, increasing the magnitude of applied voltage leads to an elevation in the pulse repetition and reduction in the time interval of pulses since the electric field is strong enough to scatter the space charges around the needle tip curvature. It was observed the that inception phase of PD shifts to the right side of the obtained pattern and discharge phase range decrease with increasing the applied

frequency [42].

Xing *et al.* employed computational approaches to study the effect of air pressure in the creation of space charge for the negative corona discharge pulses. A rod-plane electrode was used to model the corona discharge under an air pressure range of 50 kPa to 100 kPa. It was found that the drift velocities of gas particles such as electrons or ions increases significantly under low pressure which leads to obtain higher kinetic energy when subjected to an external electric field. In addition, the number of electrons and ions produced during corona discharge are much higher at low air pressure since the kinetic energy of gas particles is much less dissipated as a consequence of less collisions. It was concluded that PD inception voltage is lower at sub-atmospheric pressures and the number of charged particles increases with raising the applied voltage [43].

2.5 Partial Discharge Detection Methods

Several PD detection techniques and measurement procedures have been developed and proposed in the literature. These methods use physical symptoms for revealing partial discharges including electromagnetic emission, electrical pulses, light emission, acoustic emission, and chemical reaction. Generally, two approaches are available to detect PD in the HV equipment. For off-line testing, PD measurements are performed at an elevated voltage to initiate PDs when the test apparatus is not in the service. The advantage of this test is that the measuring device can work in the low frequency domain (LF detectors) with high detection rate due to low environmental and background noises. However, the implementation of this test requires external power supply which is expensive and not convenient. The other approach is to measure PD under operating conditions of the HV equipment. This is a non-destructive and less expensive method because of being performed at the rated voltage of the equipment. The requirement of this approach is that high frequency domain analysis (HF testing) should be carried out for PD detection due to high level of the background

noises [10, 44]. In this section, a brief summary of the detection techniques mostly used in electrical commercial PD detectors is presented.

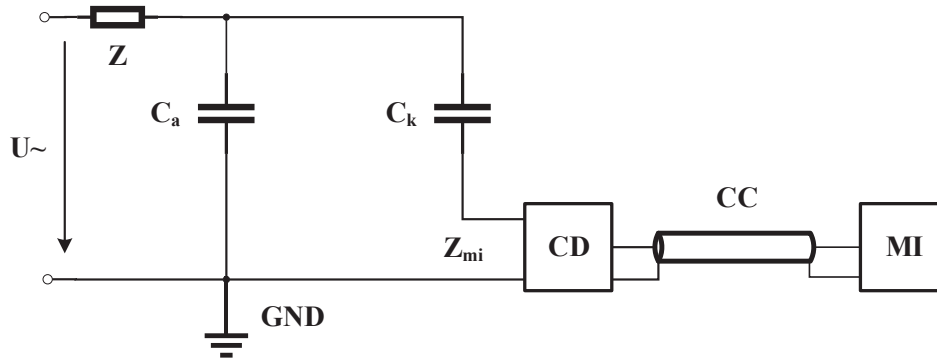
2.5.1 Electrical Method

The most direct technique to detect PD is the electrical method. This method offers many advantages in terms of convenient implementation for any type of insulation system and better suppression of the background noises in comparison to the other methods [45]. The IEC standard 60270 recommends test circuits and measuring systems for wide-band PD instruments with lower and upper cut-off frequencies of 30 and 500 kHz, respectively. The electric current discharge is measured in this method as described by the IEC standard [8]. There are two common PD test circuits illustrated in Fig.2.3. The main components of the partial discharge measurement setup are as follows: (i) test object C_a , (ii) coupling capacitor C_k to sense the partial discharge of the test object, (iii) connecting cable CC to transmit the PD signal to the measurement system, (iv) measuring instrument MI to capture and record the transmitted PD data, (v) coupling device Z_{mi} to convert the input discharge current into the voltage signal, and (vi) impedance Z to block the background noises from the side of voltage supply. It is worth mentioning that the coupling capacitor must have a low level of partial discharge compared to the test object.

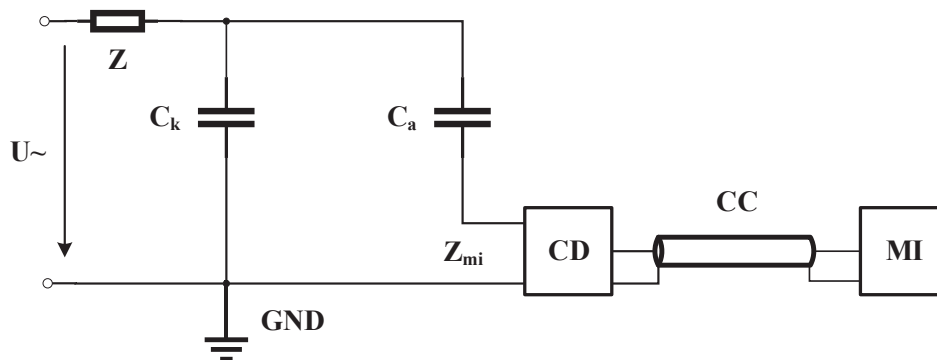
According to the IEC standard 60270 [8], the apparent charge of partial discharge injected from the terminal of the test object is measured by the measuring device. The amount of apparent charge is not equal to the local charge initiated at the site of discharge in the insulation system and expressed in picocoulombs (pC). The calibration of the system is done via injecting a known amount of charges and then measuring the PD output of the coupling device to obtain a ratio of millivolt to picocoulombs.

The conventional electrical method is mostly beneficial to perform in a laboratory due to the difficulty of performing accurate calibration for the on-line PD measurement [10,

44]. However, phase-resolved partial discharge (PRPD) pattern and time-resolved partial discharge (TRPD) pattern are obtained with respect to the phase of the applied voltage and PD waveform. Using the variation in the pattern of these two evaluation tools, the condition of insulation system can be monitored and analyzed.



(a)



(b)

Fig. 2.3: Test circuits for PD measurement [8]: (a) Coupling device in series with coupling capacitor (b) Coupling device on the ground side of the test object.

2.5.2 RF Method

Electromagnetic (EM) waves generated by partial discharge pulses can be detected far from the site of PD location. The EM radiation is comprised of radio frequencies (RF) ranging from 100 kHz to 300 GHz. Using a suitable antenna probe in conjunction with a RF sensor, allows capturing the radiated electromagnetic waves for sensing PD phenomena. The antenna probe should be capable of preserving the waveform shape of the incoming PD signal and synchronizing to the phase of applied voltage. Radio frequency method can be implemented for both of the on-line and off-line detection approaches [46]. This method has been employed for PD detection in the machine winding via moving the antenna along the stator when the stator winding is excited at rated voltage but the machine is not in service. Pinpart and Judd investigated the transient response characteristics of three ultra high frequency (UHF) sensors (disc, monopole and spiral-type) to localize PD in a power transformer. It was reported that PD sources are localized effectively using UHF sensors and the disc-type shows high accuracy for PD localization among these three sensors [47].

2.5.3 EMI Method

Partial discharge pulses have a very fast rising time (in the nanosecond range) that generate high frequency components. Hence, measuring Electromagnetic Interference (EMI) in the very high frequency (VHF) range provides a detection method of PD. An EMI PD measurement system consist of a coupling capacitor, high frequency current transformers (HFCT), and coaxial cable sensors. The role of the coupling capacitor and HFCT is to sense and transfer the PD signal to the data acquisition system. PD signals are attenuated during propagation because of the impedance along the traveling path. To enhance the signal to noise ratio, de-noising techniques are needed to process the captured PD signal and increase the detection sensitivity. For the establishment of an on-line PD diagnosis, it is also significant that the capacitors used as coupling devices be PD free at the measurement

condition. The output of HFCT and coupling capacitor, which are the PD current pulses, can be sent to an oscilloscope for recording [26, 48, 49].

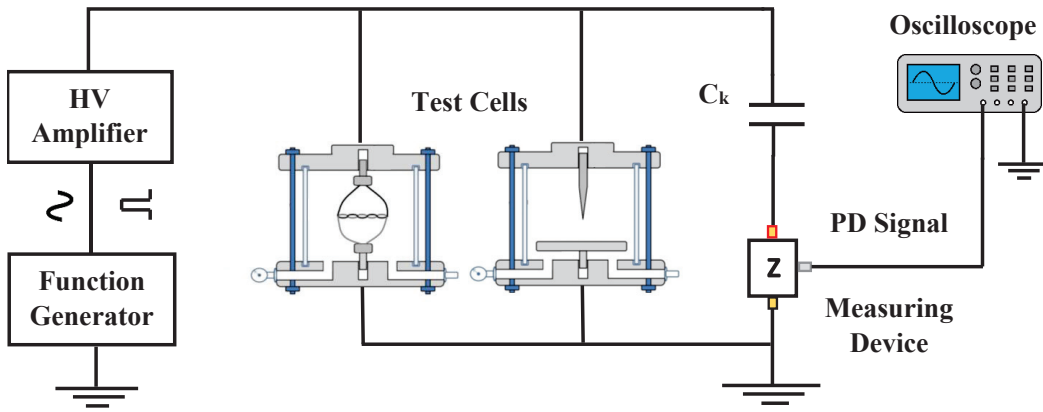
Chapter 3

PRPD Pattern Recognition

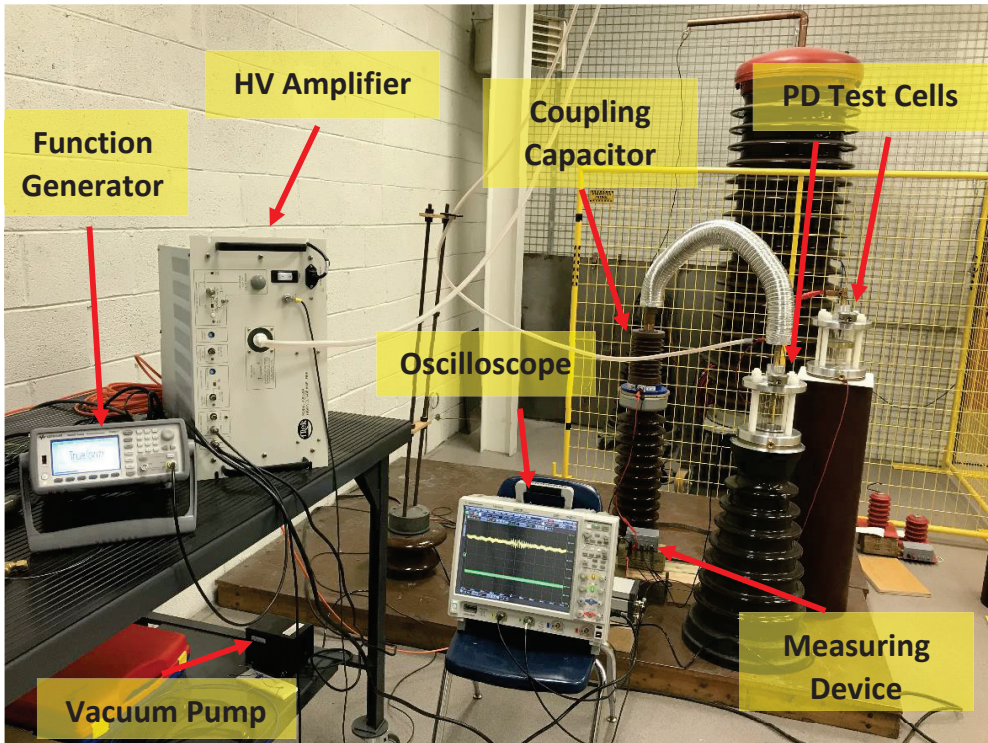
The phase resolved partial discharge (PRPD) pattern shows the occurrence of PD activities with respect to the phase of the applied AC voltage. The noise interference from external sources affects the measurement of PD signals that reduce the accuracy of the measurements. To obtain the PRPD pattern for PD recognition, a series of signal processing techniques are required to perform on the measured noisy PD data. This chapter presents a technique developed for on-line monitoring of PD for a low air pressure system and excessive noisy environment. To evaluate the developed method, PD tests are performed on two test cells under different level of air pressure and frequency. The phase-resolved patterns of the measured noisy PD signal are studied to for PD source recognition.

3.1 The Description of Experimental Setup

To detect PD pulses under different range of air pressure and applied frequency, the test setup shown in Fig. 3.1 is employed. The PD tests are performed on artificial defects in a high voltage laboratory. Two different artificial PD sources are used to produce PD pulse signals. A pressure controllable test cell is employed to simulate the defects in MEA. As shown in Fig. 3.1, the test setup is comprised of a power source for energizing the test cells,



(a)



(b)

Fig. 3.1: Experimental setup of two-source PDs consists of an HV source, a coupling capacitor, two PD source cells, a measuring device, and an oscilloscope. (a) Test circuit for partial discharge measurement. (b) Photo of the experimental setup.

a coupling capacitor ($C_k = 1nF$) to sense the partial discharge pulses, and a measuring impedance (Omicron CPL 542) to provide the means of sending PDs as voltage signals to an oscilloscope. A linear high-voltage power amplifier (TREK Model PD05034) and a signal generator are the main components of the source of high voltage. The signal generator is used to vary the frequency and the magnitude of the applied voltage. To set the desired voltage level, the output channel of the signal generator was connected in series to the HV amplifier.

3.1.1 Test Cells

In this study, two specific types of partial discharge are considered as insulation defects in an aircraft. The partial discharge between stator winding turns of motors and generators is one of predominant causes of electrical insulation failure. A random-wound stator is commonly used in low voltage electric machines. This type of stator winding structure is potentially susceptible to PD attack due to the existence of air pockets between winding turns. The winding of random-wound stator is made of magnet wires which are insulated copper conductors. Because of difference in the permittivity of air and insulation material of the magnet wires, PD may be initiated in the air gap between winding turns [10]. The second type of partial discharge is corona discharge which may be present in the non-uniform electric field generated by sharp edges, loose wire strands, or electric power transmission conductor in the power system of MEA [17].

To simulate corona discharge and the air gap between winding turns, a needle-plane electrode and a twisted pair of magnet wires are established in small-scale test cells as shown in Fig. 3.2. The test cells are able to withstand near vacuum condition and a maximum pressure of 500 kPa [50]. We used a pressure gauge and a vacuum motor to set the air pressure in the test cells. A tungsten needle with a tip diameter of 20 μm is used as the needle-plane electrode configuration. The insulation type of magnet wires (NEMA

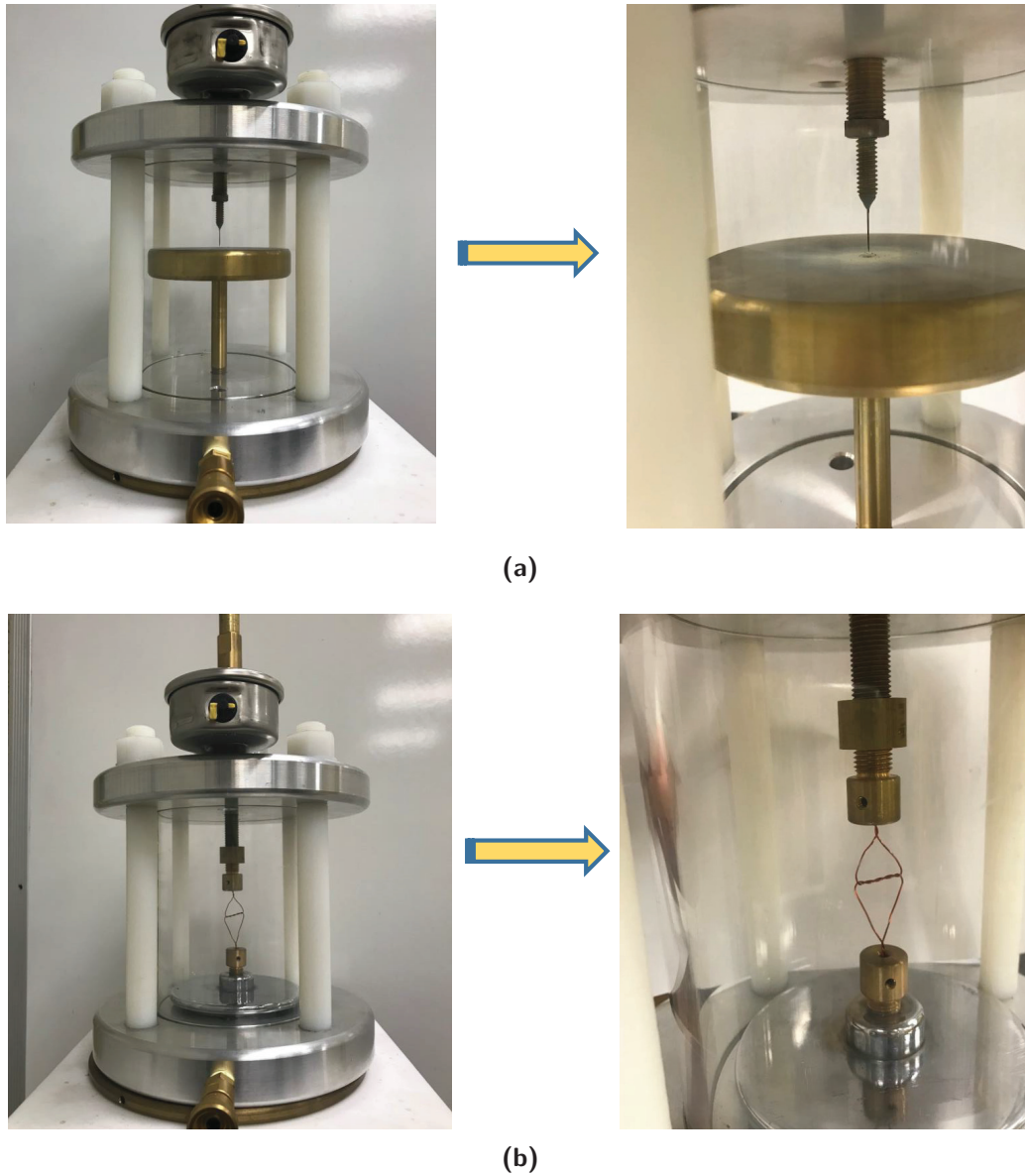


Fig. 3.2: PD source test cells, each cell consists of a pressure gauge and Perspex tube and is able to withstand vacuum pressure. (a) Needle-plane electrode configuration. (b) Twisted-pair of magnet wires.

MW 35-C) is made of a heavy polyester layer coated with a layer of polyamide to alleviate the problem of PD occurrence on the insulation surface. The magnet wires have a wire

gauge of 24 AWG and jacket diameter of 0.58 mm with a temperature rating of 200°C. The procedure for the preparation of twisted pair sample was carried out according to IEC60851-5 standard [51]. A straight piece of magnet wires was twisted back on itself for a length of 3 cm. The number of twists is three in this distance. The insulation of copper wires at both ends were removed and joined to make the test specimen.

3.1.2 PD Measurement Setup

The calibration and measurement procedures recommended by IEC60270 standard [8] are carried to conduct PD tests. The measuring impedance is placed on the ground side of the coupling capacitor. The V and PD output channels of the measuring device represent the applied voltage to the test object and the generated PD pulses, respectively. For further signal processing, the output signals of the measuring device are sent to an oscilloscope via a connecting cable. To record the PD signal, a high-speed digital oscilloscope (Agilent DSO9254A) with a bandwidth of 2.5 GHz and a sampling rate of 20 GSa/s is employed. The applied voltage to the test cell and PD signal are recored by the oscilloscope as voltage signals.

3.2 PD Detection Method

The environmental noise interference and the parasitic impedances affect the measurement of PD signal in on-line PD testing. Under sub-atmospheric pressures, PD pulses contain lower frequency contents due to the longer rise time of PD pulses (up to hundreds of microseconds) [38]. Also, the amplitude of PD pulses decreases at low air pressures which results in masking of PDs pulses by the interfering signals and background noises [26, 35]. The amplitude of corona discharge in low air pressure environment is significantly lower than the one at sea level air pressure because of the reduction in the density of the air particles and the generation rate of free electrons [34]. The background noise and corona discharge

may overlap when the reduction in corona discharge magnitude causes the PD pulse to have the same magnitude as the background noise. Because of this reason, PD pulses of corona discharge may be buried in excessive noise due to the low amplitude which causes difficulty in the detection of PD activity. In addition, traditional PD measurement is performed at a single frequency of 50/60 Hz in atmospheric pressure which cannot provide information about PD characteristics at a higher frequency at low air pressure [28, 29]. Therefore, a technique is needed to reveal the PD pulses in the measured noisy PD signal for further investigation. This assessment technique should have the capability of implementation for the on-line PD testing.

In the PD test setup shown in Fig. 3.1, the high voltage amplifier generates a wide range of switching noises. The operation of HV amplifier is based on power switches that turn electronic devices on or off at a high frequency rate. To assess the background noise of the high voltage laboratory, a commercial device (Omicron MPD 600) is employed. It was measured that the background noise of the HV lab is less than 5 pC. To accomplish an accurate PD test, the measurement setup was calibrated according to the IEC 60270 standard [8]. In this procedure, a defined charge pulse is injected into the test cell using charge calibrator (Omicron CAL 542). The ratio between the injected and the measured PD pulse is obtained and measurement system is calibrated to this value.

The captured noisy PD signal for one cycle of AC applied voltage is shown in Fig. 3.3. The needle-plane test cell is energized with a sine wave voltage and a frequency of 1 kHz under an air pressure of 67 kPa. As shown in Fig. 3.3, the recorded PD signal comprises of low-frequency switching noise, corona discharges, and background noises the recorded PD signal. Corona discharges occur at the negative half-cycle of the sine wave voltage with small magnitude. As shown in the same figure, the corona discharge recognition is difficult due to the small magnitude of the PD pulses. Because of this, a method is developed for corona discharge detection in a noisy environment. In the proposed detection approach,

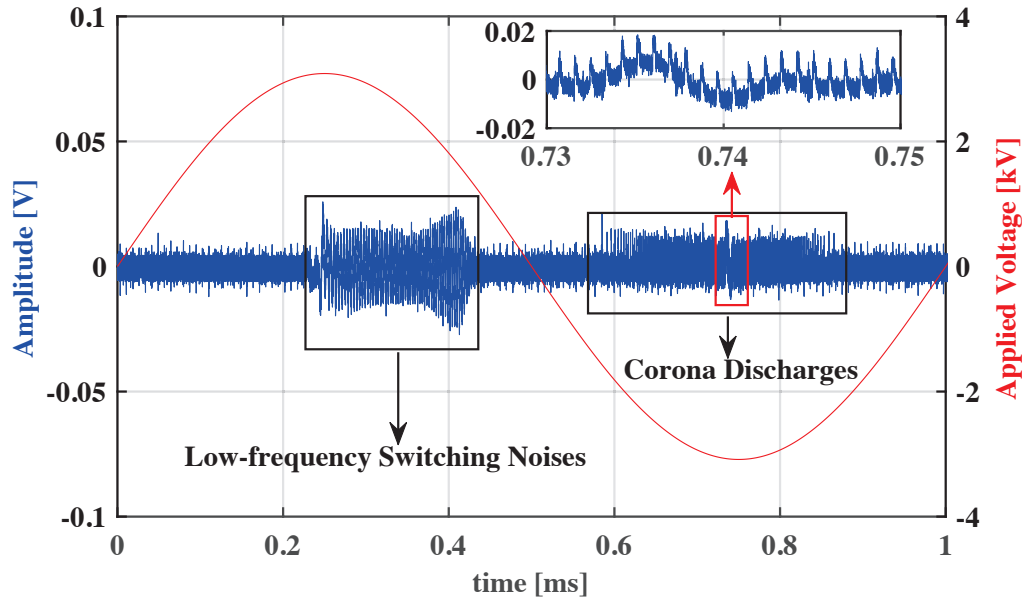


Fig. 3.3: Measured PD signals under sine wave applied voltage with the frequency of 1 kHz.

a series of signal processing techniques are carried out on the captured PD noisy signals. For this purpose, the differential energy magnitude of the PD pulses are calculated with respect to the phase of the applied voltage. This processing method consists of de-noising the measured PD signal, recognizing the PD Pulses, and corona discharge detection. Fig. 3.4 illustrates the proposed PD detection method at low air pressure over a range of the frequency of the applied sine wave. To reduce the effect of continuous background noises and low-frequency ripple of the measured PD signal, a wavelet de-noising technique is used. For removing the background noise from the PD data, a suitable wavelet mother is required. It has been indicated that Symlet family with high orders represents an acceptable outcome in the de-noising of the PD data [52, 53]. M cycles ($M=20$) of the PD signal waveform is captured by the oscilloscope that provides M data windows with a duration time of one-cycle of the applied AC voltage. The PD signal consists of corona discharge pulses and switching pulses after performing wavelet de-noising. As shown in Fig. 3.5, the magnitude

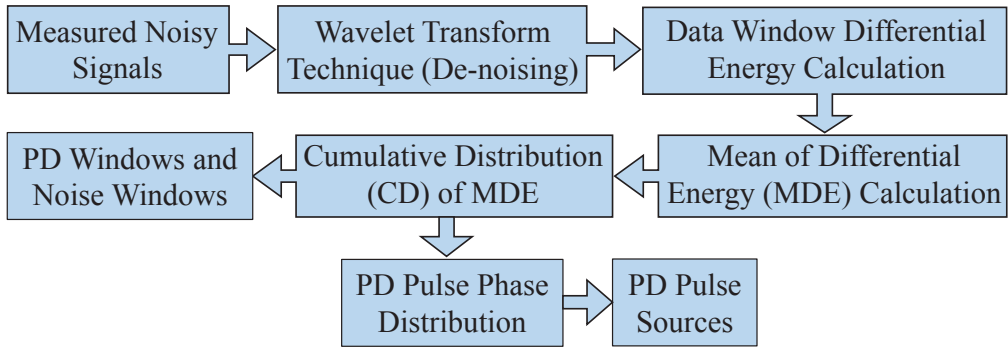


Fig. 3.4: Proposed algorithm for PD detection.

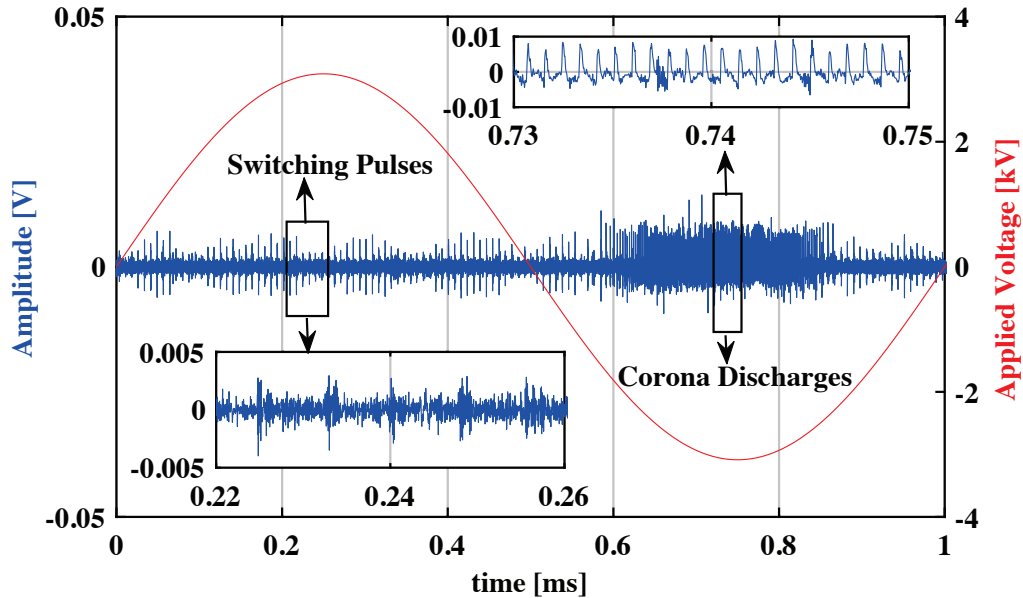


Fig. 3.5: PD signals under sine wave voltage after using wavelet transform.

of corona discharge is close to the switching pulses. In order to obtain the PRPD pattern and attenuate the switching pulses, further data processing of the PD signal is required. Hence, the one-cycle data window is divided into sub-windows with equal time length of $2 \mu\text{s}$. This brings N sub-windows in one-cycle data window which depends on the frequency.

For example, the total number of sub-windows for the frequency of 1 and 2 kHz are 500 and 250, respectively. The energy-based technique, which is called the differential energy (DE) technique, is employed to detect sub-windows with PD pulses and then discriminate them from the noisy sub-windows [54]. The differential energy of each sub-window is determined by taking the sum of squared data points considering the sign of the sampled points as given by

$$E_i = \sum_i k_i \cdot (x_i)^2 \quad (3.1)$$

where

$$k_i = \begin{cases} +1, & \text{if } x_i \geq 0 \\ -1, & \text{if } x_i < 0 \end{cases} .$$

Due to the symmetrical nature of low-frequency switching pulses, the differential energy values (E_i) of sampled signal in a sub-window data correspond to the switching signal will be approximately zero ($E_i \cong 0$). On the other hand, the differential energy (E_i) values of sub-windows related to the PD signal will be large enough compared to the differential energy of noisy sub-windows that show the phase location of the PD signal. Fig. 3.6 shows the phase-resolved pattern of partial discharge differential energy for the sine wave voltage waveform. The differential energy of all M one-cycle PD signal is calculated that results in M different values related to each sub-window. The mean of these M values is assigned to each of the $2\pi/N$ -wide phase window. Thus, a distribution of N differential energy values along 2π phase is created and given by

$$E_w = \frac{\sum_{i=1}^M E_{i,w}}{M} \quad (3.2)$$

where

$$w = 1, \dots, N.$$

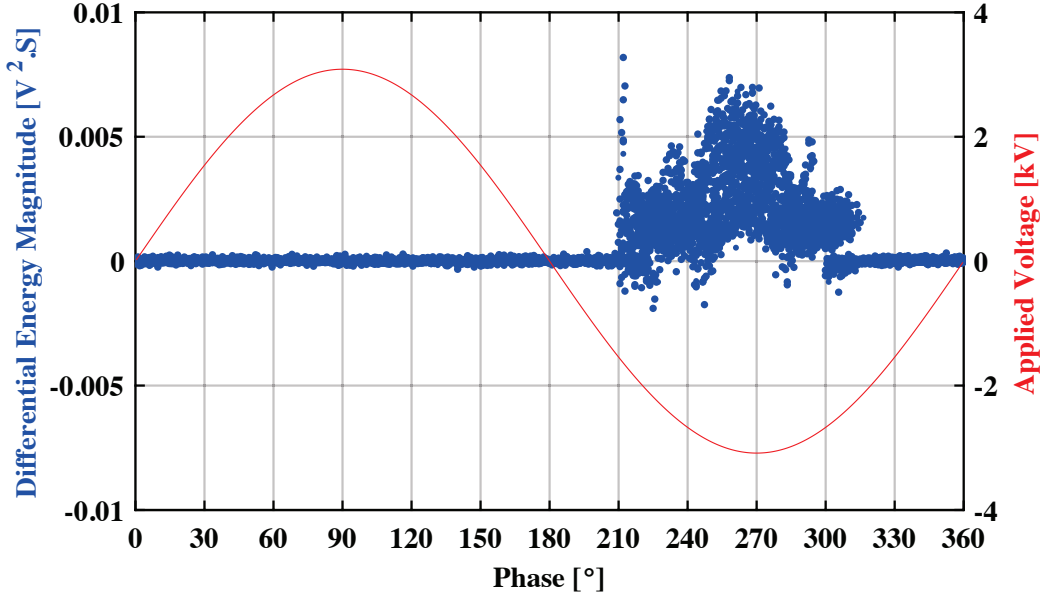


Fig. 3.6: Differential energy of signal in reference to phase angle under sine wave voltage

In (3.2), E_w is the mean of differential energies (MDE) in the corresponding phase window (w), and $E_{i,w}$ is the differential energy of a sampled signal (E_i) in the corresponding phase window (w). The N values calculated using (3.2) are allocated as the MDE in reference to phase of the applied voltage. The phase-resolved pattern of the MDE for applied voltage of sine voltages is shown in Fig. 3.7. The cumulative distribution of the MDE pattern is obtained by taking the sum of the phase window values as phase windows progresses. For instance, the phase window 3 in the cumulative distribution (CD) takes a value which is the sum of the phase window 1 and 2 in the MDE pattern. Hence, this calculation makes a new distribution of pattern along a 2π phase angle window n as given by

$$CD_n = \sum_{w=1}^n E_w, \quad n \leq N. \quad (3.3)$$

The output result of this step, which is the cumulative distribution of MDE (CDME)

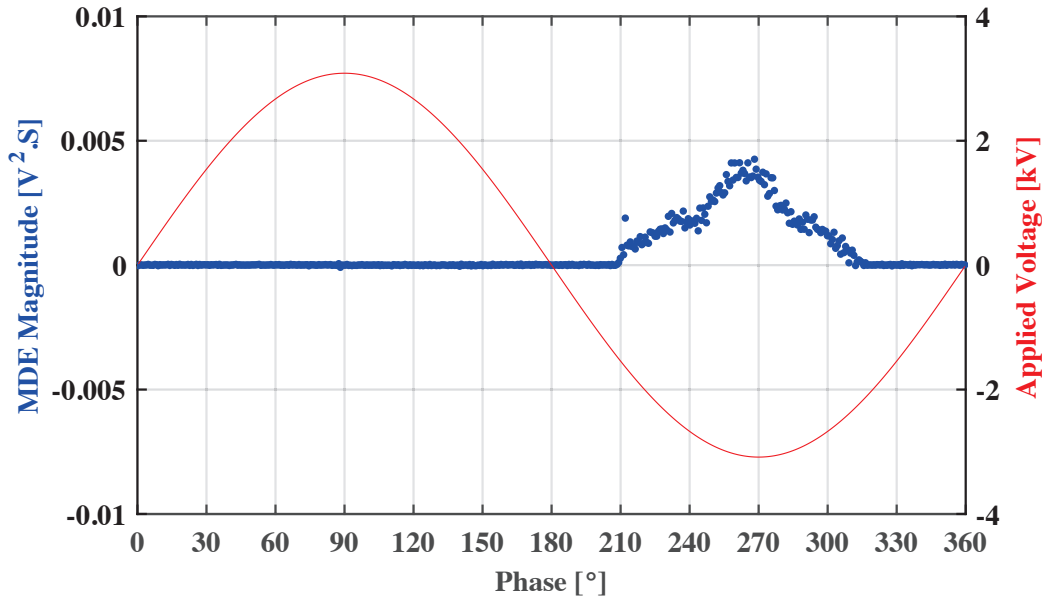


Fig. 3.7: Mean of Differential Energies (MDE) of signal in reference to phase angle under sine wave voltage

pattern with respect to 2π phase angle, is shown in Fig. 3.8. It can be observed that the CDMDE is constant when there is no PD activity, whereas the value of the CDMDE starts to increase/decrease when the PD pulses appear. The gradient of the CDMDE pattern provides a method to recognize the PD pulses in the insulation system. As illustrated in Fig. 3.8, the gradient of the CDMDE is large enough at negative half-cycle to reveal and detect the corona discharge occurrence specially at low air pressure area and noisy environment.

3.3 Effect of Air Pressure and Frequency on PDIV

In this section, PD tests are individually conducted on the needle-plane and twisted-pair wire test cells in the HV laboratory to determine the partial discharge inception voltage (PDIV). To find the PDIV, the magnitude of the sinusoidal voltage waveform is raised

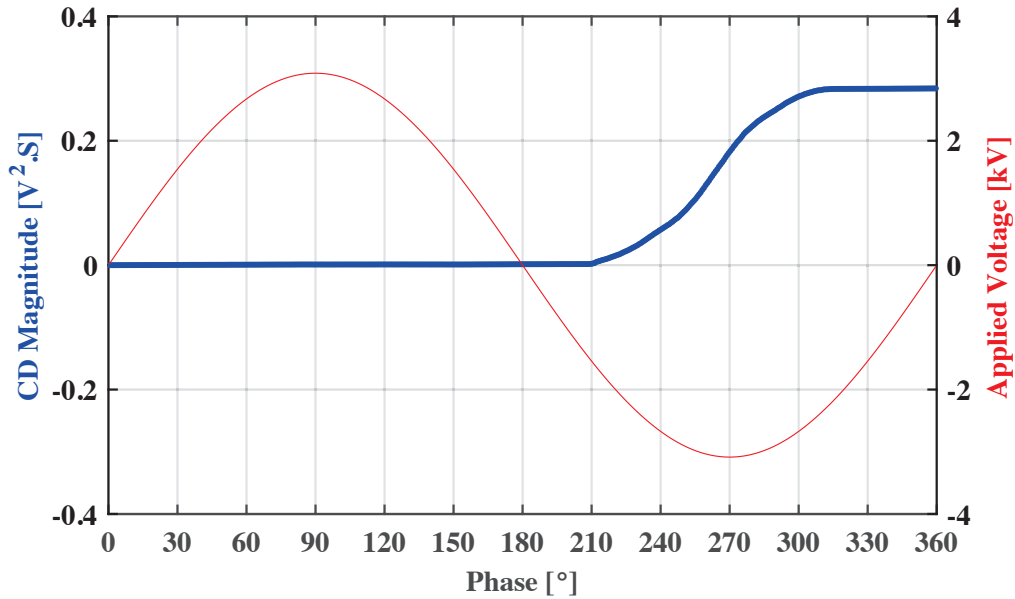


Fig. 3.8: Cumulative Distribution of MDE in reference to phase angle under sine wave voltage.

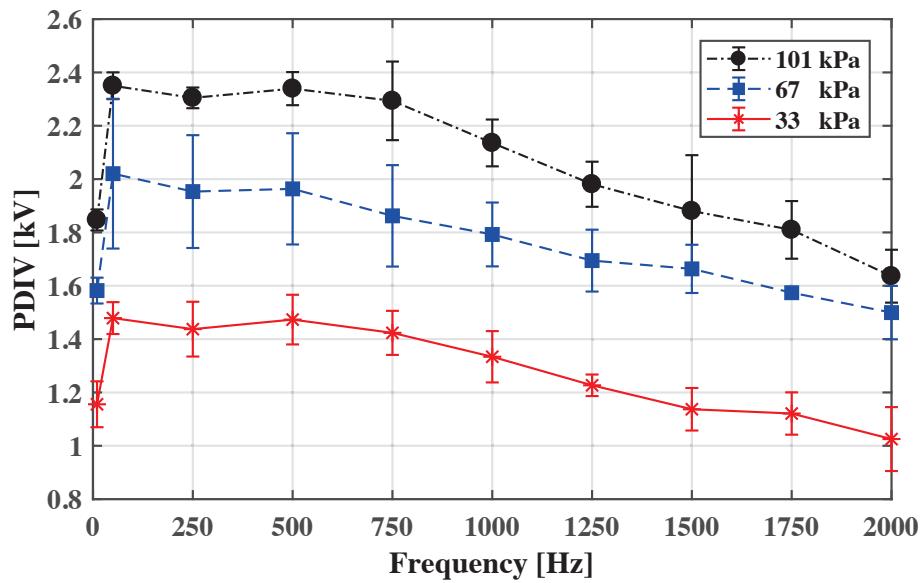
to 70% of the expected PDIV value and then steps of 100 volts (V) are used for increasing the voltage magnitude. Due to the decrease in the density of gas molecules and atoms with reducing the air pressure, each voltage step was applied for 3, 10, and 30 (s) under 101, 67, and 33 (kPa), respectively. This is because air needs more time to initiate ionization and electron avalanches at low air pressure [55].

Due to the stochastic nature of PD measurements, the PDIV values from repeated tests are significantly different. To overcome the variability in the measurements, 10 PDIV tests are carried out on the test cells to determine the PDIV value for each test condition. It is observed that the first PDIV measurement on the test cells results in higher value of PDIV compared to the subsequent PDIV measurements. The rationale for this experience can be attributed to the fact that the first electric discharge produces free electrons in the air gas. Therefore, more seed electrons will be present in the air gap for electron avalanches which causes reduction in the PDIV value of the next PDIV measurement. For this reason, the

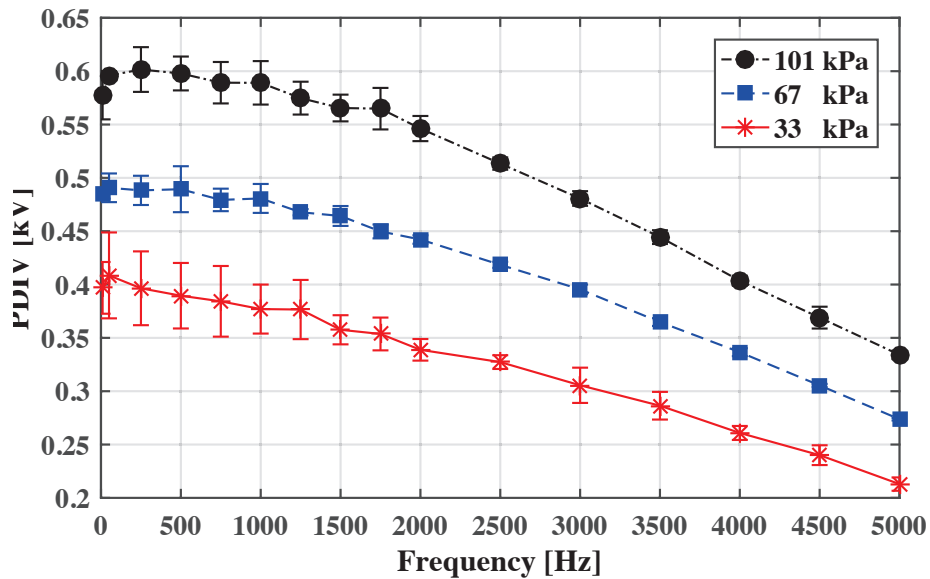
air inside the test cells is changed after performing a PDIV measurement. The mean of 10 PDIV values is calculated and determined as the PDIV at each frequency and air pressure level.

Fig. 3.9 shows the PDIV as a function of frequency under three different pressure levels. The length of the air gap for the needle-plane electrode is adjusted to 3 mm between the needle tip and plane electrode. Protection devices in the HV amplifier are capable of tripping the power supply when the electric current exceeds the maximum current limitation. For this reason, the PD tests related to the needle-plane electrodes are performed up to 2kHz. It can be observed that both the frequency and the air pressure have a significant influence on the PDIV values. As shown in Fig. 3.9, the PDIV of the needle-plane is much higher than the twisted pair of insulated wires and its value increases with air pressure. The reason of this observation is that decreasing the air pressure causes the density of air particles to decrease. As a result, an electron has less chance of collision with the other gas particles as it moves towards the anode. Because of lower collision probability, and consequently less chance of losing kinetic energy at low air pressure for an electron, a lower applied voltage will suffice to give the electron the required kinetic energy to ionize other particles via collision. Under a frequency of 500 Hz, it can be observed that the PDIV for a needle-plane electrode and twisted-pair of magnet wires decreases from 2.3 and 0.6 kV to 1.5 and 0.39 kV when the air pressure drops from 101 to 33 kPa, respectively. This reduction in PDIV demonstrates that the gap length (conductor spacing) between energized conductors as well as the insulation type used in the electric machines must be taken into account in the design of electrical insulation system of aircraft.

It can also be observed that the PDIV for a sine wave voltage waveform decreases with increasing frequency. To explain the effect of frequency on the trend in PDIV values, two factors can be considered. The first factor is the effective discharge time which is the total time duration of PD activity at one period of the applied sine wave voltage. As mentioned in



(a)



(b)

Fig. 3.9: PDIV measurement, obtained from conducting PD test on each test cell separately at different level of air pressure and applied frequency. (a) PDIV as function of frequency and pressure for needle-plane electrode. (b) PDIV as function of frequency and pressure for twisted-pair of magnet wires.

Section 2.2, the positive ions have lower mobility in comparison to the electrons. Increasing the frequency makes positive ions have less time to disperse. Hence, there always exists a number of positive ions in the vicinity of the tip of electrode. The accumulation of positive ions around the tip electrode creates an internal electric field that contribute to the external electric field at negative half-cycle of the applied voltage. The second factor is the density of the positive ions accumulated near the tip of the needle, which grows with increasing the frequency. The enhancement of external electric field because of the positive ions, causes a lower electric field intensity or a lower voltage magnitude be adequate for the initiation of electron avalanches [42]. This explanation can be used for the reduction in the PDIV of twisted-pair of magnet wires with increasing the frequency. This is because of creating non-uniform electric field in the air gap between turns. According to Fig. 3.9b, PDIV for twisted pair of magnet wires is decreased from 0.6 to 0.4 kV under atmospheric pressure when the frequency is increased from 500 to 4000 Hz.

3.4 Corona Discharge PRPD Pattern

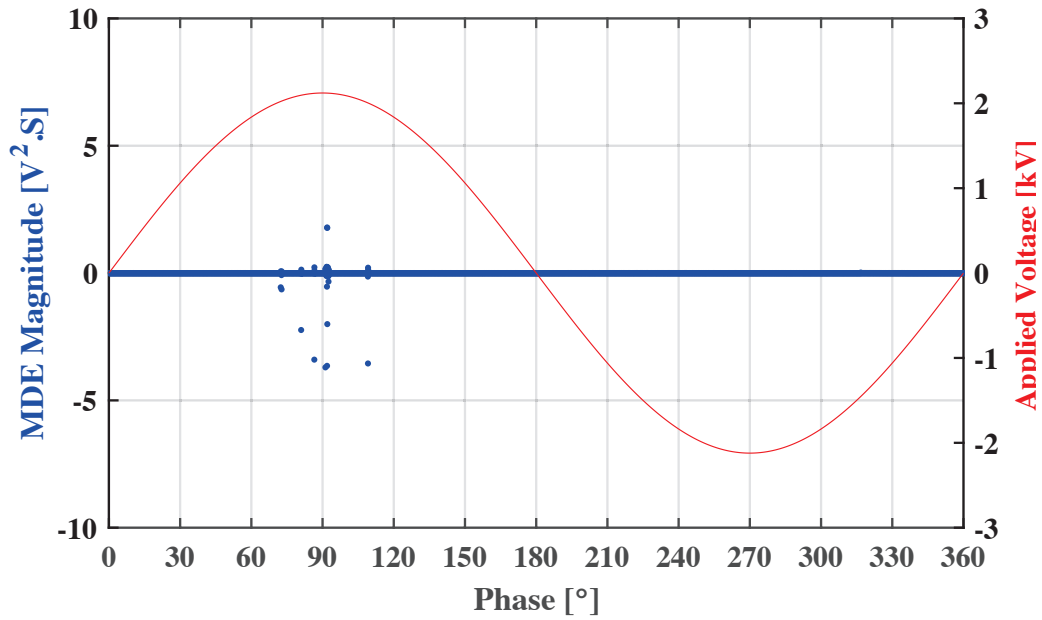
In this section, PD measurements are performed to generate the PRPD pattern for the corona discharge recognition. A needle-plane electrode configuration is mounted in a chamber with a gap length of 3 mm. The test circuit components are same as those shown in Fig. 3.1 but the twisted-pair of magnet wire is disconnected from the measurement setup, i.e. the needle-plane electrode is the only PD source for generating PD pulses. PD measurements are carried out at pressure levels of 33, 67, and 101 kPa at frequencies of 50, 250, 500, 750, 1000, 1250, 1500, 1750, and 2000 Hz. It is not possible to increase the frequency higher than 2 kHz since the power supply current is increased above the maximum current limitation of the HV amplifier. The noise interference from external sources affects the measurement of corona discharge signals that reduces the accuracy of the measurements. One of the significant external sources of interference is a switching noise that comes from the

power supply. The switching noise contains both low-frequency and high-frequency characteristics. The low-frequency and high-frequency switching interferences are created by the function generator and the amplifier. Moreover, the high level of continuous background noise of high voltage laboratory has significant effect on the measured signals. Because of these reasons, extracting corona discharge signals from noisy measured signals for further data analyzing is a challenge. To overcome the switching noises, a detection method is developed to extract the PD pulses to enable the study of the effect of the air pressure and frequency on the PRPD pattern as described in Section 3.2.

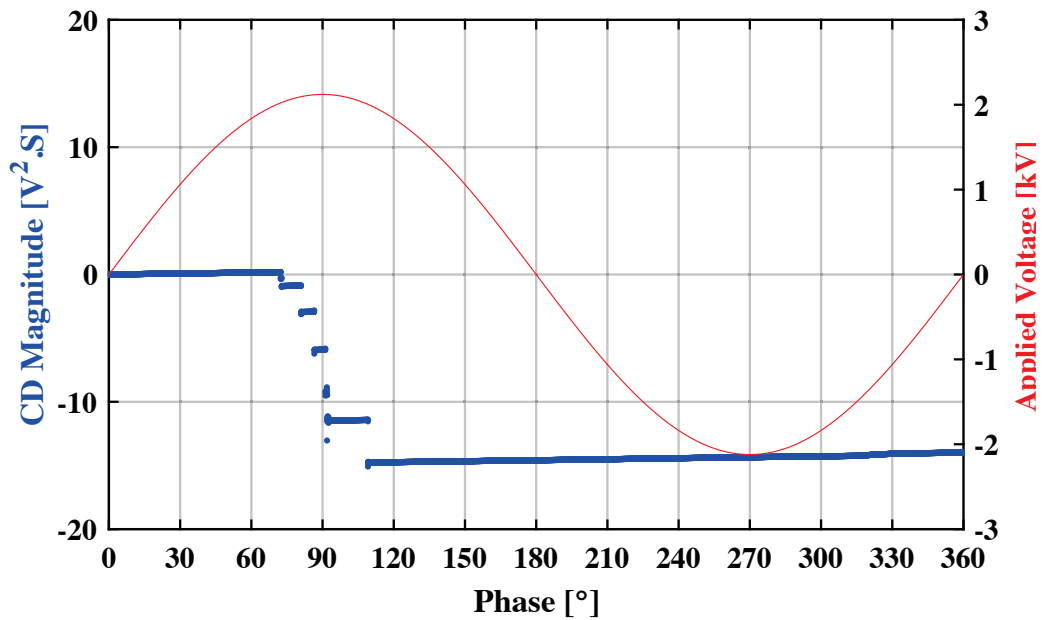
The applied voltage for PD measurement is set at 20% higher than the PDIV value at a predetermined frequency and air pressure. Due to the large number of the generated PRPD patterns, the MDE and CDMDE patterns for 50 Hz (low and power frequency) and 2 kHz (high frequency) under pressure of both 101 and 33 kPa are presented and compared.

The patterns provide the means to observe the trend in PD characteristics under variable frequency and air pressure. Fig. 3.10 and 3.11 show that at a low frequency of 50 (Hz), the PD ignition starts at positive AC cycle. The CDME pattern give an indication that at low-pressure level of 33 (kPa), PDs occur at positive half cycle of applied voltage. The occurrence phase angle of positive corona PDs is around 70° with high differential energy magnitude. While the air pressure increases, the positive corona discharges occur at a phase angle of 60° with lower differential energy magnitude which shows a shift in PD ignition phase angle. Also, negative corona discharges appear that demonstrates an increase in PD activities. The main observation is that the MDE magnitude of positive corona discharge is significantly greater than the negative corona discharge. Also, the MDE magnitude increases by reducing air pressure. At high altitude, positive corona discharge can be a dominant parameter in insulation degradation.

Fig. 3.12 and 3.13 show that at a frequency of 2 kHz, there is no positive corona discharge. However, negative corona discharges ignite at a phase of 210° with lower energy



(a)



(b)

Fig. 3.10: Obtained MDE and CD patterns for corona discharge under frequency of 50 Hz and sub-atmospheric pressure (33 kPa). (a) MDE pattern. (b) CD pattern.

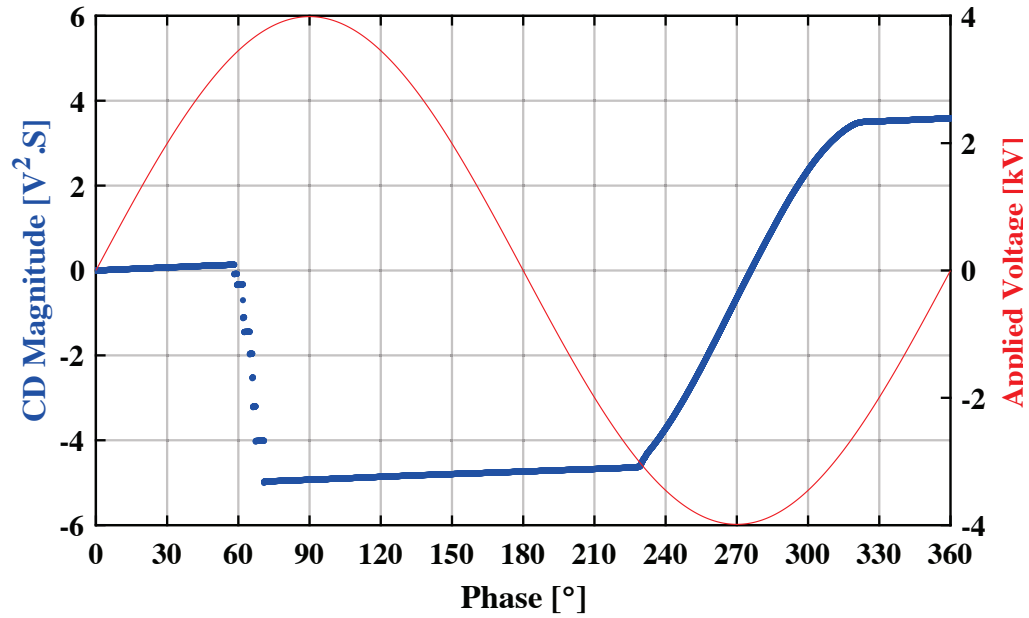
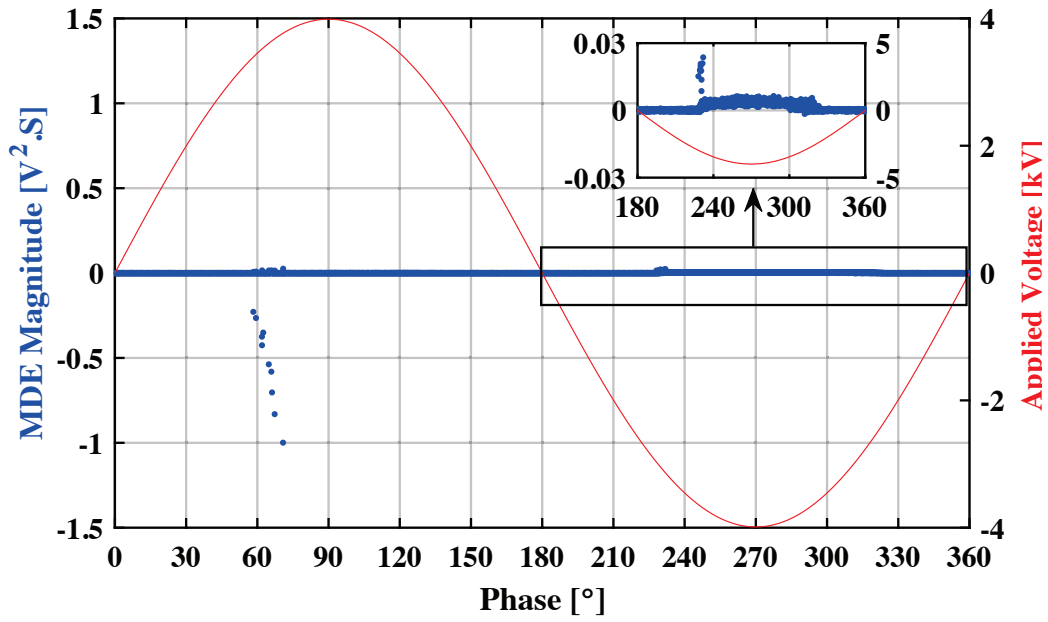
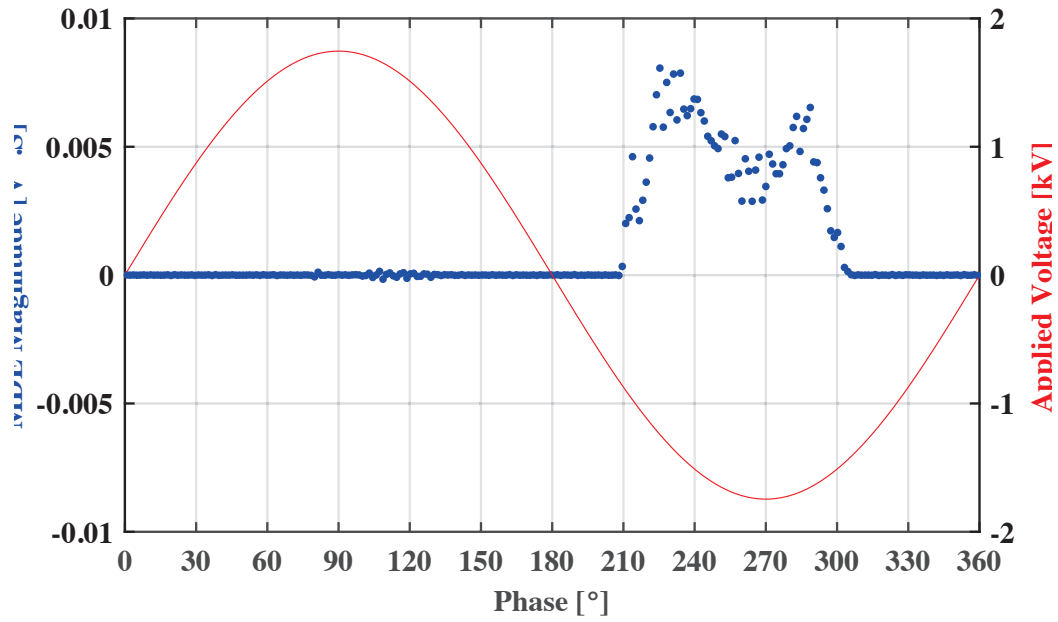
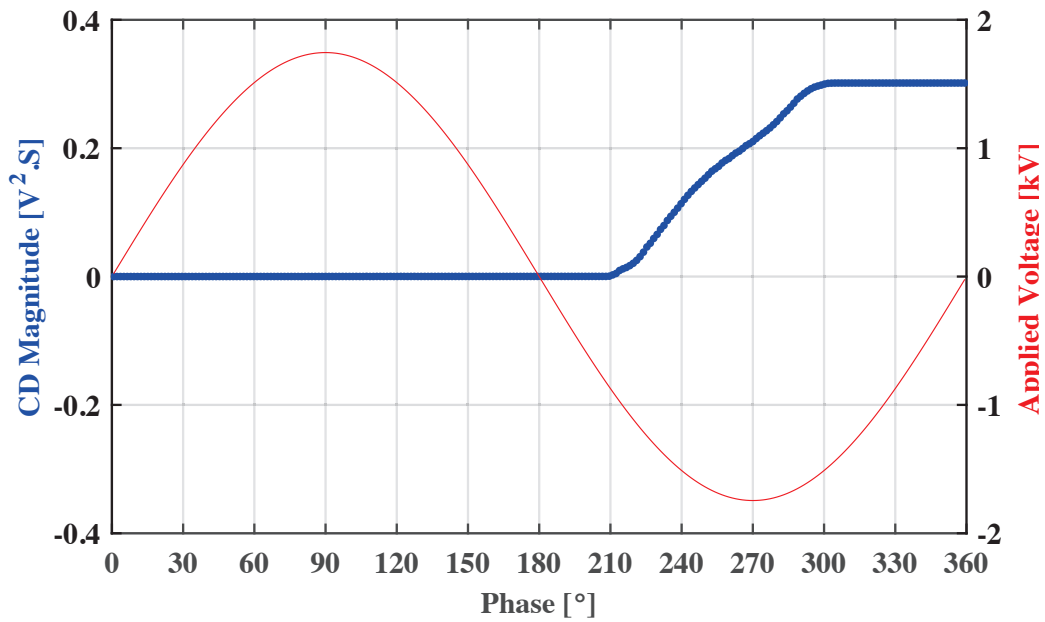


Fig. 3.11: Obtained MDE and CD patterns for corona discharge under frequency of 50 Hz and atmospheric pressure (101 kPa). (a) MDE pattern. (b) CD pattern.



(a)



(b)

Fig. 3.12: Obtained MDE and CD patterns for corona discharge under frequency of 2000 Hz and sub-atmospheric pressure (33 kPa). (a) MDE pattern. (b) CD pattern.

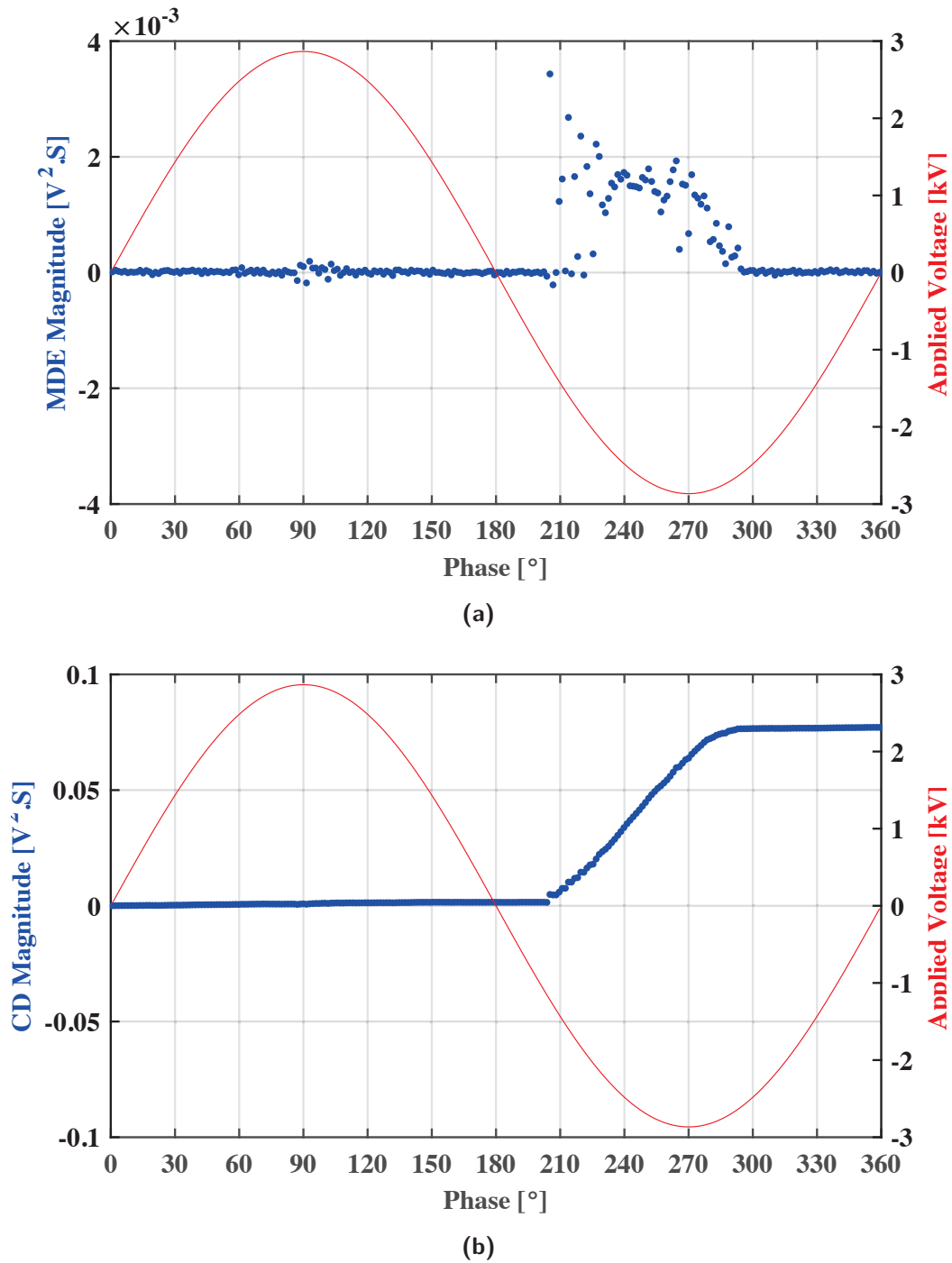


Fig. 3.13: Obtained MDE and CD patterns for corona discharge under frequency of 2000 Hz and atmospheric pressure (101 kPa). (a) MDE pattern. (b) CD pattern.

magnitude at all pressure levels. The magnitude of the MDE decreases as the frequency increases. It can be seen that the MDE pattern changes with air pressure. At a pressure level of 101 (kPa), the shape of the MDE pattern is similar to wave-like pattern. At low-pressure level, the MDE pattern is similar to rabbit-ear pattern. This pattern transformation can be easily seen at high frequencies. According to Fig. 3.11 to Fig. 3.13, it is observed that the energy magnitude of PD pulses decreases with increasing the frequency. The rationale for decreasing the amplitude is that the discharge time decreases with frequency and there is less time for electric field to be reconstructed. When a discharge occurs in the air gap, the electric field is distorted due to the movement of space charges and dropped below the PD inception electric field again. Therefore, a specific time is required for the electric field to be reformed and increased above the PD inception electric field. With increasing the frequency, there is less time for reconstructing electric field and PD occurs at lower electric field intensity with lower discharge amplitude [4, 15].

It is important to mention that PD pulses during negative half cycle of the applied voltage are of the Trichel pulses type. As shown in Fig. 3.11a, the first PD has higher amplitude than the following successive PD pulses under negative half cycle. When the needle electrode has negative voltage polarity and the applied voltage reaches to the PDIV level, the electrons formed on the needle surface will travel with high kinetic energy toward the ionization region (needle tip) to cause electron avalanches and leave behind a cloud of positive space charges. After leaving the ionization region, these electrons will not be capable of ionizing other gas particles due to the reduced speed. Some of the low speed electrons may be absorbed by the plane electrode and the rest may be absorbed by oxygen molecules and form a cloud of negative space charges. When the first pulse of Trichel corona discharge is ignited, the internal electric field formed between the negative cloud of space charges far from the needle tip and positive ions near to the discharge electrode weaken the electric field in the gap. This reduction in the electric field cause the ionization process to

stop. After clearing the gap of negative cloud space charges, the electric field again becomes high enough to start the ionization process [4, 32]. Therefore, the periodic character of the Trichel discharge can be realized using this explanation.

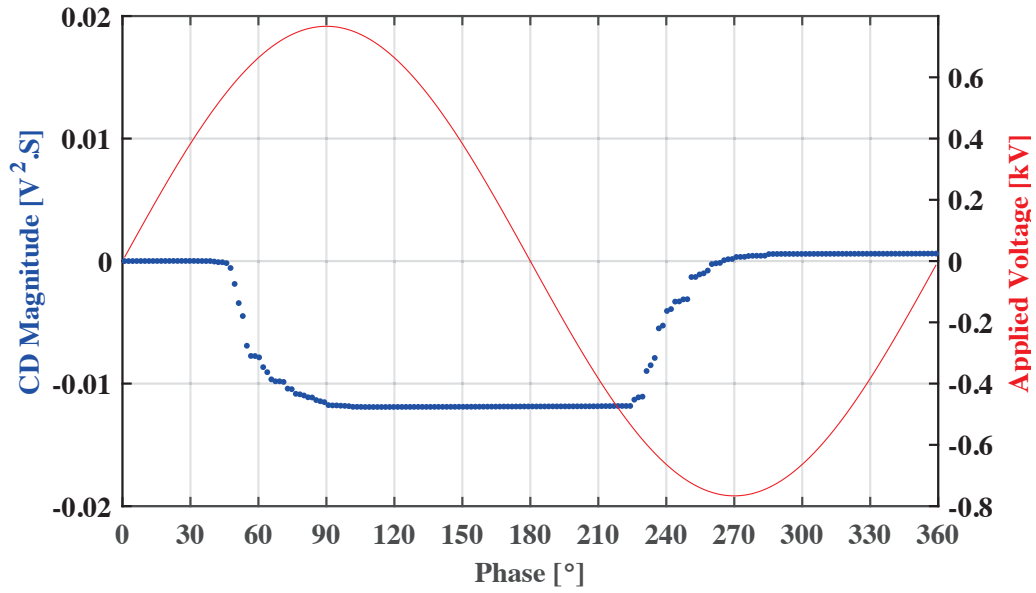
3.5 Multiple PD Sources PRPD Pattern

It was mentioned that the amplitude of corona discharge decreases at low air pressure, thus the detection and localization of the corona discharge in the aircraft power system is a challenge at sub-atmospheric pressures and noisy environment. In this section, the performance of proposed corona detection method is examined upon different measured noisy signal. The test cells are connected in parallel as shown in Fig. 3.1. The voltage magnitude is set to 120% of the PDIV of corona discharge. Thus, both of the needle-plane electrode and the twisted-pair wires generate PD pulses, simultaneously. The measurements are carried out at the pressure level of 33 kPa and for the frequencies of 1 kHz, and 2 kHz.

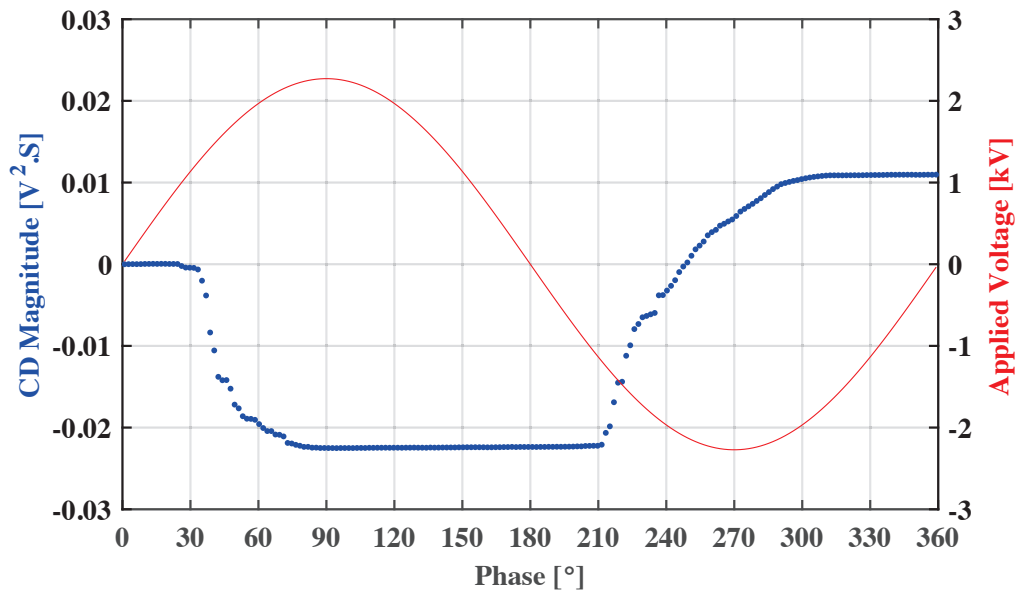
The phase-resolved patterns of the CDMDE of measured signals are shown in Fig. 3.14. As shown in Fig. 3.14a, the CDMDE magnitude relevant to twisted-pair insulated wires suddenly decreases to the value close to -0.012 and then rises to a value which is a little more than zero. It can be seen that the starting and terminus points of CDMDE plot are close to each other. The changes in CDMDE magnitude reveal that PD pulses occur at positive and negative cycle of the applied voltage. Positive and negative PD pulses start at the phase angles of 45° and 225° , respectively. By increasing the applied voltage, the corona discharges that are from the needle-plane electrode appear and result in the measurements consist of two types of PD pulses activated simultaneously. The CDMDE pattern reveals that the corona discharges occur at negative half cycle of the applied voltage. The reason is that the positive ions accumulated in the vicinity of the needle tip curvature create a internal electric field which enhances the external electric field. This results in a lower electric field intensity to suffice for electrons avalanches to be initiated. To generate corona discharge at

the positive half cycle, a little higher voltage must be applied. Fig. 3.14b indicates that the changes in the CDMDE magnitude at negative half cycle are much more than the one in positive half cycle. The phase-resolved partial discharge (PRPD) pattern for twisted-pair insulated wires is symmetrical. However, the PRPD pattern for needle-plane electrode is asymmetrical.

Fig. 3.16a shows the measured PD signal after performing wavelet de-noising for one cycle of the applied voltage to the PD sources in parallel. The frequency of the applied voltage is 2 kHz. The measured signal consists of switching noise, background noise, PD pulses and corona discharge. The PD pulses coming from the twisted-pair insulated conductor occur during the falling and rising edges of the applied voltage. It can be seen that the amplitude of corona discharges is much less than the PD pulses from twisted-pair wires. In addition, the phase-resolved patterns of the CDMDE of measured signals under a 2 kHz sine wave are shown in Fig. 3.16. When the applied voltage is less than the PDIV of both PD sources, there is no PD occurrence. The zero value and the pattern of CDMDE shows that there is no PD activity as depicted in Fig. 3.15a. As the magnitude of the applied voltage becomes greater than the PDIV of the twisted-pair of magnet wires, this PD source generates PD pulses while the needle-plane electrode is not active. According to Fig. 3.15b, CDMDE magnitude abruptly falls to a value close to -0.02 and then rises to a value close to zero. It is obvious that the PD pattern is symmetrical for PD pulses generated by twisted-pair insulated wires. In Fig. 3.16b, It can be seen that the PD pattern changes from symmetrical to asymmetrical by increasing the applied voltage to higher than 1.5 kV. The reason is that the corona discharges appear on the negative half cycle of the applied voltage that converts symmetrical PD pattern to asymmetrical. The PD phase location can be found by the absolute value of the gradient of the CDMDE. The absolute value of the gradient on phases without any PD pulses will be zero.

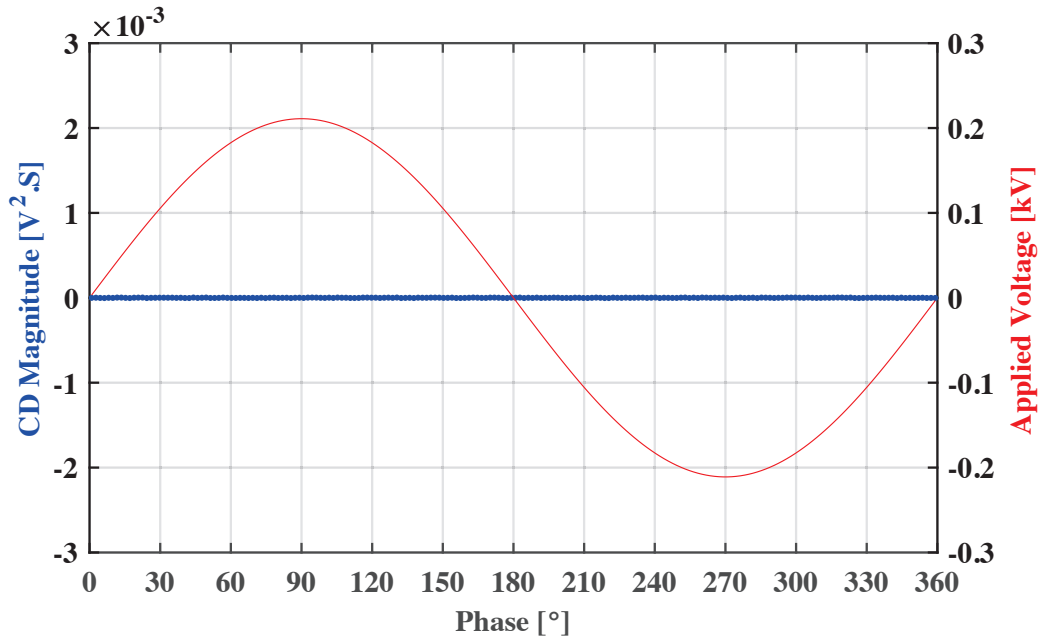


(a)

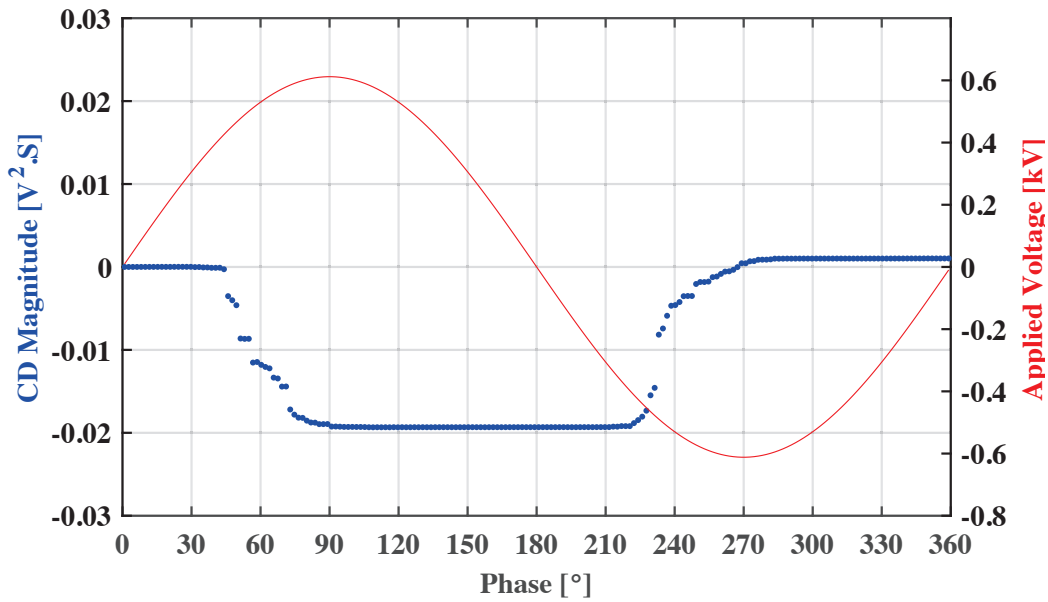


(b)

Fig. 3.14: Cumulative Distribution of MDE in reference to phase angle of measured signal with PD pulses generated by two PD sources under applied frequency of 1 kHz. (a) PRPD pattern generated by PD pulses from twisted-pair wires. (b) PRPD pattern generated by both of PD pulses sources.

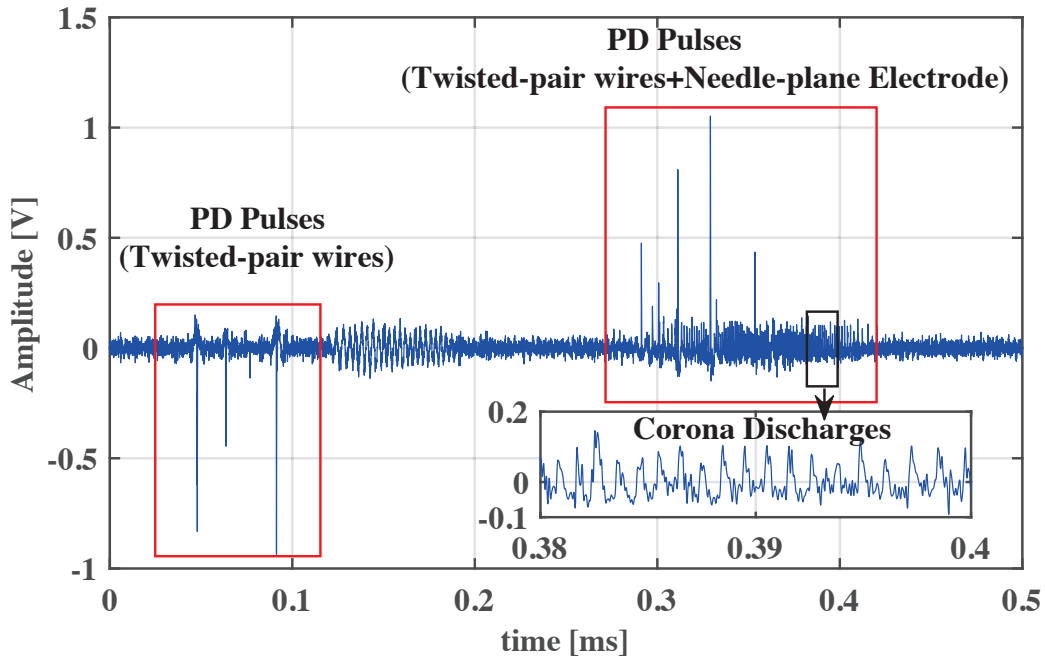


(a)

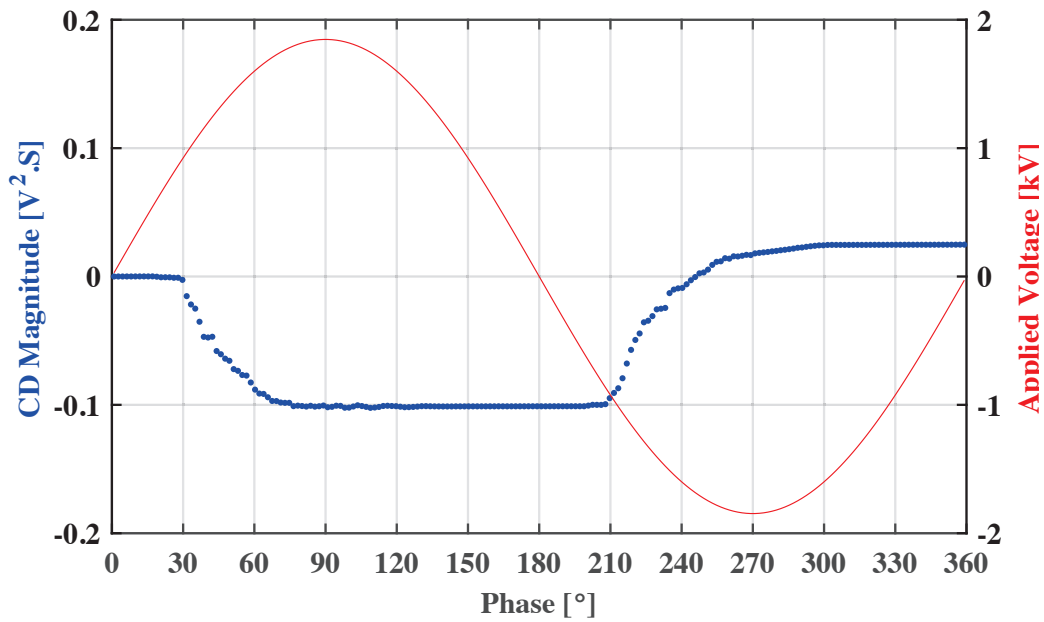


(b)

Fig. 3.15: Cumulative Distribution of MDE in reference to the phase angle of the measured signal. (a) Without any PD pulses. (b) PD pulses generated by twisted-pair wires.



(a)



(b)

Fig. 3.16: Cumulative Distribution of MDE in reference to the phase angle of the measured signal in the presence of two activated PD sources . (a) PD signals after using wavelet transform (both PD sources are activated). (b) PD pulses generated by both PD sources.

3.6 Summary

In this chapter, a PD detection procedure was presented. It was mentioned that the amplitude of corona discharges decreases as the air pressure drops. A technique was proposed to detect discharge pulses under low air pressure and excessive noisy environment that can be implemented for on-line condition monitoring of the insulation system in the aircraft electrical system. The PRPD pattern of single PD source as well as multiple PD sources can be obtained using the developed algorithm. Different patterns for investigation of corona discharge under variable frequency and air pressure were produced via implementation of energy based technique on the measured PD signal. This method is based on the combination of the wavelet and energy techniques. This method offers high performance corona discharge detection in excessive noisy environment. The CD magnitude of the recorded noisy signal was obtained using this method. The absolute value of the gradient of CD magnitude revealed the phase duration that PDs were activate in one cycle of the applied voltage. The non-zero value of gradient shows PD phase occurrence. Also, the results indicated that the phase-resolved pattern of the calculated CD for PD pulses caused by twisted-pair magnet wires is symmetrical. When the corona discharges occur, the pattern changes from symmetrical to asymmetrical. For an asymmetrical pattern, the CD magnitude increases from a negative value to a positive value much greater than zero value on a negative half cycle of the applied voltage. It was shown that both the frequency and the air pressure do affect the characteristics of PRPD patterns. The amplitude of corona discharge decreases as the frequency increases. It was observed that at low air pressure and high frequency the pattern of corona discharge has the shape of a rabbit-ear while the pattern is like wave shape in the atmospheric pressure. In addition, the PDIV measurement was performed on a needle-plane electrode and twisted-pair magnet wires experimentally. It was shown that the PDIV decreases with increasing the frequency and decreasing the air pressure.

Chapter 4

Classification of Concurrent PD Sources

In the previous chapter, a high performance localization and detection method for both single PD source and multiple PD sources was developed. It was demonstrated that the CD pattern is capable of detecting PD activity in the insulation system even when the PD pulses were buried in the noisy recorded PD signal. However, the disadvantage of this pattern is that multiple, simultaneous PD sources make recognition of PD sources very hard due to overlapped patterns. There are many real situations where PD measurement is affected by multiple concurrent activated PD sources. The PRPD patterns produced by simultaneously activated PD sources are partially overlapped. PD source identification based on the PRPD pattern may lead to false interpretation of the measured PD signals [56, 57]. In this regards, recognition of PD sources has been continually investigated in order to perform comprehensive assessment of the insulation condition. For separation of PD pulses, various methods and algorithms have been developed and proposed based on the PD pulse waveform analysis [56, 58]. The PRPD pattern related to each PD source was used for the discrimination of the PD sources in most of the proposed methods. The

drawback of using PRPD patterns associated with each single PD source for classification, is misclassification of PD sources due to overlapped patterns.

The recognition of two simultaneous PD sources has been done using a five-parameter additive Weibull distribution by Cacciari *et al.* [59]. It is reported that this function fits well on the partial discharge height distributions which provides a means to analyze the probability distribution associated with each concurrent PD defect [59]. It has also been reported that there exists a correlation between different kinds of defects with their PD pulse waveforms. This means that PD sources of the same nature generate PD pulse waveforms with the similar characteristics [60]. For classification of multiple PD sources occurring in practical insulation systems, auto-correlation function (ACF) of the measured signals were compared under the assumption that there is similarity between the ACF of the recorded PD shape signals generated from the same nature of the PD source [61,62]. When the captured signals contain dissimilar PD shape signals, ACF differ that can provide a correlation index for comparison [61,62]. In order to discriminate the collected pulses into homogeneous clusters and considering noise disturbance, time-frequency analysis method has been proposed using a fuzzy classifier (FC) [63]. In this procedure, the separation was carried out via the transformation of the recorded pulse waveforms into a two-dimensional (time-frequency) space. The features were considered for mapping the pulse waveforms are the average time and dominant frequency that contains the total energy of the signal [63]. To classify multiple concurrent PD defects, the comparison of ultra-high-frequency (UHF) envelopes were performed through applying a Gaussian kernel smoothing to the data set [64]. The use of mathematical morphology for feature extraction from optical PD data and sparse representation classification has been presented [65]. This classification technique discriminates the PD sources on the principle of using least amount of resources which is used for the imperfect and noisy PD signal [65]. A new method based on two-step logistic regression (LR) model for the probabilistic identification of PD pulse signals has been introduced [57]. In

this method, principal component analysis (PCA) was used to reduce the high dimensional space related to a single PD source. The PD data of multiple PD sources were fed into the feature space and one-class kernel support vector machine (KSVM) was employed to differentiate the multiple PD sources. Partial discharge identification of multiple activated sources has been studied in [66]. In this work, principal component analysis (PCA) was used for reducing the dimensionality of the PD data. Wavelet coefficient energies associated with a single-PD source were compared for separating PD sources. Spectral power analyses of the recorded PD pulses has been performed under the assumption that pulses of different PD types, as well as noise, generate spectrum at different frequency band [67–69]. For this purpose, spectral power ratios were calculated at different frequency intervals for the separation of PD pulses.

In this chapter, PD measurements under AC voltage are performed to investigate and analyze various time-domain features of the PD pulse waveforms comprehensively. In this regards, several PD pulse parameters such as rise time, fall time, slew rate and pulse width are computed to generate time-domain features. These pulse parameters describe important fingerprints of the PD sources. The statistical moments of the features distributions are utilized for discriminating PD pulse sources. In this approach, PD pulses are recognized and separated from noise pulses based on pulse signal parameters. After separation, the classification of PD concurrent sources are achieved using a nonlinear version of support vector machine (SMV). The results demonstrate an accurate, powerful and robust algorithm for on-line monitoring of HV components operating under sub-atmospheric air pressures as well as classification of simultaneous PD sources.

4.1 PD Pulse Waveform Analysis

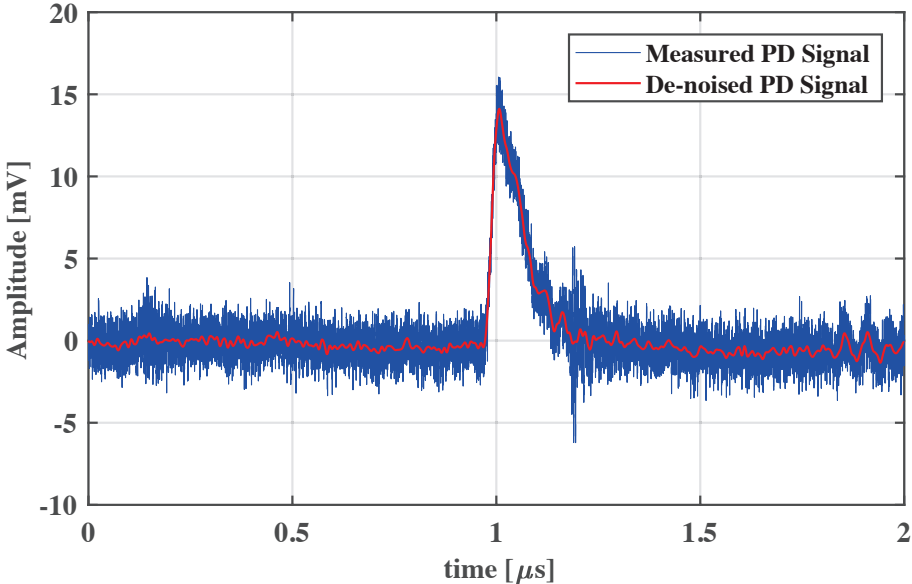
The phase resolved PD (PRPD) technique offers many merits to analyze the condition of almost any type of insulation system. However, the implementation of this well-known

method for on-line PD measurement brings about several key challenges that reduce the reliability of this technique. Due to a high level of noises in on-line PD testing, the use of this method may lead to false interpretation of the PD pattern. In addition, the presence of multiple, simultaneously activated PD sources may undermine the performance of this method because of overlapped patterns [67–69]. Hence, PD waveform analysis has been carried out to separate and classify two simultaneous PD sources in the presence of noisy environment. It is assumed that the same PD source generates signal having same waveform similarity. For this purpose, the time-resolved of PD signal are analyzed to extract time-domain pulse parameters which include rise time (RT), fall time (FT), slew rate (SR) and pulse width (PW) for pulse source separation under different range of air pressure and applied voltage frequency. The value of all these pulse parameters depends on the air pressure that varies during ascending and descending of the aircraft.

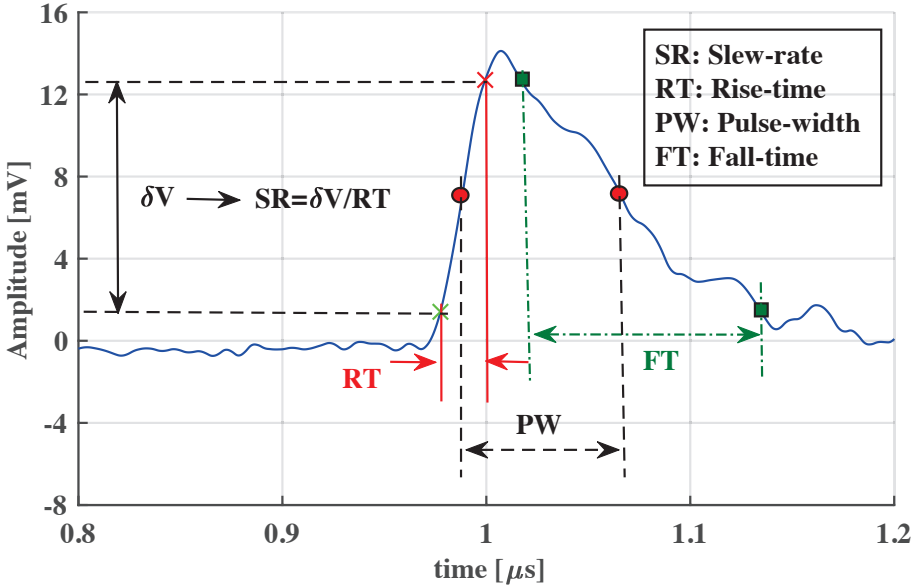
As shown in Fig. 4.1, the rise time is defined as the time taken by the PD pulse to increase from 10% to 90% of its maximum value. The fall time is the time taken by the PD pulse to drop from 90% to 10% of its maximum value. The slew rate is the rate of change of PD pulse which is defined as the slope of the line connecting the 10% and 90% of PD signal maximum value. Finally, the pulse width is the duration time of two same level instants which are defined as the 50% of PD signal peak value.

4.1.1 PD Pulse Waveform Measurement

PD tests are performed on two types of PD sources (twisted-pair of magnet wires and needle-plane electrode) individually and simultaneously according to the recommended procedure of IEC60270 standard [8]. The experimental setup for recording the PD pulse waveform is the same as that shown in Fig. 3.1. Due to the effect of noise pollution of high voltage laboratory on the PD pulse waveform measurement, the voltage threshold trigger of oscilloscope is employed. The test cells are energized with the 70% of PDIV as the applied voltage



(a)



(b)

Fig. 4.1: PD signal shape, recorded from PD measurement on needle-plane electrode under voltage applied frequency of 500 Hz and atmospheric pressure. (a) Measured signal by oscilloscope (b) Definition of time-domain parameters.

magnitude. Because there is no active PD pulse in the test circuit, the oscilloscope only displays the noise signal under this level of the applied voltage. Next, the trigger level of the oscilloscope is adjusted to a level higher than the amplitude of continuous background noise signals. In this approach, the oscilloscope only records the pulses having a magnitude greater than the noise signal. Afterwards, the applied voltage is set to 20% higher than the PDIV. The PD pulses are observed under this level of the applied voltage. To capture the waveform of the PD pulses, the PD tests are conducted at 20% higher than the PDIV of the test cells. Since the measured PD pulse waveform is polluted by the background noise signals, a wavelet filter was applied to the signal to get rid of the background noise signals as described in [70]. In this way, a cleaner PD pulse signal is present for further investigation. The noisy PD pulse waveform and de-noised signal recorded by the oscilloscope, are shown in Fig. 4.1a. The PD measurement is conducted on needle-plane electrode (corona discharge defect) under the applied voltage frequency of 500 Hz and air pressure level of 101 kPa.

For performing an investigation into the detailed characteristics of the PD pulse waveform, it is necessary to generate an adequate PD data. For this reason, more than 100 PD pulse waveforms are recorded at each frequency and air pressure level.

To visualize the separation of concurrent PD sources, a three dimensional space (3D) is selected in which three features of the PD pulses constitute the coordinates system. In this way, the position of all PD pulses in 3D space is determined according to the values of these three features. In addition, the probabilistic analysis of the PD data is done to provide diagnostic tools for insulation assessment. It is common to use Normal and Weibull functions for fitting distribution to a set of PD data in the presence of one PD source. However, when the first PD phenomenon is overlaid with other different types of PD sources, the probabilistic analysis may be ineffective. After the probability distributions of the PD pulse features have been plotted, the values of statistical parameters of probability

distributions are known for further comparison.

4.2 Probabilistic Analysis

After the separation of the PD sources, the clusters associated with each PD source are investigated using Normal and Weibull probability density functions. The distribution of each time-domain feature related to each cluster, is fitted by both of these probability function to generate informative fingerprints. Normal distribution is described completely by two parameters of mean (μ) and standard deviation (σ) and the Weibull probability function is defined in terms of two parameters of scale (α) and shape (β), which are obtained using maximum likelihood estimation. The probability density function (PDF) of these two commonly used distributions are given by [71]

$$N(x|\mu, \sigma) = \frac{1}{\sqrt{2\sigma^2}} \cdot \exp\left(-\frac{(x - \mu)^2}{2\sigma^2}\right) \quad (4.1)$$

$$W(x|\alpha, \beta) = \frac{\beta}{\alpha} \left(\frac{x}{\alpha}\right)^{\beta-1} \cdot \exp\left(-\left(\frac{x}{\alpha}\right)^\beta\right) \quad (4.2)$$

where x is the measured value.

Skewness (third moment) and kurtosis (fourth moment) are two descriptive statistic moments that provide information about the symmetry and flatness in the PDF histogram of the Normal distribution, respectively. For a Normal distribution, the skewness and kurtosis are normalized and given by [71]

$$S = \frac{\sum_1^N (x_i - \mu)^3}{N \cdot \sigma^3} \quad (4.3)$$

$$K = \frac{\sum_1^N (x_i - \mu)^4}{N \cdot \sigma^4} \quad (4.4)$$

where x_i is the value of each data point, N is the total number of data points, μ is the mean

of the distribution and σ is the standard deviation of the distribution. A positive skewness indicates that a distribution is skewed at the right of the mean value whereas a negative value of skewness shows that the bulk of the distribution is at the left side of the arithmetic mean. A positive kurtosis means that the distribution curve of the data points has a sharper and higher maximum than the curve of normal distribution. By contrast, the distribution of data points with negative kurtosis represents a flatter peak in comparison with the normal curve. In order to generate features associated with each PD source, statistical moments (S, K, α, β) related to the distributions of the PD pulse waveform parameters are taken into account. In this way, there are sixteen statistical moments that can be used for the classification and evaluation of unknown PD source.

4.3 Support Vector Machine

Several classification algorithms such as probabilistic network machine [72], support vector machine [73, 74] and fuzzy logic algorithm [75] have been put forward in the literature to classify the concurrent PD sources. Although choosing informative, discriminating and non-redundant features as the basis of the classification, is a key step to have an effective algorithm and high classification success rate, however, support vector machine (SVM) has shown a very powerful and high accuracy performance in the classification of multiple PD sources among all algorithms employed. The objective of the SVM algorithm is to find optimum hyperplanes which can accurately classify the training data points. In other words, the SVM (supervised learning) outputs hyperplanes that maximize the margin for a given set of training data. The data points that are placed within the margin are considered as the cost of misclassification. Based on the complexity of feature values, linear and nonlinear classifiers can be employed to separate a number of classes. Inaccurate and indeterminate classification may be obtained using a linear classifier when the classes are nonlinearly separable. In this thesis, a nonlinear version of SVM is employed for classifying different

classes known as Kernel-SVM algorithm. A set of Kernel functions are used to transform the features space into infinite dimensional features space in this algorithm. Since the kernels functions are non-linear transformation, no assumption and beforehand human assessment is required to determine whether data is linearly separable or not. Therefore, using the SVM algorithm provides a good generalization for implementing in practical condition. SVM algorithm outputs unique solution in the optimization problem while other algorithms such as neural networks may have multiple solution in solving the problem and for this reason are not robust.

The KSVM classification algorithm for the discrimination of multiple concurrent PD sources is developed based on the time-domain fingerprints. These fingerprints are calculated from the statistical moments of the PD pulse parameters.

4.4 The Algorithm of Concurrent Multiple PD Source Classification

To separate and classify the multiple PD sources concurring at different levels of air pressure and applied frequencies, an algorithm is proposed and presented in this section. Once the PD source fingerprints are calculated from the probabilistic analysis on the separated data points (clusters), fingerprints data sets are fed into the KSVM algorithm for the classification. To evaluate the performance of the SVM algorithm, the classification error rate is calculated. The proposed algorithm is organized into two steps; training and testing. In order to validate the proposed algorithm, leave-one-out technique has been used due to its low computational burden and efficient functioning [76]. In this method, N multi-source test samples, containing samples from each of the classes, are used. From the captured test samples, m samples are left out for testing and $N - m$ samples are used for forming the training part of the algorithm. Then, the test samples are fed through the trained classifier

and the misclassification error is calculated. This validation process is then repeated N times, where each of the multi-source test samples is used exactly once for testing. In this way, all the measured samples are used for training and exactly once for testing. As explained in Section 3.1, two test cells with different electrode configurations have been selected for measuring the PD data that creates two concurrent PD sources. In order to carry out a comprehensive performance evaluation of the SVM classifier, the 500 successive PD pulses are captured from the experimental setup shown in Fig. 3.1. The applied voltage is increased to 20% higher than the maximum PD inception voltage of the two test cell combination. This multi-source data set is divided equivalently into 20 subsets ($N=20$). Based on the leave-one-out method, 19 subsets (475 data points) are used for training and 1 subset (25 data points) assigned for testing. This procedure is repeated 20 times, in which the data points were separated into three classes, corona discharges, twisted-pair wires and noises. In the KSMV algorithm, the generated statistical fingerprints of test subsets are compared to the trained model for classification. When a wrong estimation is made, it is counted as an error. Finally, the efficiency of the developed algorithm is examined by reporting classification accuracy (CA) which is calculated by means of the confusion matrix (CM) to visualize the algorithm performance. This matrix shows the number of correct predictions for each of the classes (class i) with diagonal elements ($CM(i, i)$) while the other elements ($CM(i, j), i \neq j$) represent mislabeled classes. Each row of confusion matrix indicates an expected class whereas each column represents a predicted class [76]. The classification accuracy (CA) and error rate (ER) for the confusion matrix are given by [76]

$$CA = \frac{1}{C \times N} \sum_{i=1}^C CM(i, i) \quad (4.5)$$

$$ER = 1 - CA \quad (4.6)$$

where N is the repetition number ($N=20$) and C is the number of classes ($C=3$).

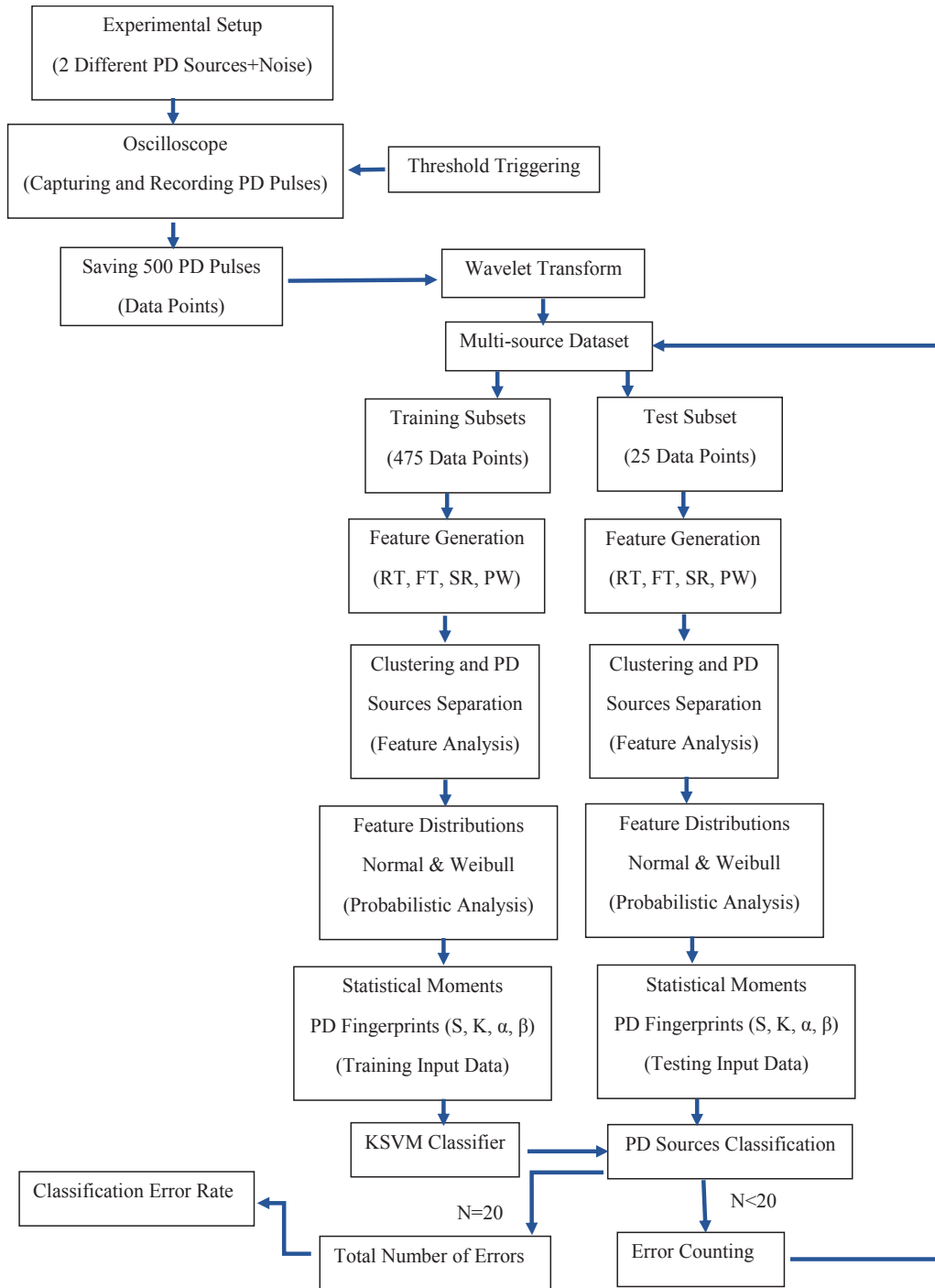


Fig. 4.2: Flowchart of the proposed algorithm.

Table 4.1: PD pulse rise time occurred at positive and negative half voltage cycles for needle-plane electrode (corona discharge).

Rise-Time [ns]						
	P=101 kPa		P=67 kPa		P=33 kPa	
f [Hz]	Pos. half-cycle	Neg. half-cycle	Pos. half-cycle	Neg. half-cycle	Pos. half-cycle	Neg. half-cycle
10	62.6	19.9	85.0	20.4	70.4	65.1
50	52.4	20.1	54.2	20.5	67.2	53.5
250	49.8	19.8	63.0	48.9	68.0	51.4
500	35.3	23.1	61.3	52.3	64.4	52.5
750	24.0	24.7	-	54.1	-	53.1
1000	-	25.2	-	37.4	-	51.0
1250	-	25.4	-	35.7	-	53.2
1500	-	24.7	-	34.0	-	54.4
1750	-	24.7	-	32.3	-	52.9
2000	-	22.8	-	36.3	-	53.3

4.5 Results and Discussions

4.5.1 Detailed Characteristics of PD Pulse Waveforms

The rise time of the measured PD pulses occurred at positive and negative half cycles are shown in Tables 4.1 and 4.2 for both of the corona discharge and twisted-pair of magnet wires. It was observed that both the frequency and air pressure have a considerable influence on the rise time of the PD pulses produced by the PD sources. The frequency has less effect on the PD rise time compared to the air pressure. The rationale for this observation is that the PD pulse requires the total time duration of several microseconds to be completed. If a frequency (in the range of kHz) is applied to the test cells, the time-domain parameters of the PD pulse waveform will not be affected and a higher frequency (in the range of MHz) is needed. As shown in Tables 4.1 and 4.2, the rise time of PD pulses increases with decreasing the air pressure for both of the PD pulses generated by needle-plane and twisted-pair wires. Under a pressure level of 33 kPa and a frequency of 750 Hz and higher, the PD pulse does not appear at positive half cycle of the AC applied voltage, but PD pulses appear at the

Table 4.2: PD pulse rise time occurred at positive and negative half cycles of AC applied voltage for twisted-pair of magnet wires.

Rise-Time [ns]						
	P=101 kPa		P=67 kPa		P=33 kPa	
f [Hz]	Pos. half-cycle	Neg. half-cycle	Pos. half-cycle	Neg. half-cycle	Pos. half-cycle	Neg. half-cycle
10	20.8	17.6	22.1	19.5	30.4	33.2
50	20.8	18.0	23.0	19.6	30.4	31.8
250	20.6	16.9	23.2	19.1	35.3	33.3
500	20.8	16.9	23.8	19.2	33.0	30.3
750	20.9	17.3	24.0	19.0	32.7	27.5
1000	21.1	17.3	23.9	19.2	32.6	26.4
1500	21.5	17.3	24.5	18.7	31.5	25.1
2000	21.5	17.1	24.3	19.2	30.3	25.2
2500	20.9	17.5	24.2	19.2	31.2	24.9
3000	21.2	17.1	24.9	19.0	31.3	26.9

negative half cycle. It can be seen that the PD rise time for the twisted-pair of magnet wires, is varied by the frequency less than the air pressure as shown in Table 4.2.

The pulse width of the recorded waveform of PD pulses for both of the corona discharge and twisted-pair magnet wires are shown in Tables 4.3 and 4.4, respectively. It can be observed that the pulse width of the PD pulses generated by needle-plane electrode is more affected by the frequency under low air pressure level whereas there is no change with frequency in the pulse width of the PD pulses produced by the twisted-pair wires. The frequency has a considerable effect on the values of the PD pulse width at the air pressure level of 33 kPa. Under an air pressure level of 33 kPa, the pulse width increases from 141 to 325 [ns] with decreasing the frequency from 2 kHz to 50 Hz during the negative half-cycle. It is observed that the atmospheric pressure has significant influence on the pulse width of the PD pulses. The value of this time-domain parameter of the PD pulse waveform, decreases with increasing the air pressure level for both of the electrode arrangements. The pulse width decreases from 309 to 89.3 [ns] when the air pressure is raised from 33 to 101

Table 4.3: PD signal pulse width occurred at positive and negative half voltage cycles for corona discharge

Pulse-Width [p.u/s]						
	P=101 kPa		P=67 kPa		P=33 kPa	
f [Hz]	Pos. half-cycle	Neg. half-cycle	Pos. half-cycle	Neg. half-cycle	Pos. half-cycle	Neg. half-cycle
10	133	103	206	183	529	542
50	126	104	207	186	480	325
250	125	106	200	196	502	320
500	93.1	89.3	201	181	501	309
750	90.0	89.0	-	177	-	315
1000	-	93.1	-	150	-	313
1250	-	93.4	-	183	-	264
1500	-	93.2	-	168	-	174
1750	-	92.3	-	152	-	168
2000	-	93.4	-	143	-	141

kPa at a frequency of 500 Hz.

As defined in the Section 4.1, the value of slew rate depends on the magnitude and rise time of the PD pulse. Hence, the voltage magnitude, air pressure, and frequency change the amplitude of the PD pulse. In the investigation of the detailed characteristics of the PD pulse waveform, all the PD tests were conducted at the voltage magnitude of 20% higher than the PDIV for each air pressure and frequency. In this approach, the same ratio of applied voltage to PDIV was utilized for the energizing the test cells. The slew rate of the recorded PD pulses generated by the corona in air and twisted-pair wires are presented in Tables 4.5 and 4.6, respectively. It can be seen that the value of slew rate does not vary with frequency for PD pulses produced by the twisted-pair wires whereas the frequency has a great impact on the slew rate of corona PD pulses. As shown in Table 4.5, it can be observed that increasing the frequency reduces the value of slew rate under the air pressure level of 67 kPa for both of the positive and negative corona in air. The value of the slew rate increases as the air pressure raises and this tendency is noticed for all the measured

Table 4.4: PD signal pulse width occurred at positive and negative half voltage cycles for twisted-pair of magnet wires

f [Hz]	Pulse-Width [ns]					
	P=101 kPa		P=67 kPa		P=33 kPa	
	Pos. half-cycle	Neg. half-cycle	Pos. half-cycle	Neg. half-cycle	Pos. half-cycle	Neg. half-cycle
10	31.8	29.3	36.6	35.6	64	67
50	31.4	31.1	39.2	35.6	69.3	72.2
250	32.3	29.4	38.5	33.8	63.1	59.2
500	32.3	28.6	40.6	34.0	64.4	59.4
750	32.1	28.3	41.4	32.3	64.8	56.4
1000	32.3	28.4	40.1	32.9	65.3	55.8
1500	32.6	28.5	43.3	32.3	66.1	55.1
2000	34.6	28.4	33.3	39.5	66.4	52.1
2500	32.4	29.2	41.5	32.7	65.2	55.4
3000	34.3	29.0	42.4	32.2	67.7	53.8
3500	34.4	28.9	42.8	32.2	65.6	51.3
4000	33.5	28.3	40.5	31.1	66.7	51.7
4500	32.7	28.4	38.3	32.6	64.9	52.3
5000	31.6	27.8	40.6	31.6	65.7	53.6

PD pulses generated by both of the simulated PD sources.

The fall time of the recorded PD pulses generated by both of the PD sources are presented in Tables 4.7 and 4.8 for corona in air and twisted-pair wires. It can be seen that fall time of corona PD pulse is notably affected by the frequency whereas the fall time of PD pulses generated by the twisted-pair wires is slightly varied. According to Table 4.7, it is observed that the value of fall time increases with decreasing the frequency for all the measurements. The fall time increases from 181 to 329 [ns] as the frequency is reduced from 2 kHz to 50 Hz under the air pressure level of 67 kPa. Under the frequency of 500 Hz and negative half-cycle, the fall time increases from 116 to 736 [ns] when the air pressure is dropped from 101 to 33 kPa. The fall time of the PD pulses generated by the twisted-pair wires increases with decreasing the frequency at negative half cycle whereas the frequency has a slight impact on the fall time of PD pulses during positive half cycle.

Table 4.5: PD pulse slew rate occurred at positive and negative half voltage cycles for corona discharge

Slew-Rate [V/ μ s]						
	P= 101 kPa		P= 67 kPa		P= 33 kPa	
f [Hz]	Pos. half-cycle	Neg. half-cycle	Pos. half-cycle	Neg. half-cycle	Pos. half-cycle	Neg. half-cycle
10	1.76	2.85	2.36	3.33	2.46	1.78
50	8.51	4.58	7.32	7.52	6.42	1.4
250	3.49	1.91	4.1	3.13	5.49	0.81
500	0.45	0.49	0.64	0.43	5.58	0.58
750	0.44	0.46	-	0.38	-	0.43
1000	-	0.42	-	0.35	-	0.32
1250	-	0.40	-	0.39	-	0.17
1500	-	0.41	-	0.25	-	0.20
1750	-	0.41	-	0.25	-	0.21
2000	-	0.42	-	0.19	-	0.22

Table 4.6: PD pulse slew rate occurred at positive and negative half voltage cycles for twisted-pair of magnet wires

Slew-Rate [V/ μ s]						
	P= 101 kPa		P= 67 kPa		P= 33 kPa	
f [Hz]	Pos. half-cycle	Neg. half-cycle	Pos. half-cycle	Neg. half-cycle	Pos. half-cycle	Neg. half-cycle
10	19.1	21.2	17.6	20.6	14.4	16.2
50	24.2	23.4	22.4	24.2	18.1	18.1
250	19.2	17.2	17.7	18.9	9.1	10.3
500	17.4	15.0	14.7	17.3	10.8	9.58
750	16.3	16.4	13.1	15.9	10.6	12.9
1000	16.5	16.5	13.6	15.8	10.2	12.4
1500	17.3	16.2	12.2	15.7	10.3	13.2
2000	15.4	15.8	12.7	15.3	11.2	12.5
2500	15.3	14.9	12.3	15.4	9.98	12.8
3000	15.9	15.3	11.9	15.3	9.9	13.0
3500	14.8	15.8	12.2	15.3	10.1	11.9
4000	14.5	14.8	12.5	15.2	10.6	12.2
4500	13.5	15.6	12.9	15.2	10.1	12.3
5000	13.4	15.4	12.6	15.6	10.2	12.4

Table 4.7: PD pulse fall time occurred at positive and negative half voltage cycles for corona discharge

Fall-Time [ns]						
	P=101 kPa		P=67 kPa		P=33 kPa	
f [Hz]	Pos. half-cycle	Neg. half-cycle	Pos. half-cycle	Neg. half-cycle	Pos. half-cycle	Neg. half-cycle
10	187	184	354	307	820	773
50	190	204	372	329	883	621
250	193	192	363	360	850	603
500	159	116	368	349	857	736
750	150	116	-	233	853	582
1000	-	117	-	253	-	472
1250	-	114	-	241	-	308
1500	-	114	-	252	-	300
1750	-	109	-	207	-	270
2000	-	112	-	181	-	230

Table 4.8: PD pulse fall time occurred at positive and negative half voltage cycles for twisted-pair of magnet wires

Fall-Time [ns]						
	P=101 kPa		P=67 kPa		P=33 kPa	
f [Hz]	Pos. half-cycle	Neg. half-cycle	Pos. half-cycle	Neg. half-cycle	Pos. half-cycle	Neg. half-cycle
10	70.5	60.9	84.6	69.1	116.3	93.7
50	68.8	63.8	87.0	70.1	118.1	101.2
250	71.7	58.1	82.6	68.3	114.6	88.4
500	69.4	52.2	85.9	64.9	108.7	84.4
750	72.0	49.7	89.3	64.4	108.5	84.9
1000	72.2	52.0	86.4	65.7	107.7	83.6
1500	72.4	53.2	87.4	68.8	106.4	79.8
2000	78.0	50.1	86.3	64.6	108.4	81.8
2500	69.0	55.7	87.8	65.8	106.3	80.8
3000	71.5	48.6	89.6	66.1	103.7	80.7
3500	69.4	48.9	88.3	65.8	106.5	78.8
4000	71.2	46.4	85.5	65.5	105.4	77.7
4500	69.3	42.5	84.3	65.5	105.2	78.4
5000	69.3	40.8	82.1	62.8	101.5	74.2

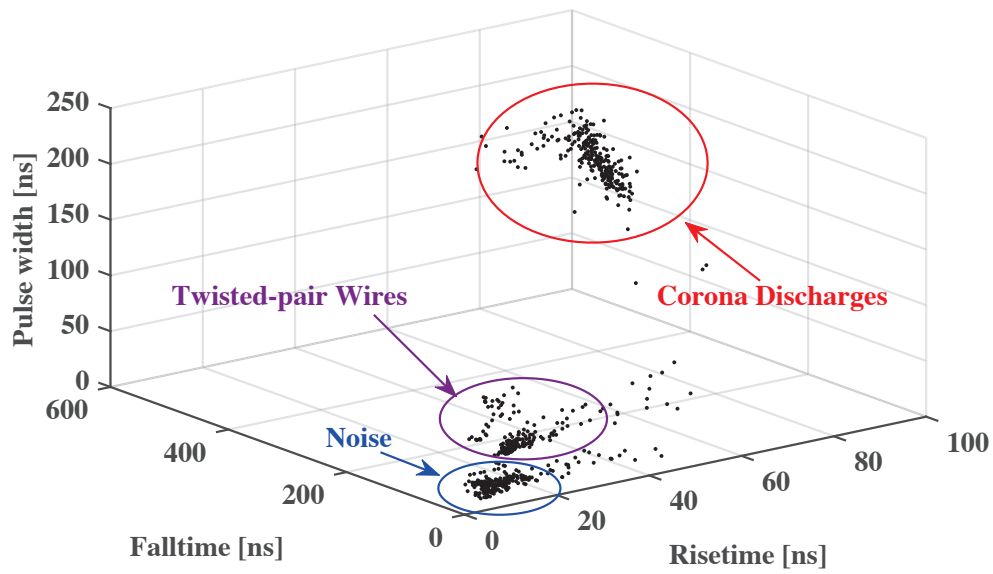
To explain the influence of air pressure on PD pulse waveform characteristics, let's assume that a positive voltage polarity is applied to a needle tip. If the magnitude of the applied voltage exceeds the PDIV value, electron avalanches start to develop in the direction of the needle electrode. The density of charged particles such as negative ions, positive ions, and negative electrons is small at the beginning of the PD pulse. A typical corona PD pulse waveform is shown in Fig. 4.1. In the time duration of rise time (RT), the densities of these charged particles rapidly grow due to the electron avalanches in the air gap. Therefore, the magnitude of corona pulse quickly increases to the maximum point. Because of lower drift velocity of ions compared to the electrons, the corona pulse during rise time is dominantly governed by the role of electrons in the ionization region. With increasing the air pressure, more free electrons can be produced via ionization due to the higher number of gas particles. This results in the decrease of PD pulse rise time at higher levels of air pressure. During the fall time interval, the magnitude of corona pulse starts to decrease due to the reduction in the density of electrons. These electrons will be absorbed rapidly by the needle tip and leave behind positive ions. The positive ions surrounding the needle tip curvature create an internal electric field that weakens the local electric field nearby the tip of electrode (ionization region) which causes the formation of the electron avalanches to stop. However, the internal electric field generated between positive ions and plane electrode enhances the external electric field and has higher value as the number of positive ions increase (higher air pressure). Since all the PD measurements have been performed at 120% of PDIV, it is reasonable to assume that the external or applied electric field is constant for all measurements. Therefore, the positive ions during fall time drift with higher velocity at higher pressures [39]. The increase in the risetime and the reduction in the magnitude of the PD pulse cause slew rate to have smaller values at lower pressures. Since the fall time and rise time increase under low air pressure, more time is required for pulse to be completed (pulsewidth).

4.5.2 Separation and Classification of Multiple Concurrent PD Sources

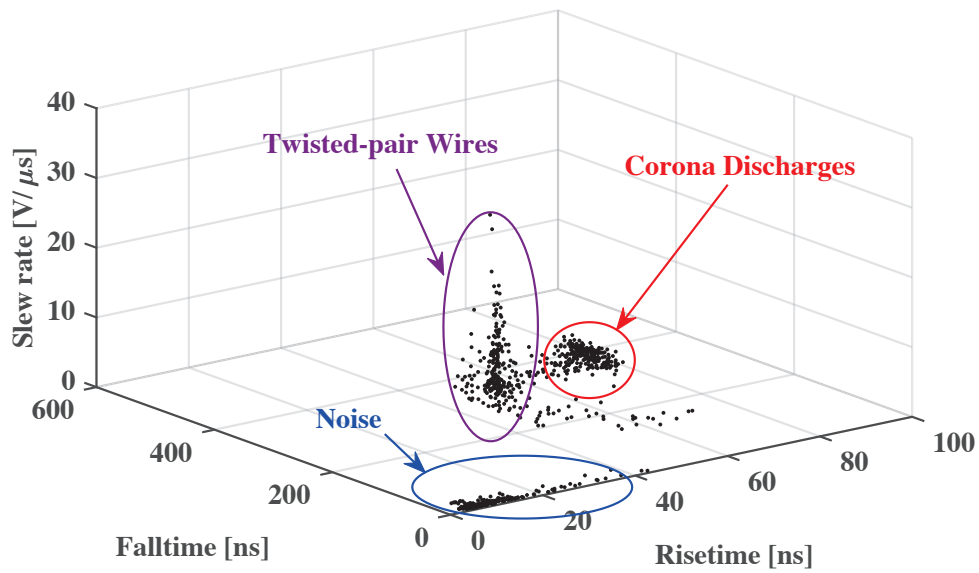
In order to generate the multi-source PD data, the parallel combination of the test cells is energized by AC voltage waveform. The twisted-pair wires have a lower PDIV compared to the needle-plane electrode. The applied voltage is increased to 120% of the maximum PDIV of parallel combination of the test cells. Under this level of applied voltage, the measured PD signal comprises of PD pulses related to both of the test cells and switching noises. The time duration of recorded PD signal is set for each level of air pressure and applied frequency to capture more than 500 successive PD pulse waveforms. As mentioned in the previous chapter, implementing the PRPD pattern for PD source identification may give inaccurate information about the source of the PD signal. In this section, the results of the proposed algorithm for the classification of multiple PD sources are discussed.

It was observed that the rise and fall time of PD pulses generated by the twisted-pair wires are smaller than the corona discharge created by the needle-plane electrode, thus the corona PD pulses in air are slower than PD pulses caused by the twisted-pair wires. The pulse width of PD pulses created by the twisted-pair wires is lower in comparison to the corona pulses in air where its slew rate is higher. Because of the impact of air pressure and applied frequency on the time-domain parameters of the PD pulse waveform, the distribution of the PD pulse parameters may overlaid with each other. Therefore, it would be useful to consider all the calculated features to perfectly discriminate the clusters related to the PD sources.

Fig. 4.3 shows the separation map of two active PD defects and noise source based on PD pulse waveform analysis. The voltage frequency and air pressure level are 500 Hz and 67 kPa, respectively for PD measurement. Each data point (PD pulse) is mapped into a point in the 3D space. The data points that have similar PD pulse parameters (same nature) form a cluster. The cluster placed in the upper part of Fig. 4.3a is associated with PD pulses generated by the needle-plane electrode (corona discharges) because its pulse width is much



(a)



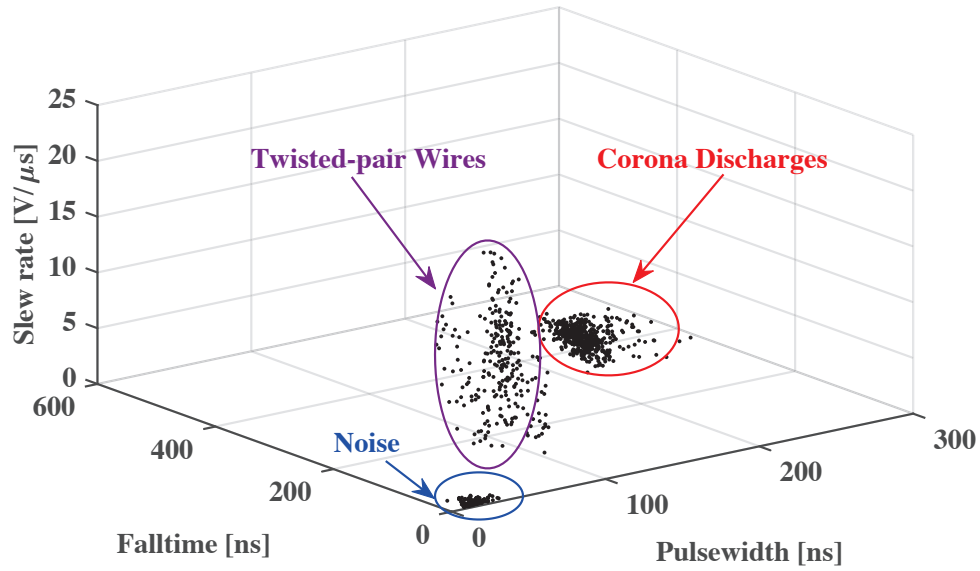
(b)

Fig. 4.3: The separation map of PD sources under the applied frequency of 500 Hz and sub-atmospheric pressure of 67 kPa. (a) (RT, FT, PW) (b) (RT, FT, SR)

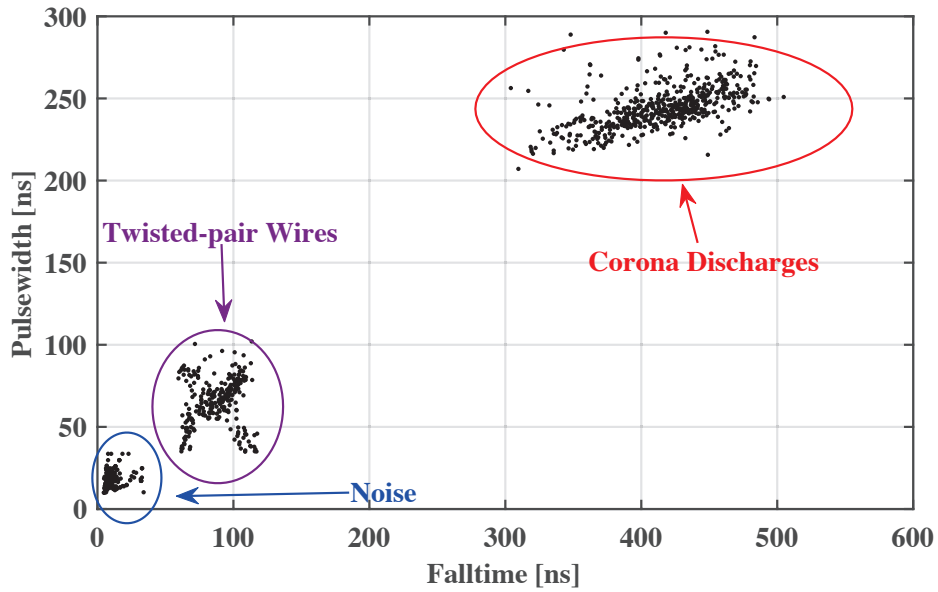
bigger in comparison to other clusters of the data points. It can be seen that the pulse width parameter is an effective feature for the separation of these two PD sources. However, it is observed that the two cluster located in the lower part of the map overlap because their rise time and pulsewidth parameters are close to each other. To discriminate between these two clusters the slew rate is selected for the map space instead of pulse width as shown in Fig. 4.3b. It is clear that the cluster related to PD pulses caused by the twisted-pair wires, is separated from the other cluster completely but is overlapped with the corona cluster. It can be seen that the data points inside noise cluster are squeezed together in the smallest cluster.

The separation of concurrent activated PD sources is shown in Fig. 4.4. The PD measurement is conducted under an air pressure of 33 kPa and a frequency of 1000 Hz. slew rate, fall time, and pulse width are selected as the separation features. There are three separated clouds of data points related to the PD sources. The dense cluster located on the right side of the separation map, is related to the PD pulses caused by corona in air. This PD sources is separated perfectly from the other clusters because of higher value of fall time and pulse width. The cluster associated to the twisted-pair wires is the biggest cluster due to the high dispersion in the value of its slew rate feature. To better illustrate the discrimination of these three clusters, 2D map space considering pulse width and fall time as separation features, is shown in Fig. 4.4b. It demonstrates that the feature values of pulses generated by switching noises vary in a very small range in comparison to the other cluster and the noise points get lumped into high density cluster.

It is clearly shown in Fig. 4.3 and 4.4 that the separation of simultaneous PD sources can be effectively done by the time-domain features of PD pulses. This approach leads to organize the PD data into discriminated classes, which is called unsupervised learning approach. In order to find a class label for large amount of PD data points, clustering criterion is an essential part of the separation task. In this thesis, the clustering structure



(a)



(b)

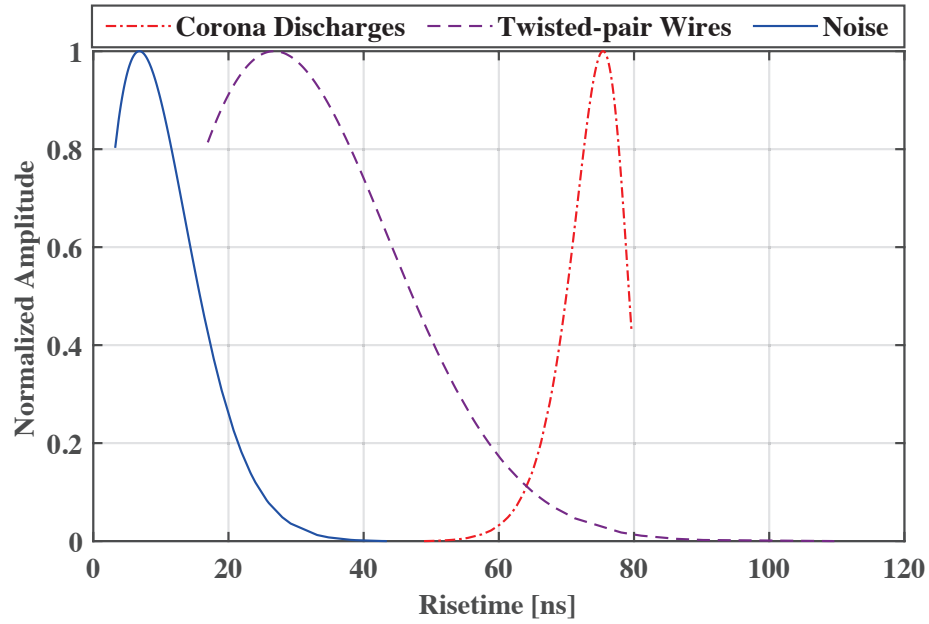
Fig. 4.4: The separation map of PD sources under the applied frequency of 1000 Hz and sub-atmospheric pressure of 33 kPa. (a) (PW, FT, SR) (b) (FT,PW)

is based on the distribution of PD pulse parameters, which is presented in Section 4.5.1. To generate fingerprints for the classification of the PD sources, Normal and Weibull functions are fitted on the parameter distributions of PD pulses. The probabilistic analysis for PD identification of mixed PD data is presented in the following.

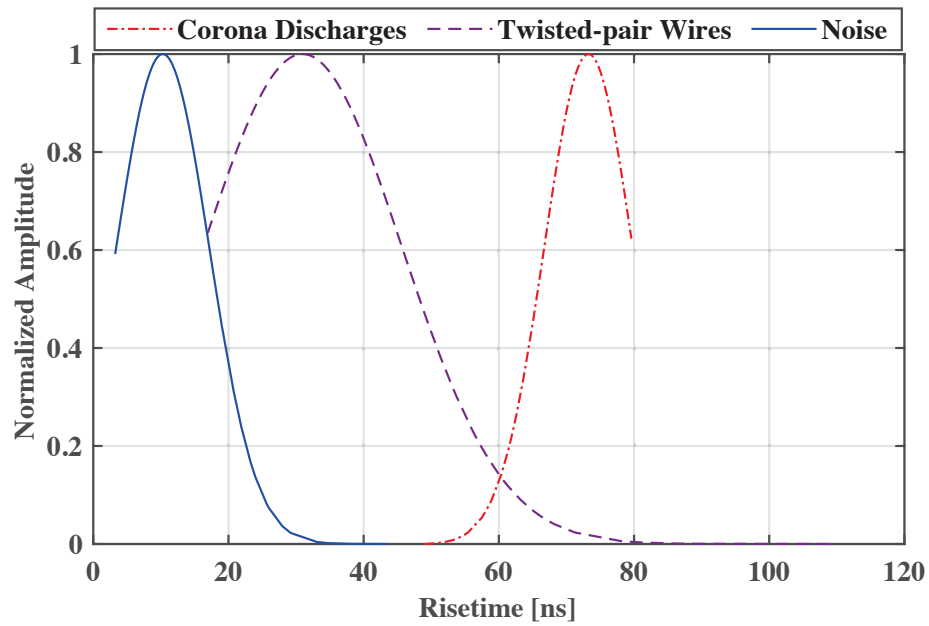
Fig. 4.6 shows the probability density function (PDF) of rise time for both of the Weibull and Normal functions. It indicates that the rise time of PD pulses generated by the corona discharges are higher than the PD pulses occur between the turns of the twisted-pair magnet wires. The separation of pulses caused by corona discharge and switching noises can only be performed by considering the rise time as the discrimination feature. However, a significant overlap exist between the PDF of all pulse sources in both of the fitted functions. Therefore, it is not accurate to conduct PD identification in the presence of concurrent PD sources specially under sub-atmospheric pressures. It is evident that the separation of pulse sources based on the rise time results in incorrect PD source identification as depicted in Figs. 4.6a and 4.6b. As such, other pulse parameters must be considered in the PD identification procedure to facilitate the discrimination of PD sources.

Figs. 4.7 and 4.8 indicate the PDF of slew rate distribution for different pulse sources. It can be seen that the slew rate of twisted-pair wires varies in a wide range and is completely separated from other sources due to the higher values. The comparison between the slew rate of corona discharge and switching noise, shows that these pulse sources have small values of slew rate and are close to each other. PD identification of twisted-pair and corona discharges can be carried out based on slew rate feature while it is impractical for switching noises and corona discharges.

Therefore, multiple PD source identification based on one feature leads to incorrect results due to the overlapping between the distribution of features. Hence, an effective approach is to perform the discrimination of simultaneous PD sources based on different pulse parameters. For instance, the feature of rise time can be employed to separate corona

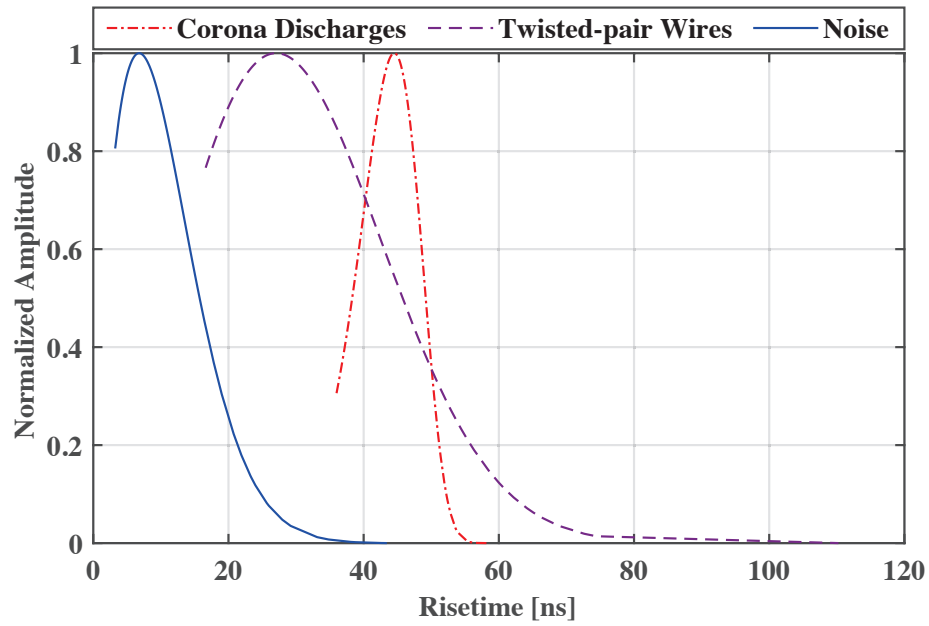


(a)

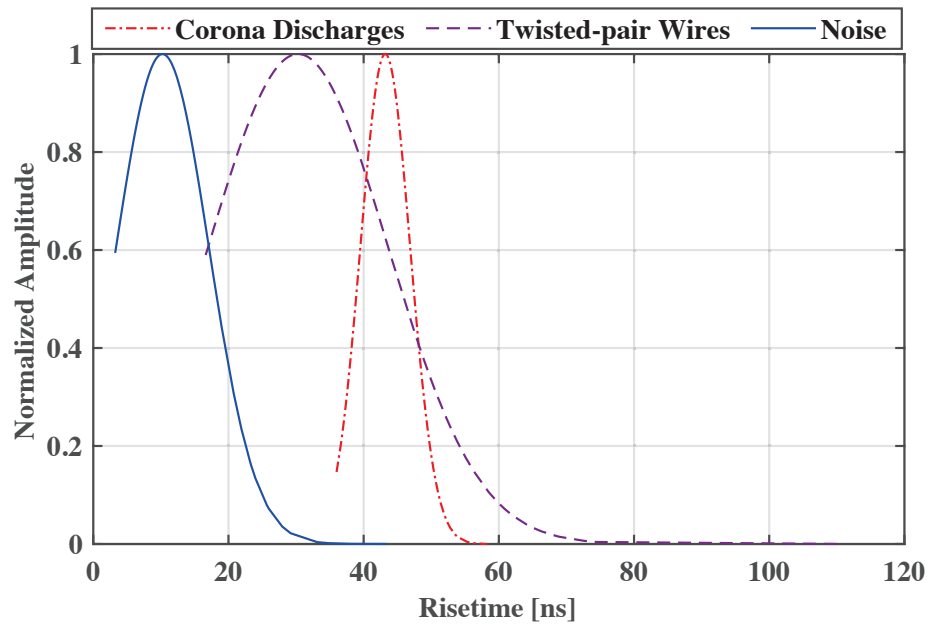


(b)

Fig. 4.5: Weibull and Normal distribution of rise time for applied frequency of 500 Hz and air pressure level of 67 kPa. (a) Weibull distribution. (b) Normal distribution.

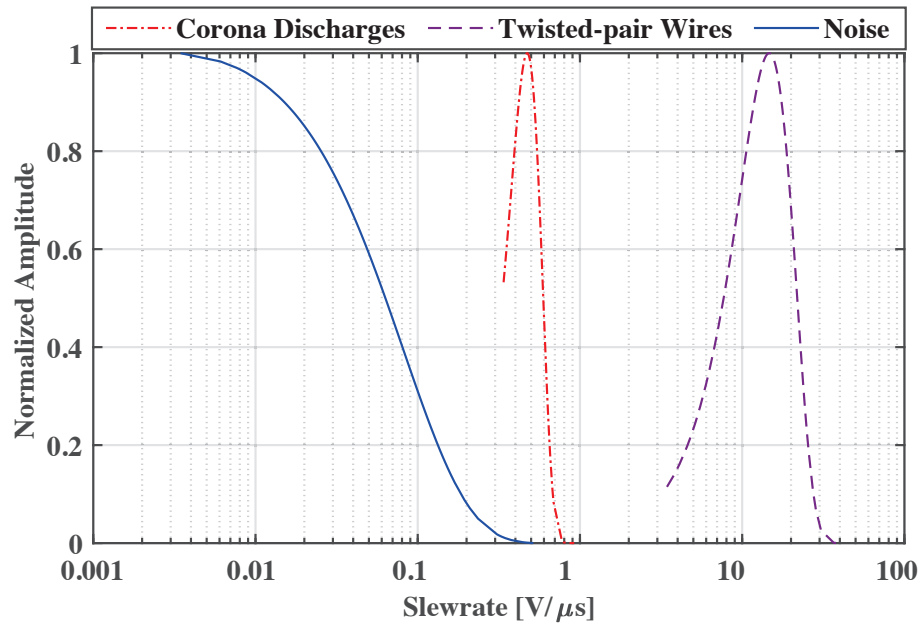


(a)

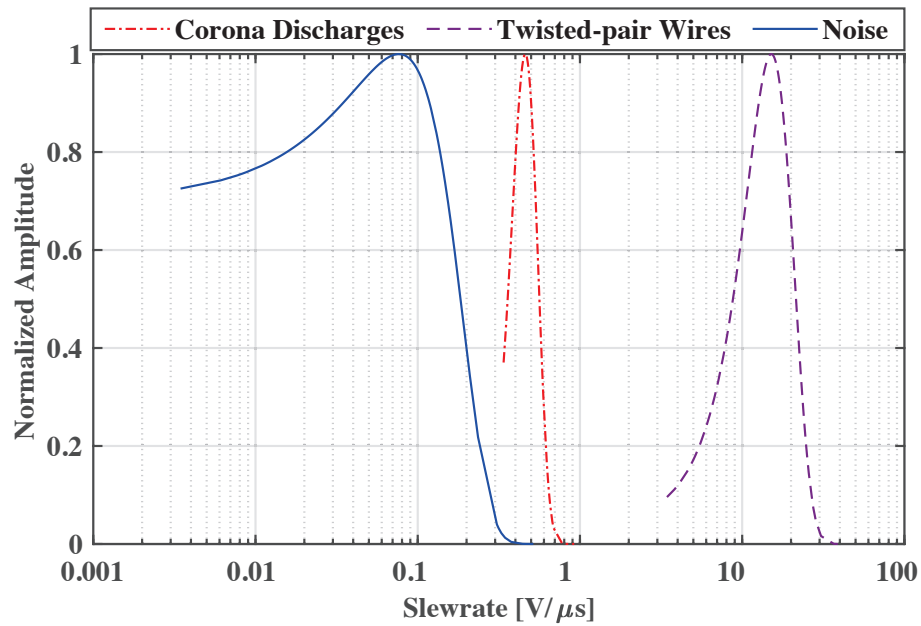


(b)

Fig. 4.6: Weibull and Normal distribution of rise time for applied frequency of 1000 Hz and air pressure level of 33 kPa. (a) Weibull distribution (b) Normal distribution

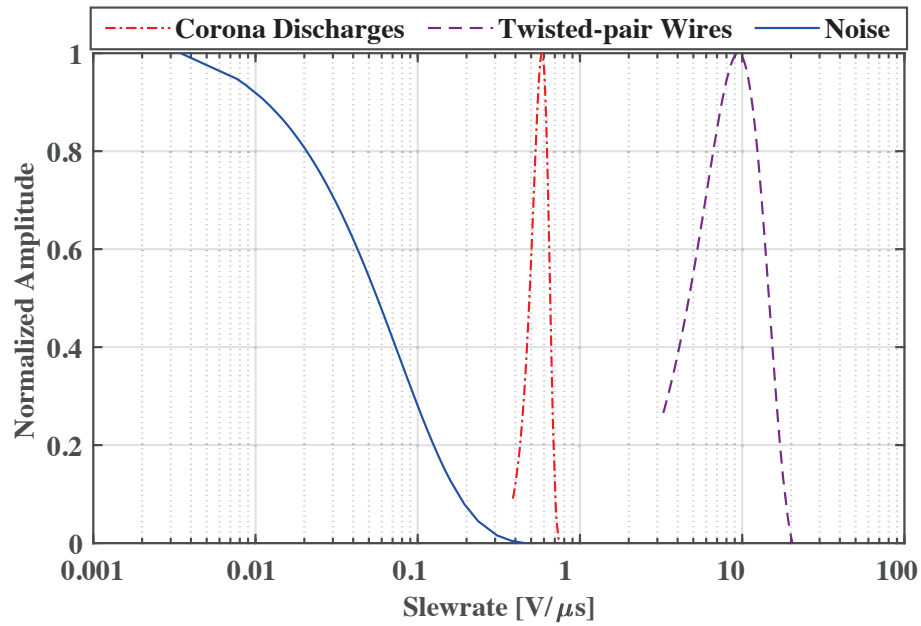


(a)

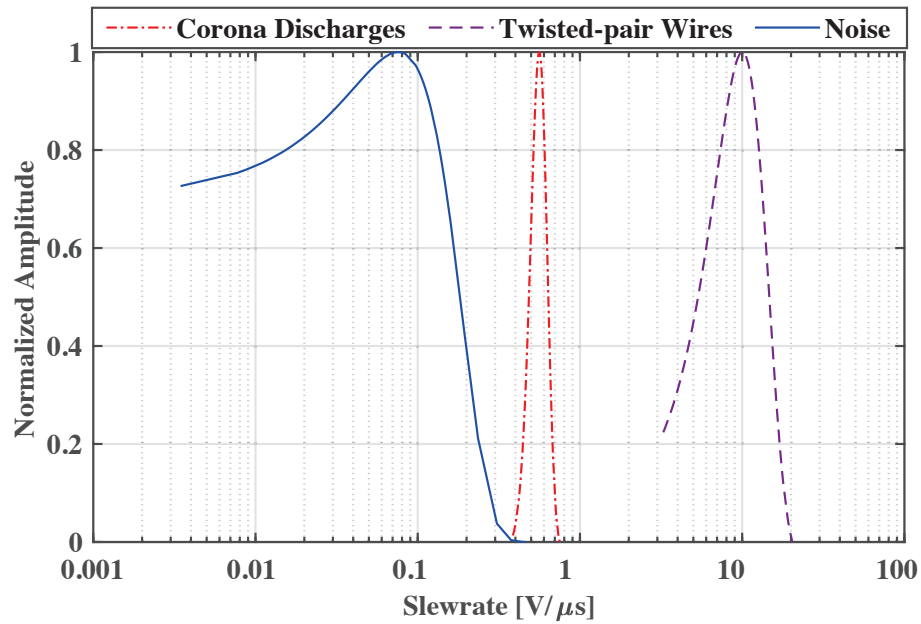


(b)

Fig. 4.7: Weibull and Normal distribution of slew rate for applied frequency of 500 Hz and under air pressure level of 67 kPa. (a) Weibull distribution. (b) Normal distribution.



(a)



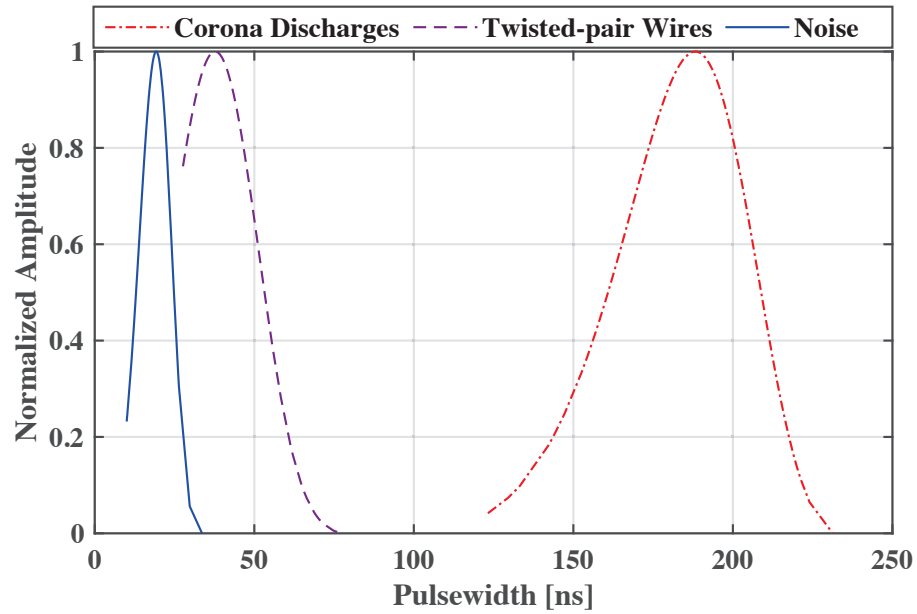
(b)

Fig. 4.8: Weibull and Normal distribution of slew rate for applied frequency of 1000 Hz and under air pressure level of 33 kPa. (a) Weibull distribution. (b) Normal distribution.

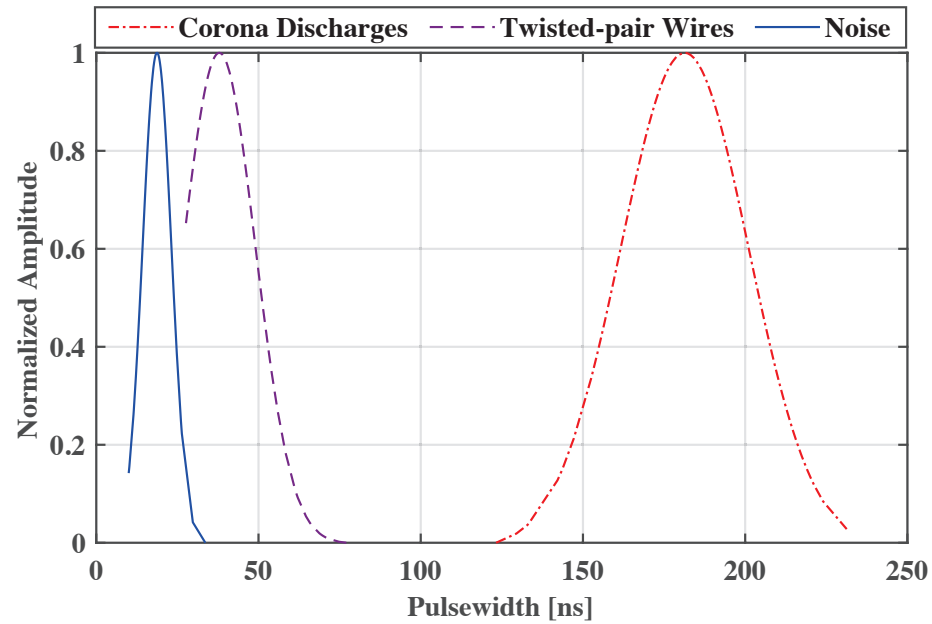
discharge from switching noise, however it is not effective to discriminate twisted pair from corona discharge. For the identification of twisted-pair from other sources, slew rate can be used. The same explanation for pulse width and fall time can be presented as shown from Fig. 4.9 to Fig. 4.12. To develop a powerful approach for the separation of pulse sources, different pulse parameters such as rise time, slew rate, fall time and pulse width are taken into account as the discriminating features.

As mentioned before, to produce a dataset from the distributions of PD pulse parameters, a probabilistic analysis is performed. For this purpose, the skewness and kurtosis parameters of the Normal distribution of time-domain pulses are calculated under each pre-determined frequency and air pressure. In addition, the scale (α) and shape (β) of Weibull distribution are obtained via data fitting. Each parameter of the distribution generates four statistical moments as the fingerprints of each PD pulse source. Totally, there are sixteen fingerprints of each pulse source. Due to low dimensionality of the features space associated with single-source PDs, principal component analysis (PCA) is not required to construct a low dimensional space. In fact, this dimensionality-reduction technique is useful when there is a high dimensional feature space [76]. The calculated statistical moments for the two case studies are presented in Table 4.9. The results for case (A) are obtained from performing PD measurements under the applied frequency of 500 Hz at the air pressure level of 67 kPa and the results for case (B) are calculated from conducting PD test under frequency of 1 kHz and sub-atmospheric pressure of 33 kPa. The results of probabilistic analysis can be used to design a classification system of multi-source PD.

To conduct a comprehensive assessment of the proposed algorithm, PD measurements were performed under the applied frequencies of 500 , 1000 and 2000 Hz at air pressure levels of 101, 67 and 33 kPa. First, multi-source dataset is separated based on the feature analysis and projected into the mapped space. The benefit of this separation is that the overlapping level of the PD sources is reduced which results in the improvement of the classification

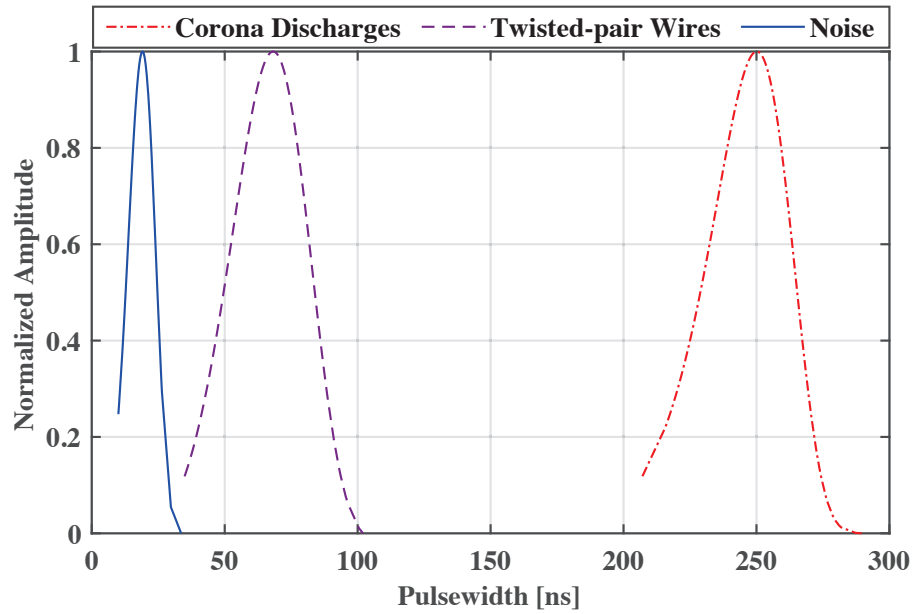


(a)

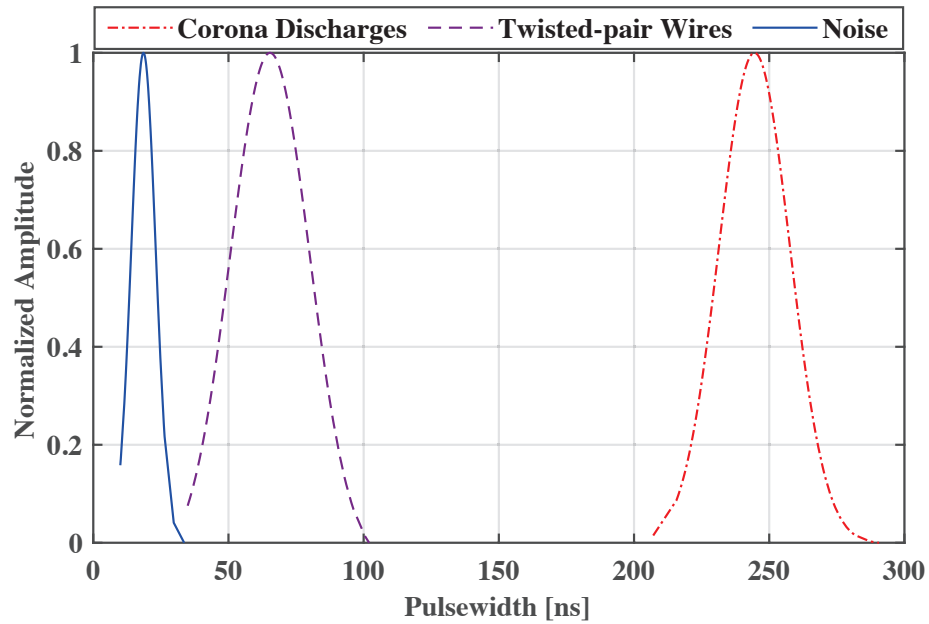


(b)

Fig. 4.9: Weibull and Normal distribution of pulse width for applied frequency of 500 Hz and air pressure level of 67 kPa. (a) Weibull distribution. (b) Normal distribution.

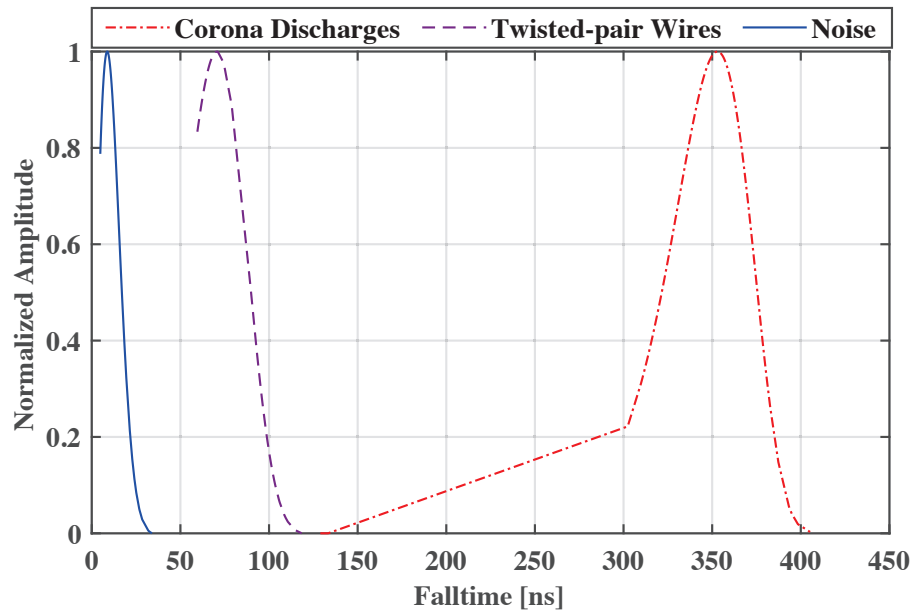


(a)

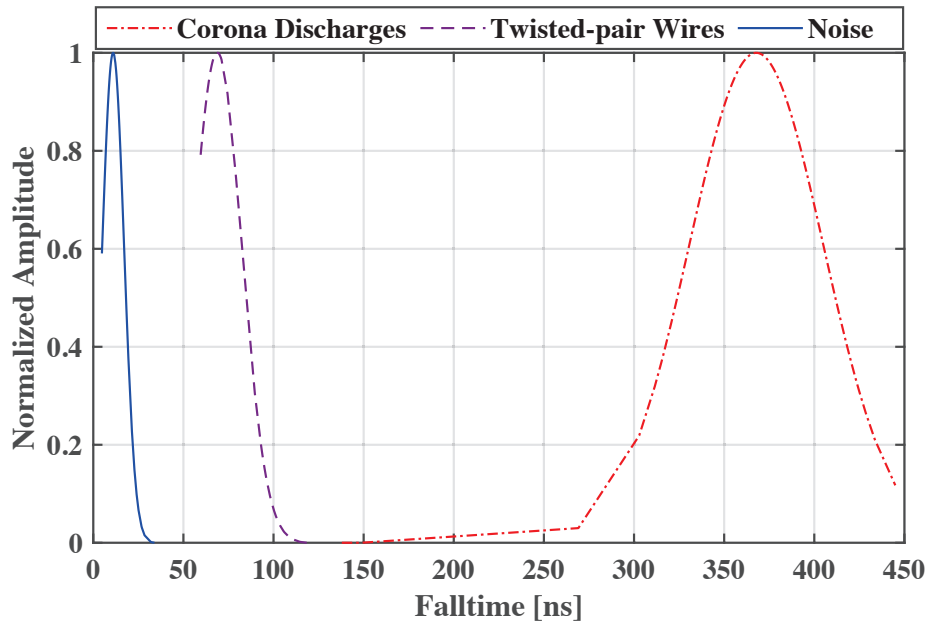


(b)

Fig. 4.10: Weibull and Normal distribution of pulse width for applied frequency of 1000 Hz and air pressure level of 33 kPa. (a) Weibull distribution. (b) Normal distribution.

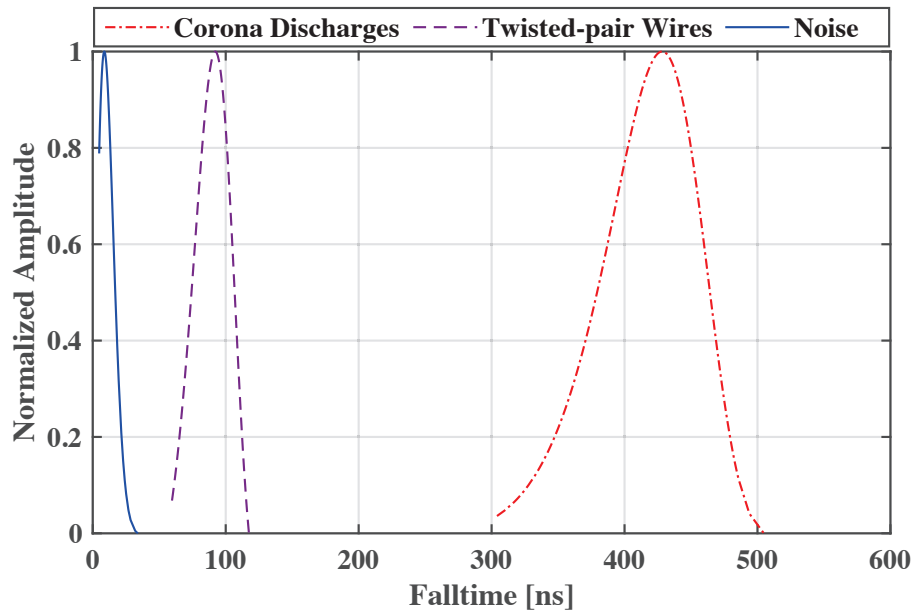


(a)

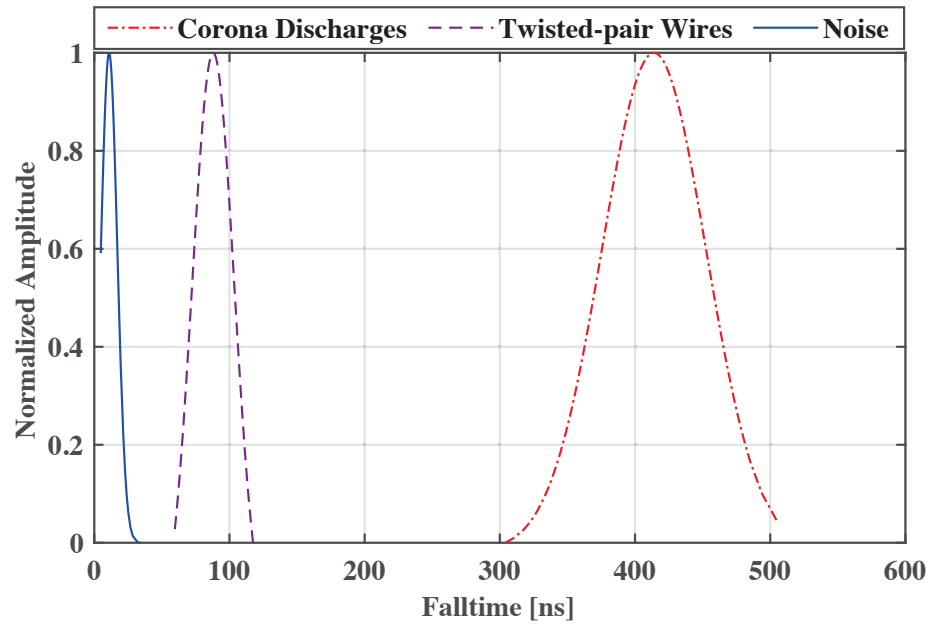


(b)

Fig. 4.11: Weibull and Normal distribution of fall time for applied frequency of 500 Hz and air pressure level of 67 kPa. (a) Weibull distribution. (b) Normal distribution



(a)



(b)

Fig. 4.12: Weibull and Normal distribution of fall time for applied frequency of 1000 Hz and air pressure level of 33 kPa. (a) Weibull distribution. (b) Normal distribution.

Table 4.9: The Statistical Moments of Feature Distribution associated with different sources of pulses

PD pulse sources		Corona in air		Twisted-pair wires		Switching noise	
PD pulse features		A	B	A	B	A	B
Rise time	S	-2.107	0.984	2.018	2.080	2.415	2.450
	K	6.942	4.684	7.774	8.743	9.545	9.751
	α (e-8)	7.559	4.496	3.509	3.428	1.173	1.163
	β	20.101	10.309	2.203	2.351	1.686	1.685
Fall time	S	-4.141	-0.352	-0.024	-0.136	2.343	2.329
	K	31.288	2.626	1.353	1.824	8.241	8.239
	α (e-8)	35.432	43.122	9.312	9.442	1.250	1.249
	β	16.308	12.539	5.434	6.622	1.965	1.972
Slew rate	S	1.532	0.125	1.050	0.281	2.734	2.757
	K	7.447	2.889	5.500	2.547	10.770	10.972
	α (e+7)	0.049	0.059	1.162	1.106	0.007	0.0077
	β	4.742	8.649	2.304	2.711	0.000	1.027
Pulse width	S	0.282	0.579	-0.162	-0.217	0.575	0.576
	K	2.657	3.852	1.834	2.439	4.107	4.022
	α (e-8)	18.343	25.102	6.776	7.114	2.045	2.036
	β	9.698	17.080	4.350	5.149	4.321	4.282

of multiple-source PDs. In this low dimensional map space, the multi-source classes are relatively discriminated. Generally, the probability estimation of multi-source data points is performed with respect to the individual single-source classes. The outcome of this analysis is the generation of PD sources fingerprints. However, the value of these estimated fingerprints will not indicate which one of the single-sources had contribution in constructing the mixed PD sample. This occurs sometimes due to the scattering of multi-sources data points close to the single source which had no role in the forming of those samples. Placing reliance on the estimated fingerprints obtained from the probabilistic analysis may mislabel the class of PD pulse sources instead of the constitutive PD source. However, performing a correct and powerful feature engineering in conjunction with utilizing a high performance classifier such as support vector machine (SVM) can enhance the estimation power of the classification algorithm by generating discriminating features from raw PD signals. This

Table 4.10: The Classification Error Rate for Each of PD Measurements Using the Proposed Algorithm

Air pressure (kPa)	33				67				101			
f (Hz)	Error Rate %	C1	C2	C3	Error Rate %	C1	C2	C3	Error Rate %	C1	C2	C3
500	1.7	19	1	0	0	20	0	0	1.7	20	0	0
		0	20	0		0	20	0		0	19	1
		0	0	20		0	0	20		0	0	20
1000	1.7	19	1	0	0	20	0	0	0	20	0	0
		0	20	0		0	20	0		0	20	0
		0	0	20		0	0	20		0	0	20
2000	11.7	17	2	1	26.7	5	10	5	1.7	20	0	0
		0	20	0		0	20	0		1	19	0
		0	0	20		0	0	20		0	0	20
Overall %	5.02											

Class C1. Corona in air; Class C2. Twisted-pair wires; Class C3. Noises

will help to recognize the constitutive single-sources which contributed to the mixed-sources PD sample. Tackling these points by the developed algorithm demonstrates its importance to have a high rate of classification for the multiple concurrent PD sources.

Table 4.10 shows the classification error rates for a different range of air pressure and frequency. The proposed algorithm shows low error rates under a wide range of frequency and sub-atmospheric pressures. It is observed that the error rate is increased with increasing the frequency under sub-atmospheric pressure of 67 kPa. This can be attributed to the impact of frequency on the time-domain parameters of PD pulse waveform as comprehensively presented in Section 4.1. Further, It can be clearly seen that the classification accuracy rate is lower at high frequency range of 2000 Hz and sub-atmospheric pressures. This outcome demonstrates the complexity of implementing separation and classification of concurrent PD sources at sub-atmospheric pressures, however, the error rates of the

developed algorithm is low enough at low air pressure levels.

4.6 Summary

In this chapter, an algorithm has been proposed for the separation and classification of multi-source PDs which may be present in the electric power system of aircraft. Multi-source PDs generate PRPD patterns which may be partially overlapped. Therefore, it would be extremely hard to identify the source of the PD pulses. To overcome this difficulty, a comprehensive method was proposed based on the statistical moments of the distributions of the time-domain PD pulse parameters. In this thesis, PD pulse waveforms related to PD sources were recorded and analyzed. The parameters that represents the time-domain characteristics of PD pulse waveform are rise time, slew rate, fall time and pulse width. It was assumed that the PD sources having the same nature, create PD pulse waveforms with similar characteristics.

To separate the multi-source PDs, the mixed PD dataset was projected into a mapped space. Each PD pulse, which was associated with a data point, was located in the mapped space depending on its time-domain parameters. The output of this step was the formation of discriminated clusters of data points in the separation map. Afterwards, Normal and Weibull distribution functions were used to fit on the distribution of each cluster to generate features for training and testing parts of the algorithm. The skewness and kurtosis parameters related to the Normal distribution and scale (α) and shape (β) parameters related to the Weibull distribution were calculated to create fingerprints of the each cluster. To classify the multiple PD sources, KSVM was selected as a classifier algorithm.

The variation of PD pulse parameters was investigated from low frequencies ranges to high frequencies and under air pressure levels of 33 kPa, 67 kPa and 101 kPa. It was observed that the rise time, fall time and pulse width of PD pulses increases with reducing the air pressure while the slew rate decreases.

Chapter 5

Conclusions

In this thesis, the development, testing, and evaluation of two methods for the identification of single and multiple concurrent PD sources at different levels of air pressure and applied frequency were proposed. The first method, which was based on the combination of wavelet and differential energy techniques, was able to detect PD pulses under noisy contaminated environment and low air pressure. This PD recognition system contains of two parts; a high order of Symlet wavelet family for removing the background noise from the measured PD signal in order to have a stable PD signal waveform and a differential energy based technique to extract the PD pulses from the PD signal for generating the PRPD pattern. The variation in the obtained PRPD pattern can be used for monitoring the insulation condition in the presence of single and simultaneous multi-source PDs.

The drawback of the PRPD pattern is that this pattern is partially overlapped if more than one PD source exists in the insulation system which results in difficulty for PD source identification. To mitigate this disadvantage, a second algorithm was developed for the separation and classification of multi-source PDs. This algorithm is based on the assumption that there exists a correlation between the nature of PD sources and the their PD pulse waveforms. In algorithm, a probabilistic analysis was conducted on the PD pulse parameters

related to each PD source in order to generate fingerprints for the classification of multiple, simultaneously-activated PD sources. For this purpose, Normal and Weibull distributions of the PD pulse parameters were estimated. Next, kernel support vector machine was adopted as an effective classifier using the statistical moments of the pulse parameters distributions as the feature vectors.

To evaluate the effectiveness of both proposed methods, two artificial laboratory test cells were simulated in small scales to model two different PD sources which may occur in the insulation system of an aircraft. The first test cell contains a needle-plane electrode to model the corona PD in air. The second test cell was designed to simulate PDs which may happen in the windings of electric machines. The air pressure of the test cells was adjustable by using a vacuum motor. The PD measurements were performed on the test cells individually and simultaneously at air pressure levels of 33, 67 and 101 kPa. The applied frequency for PD tests on the individual test cell was varied from 10 to 2000 Hz for the needle-plane electrode and 10 to 5000 Hz for the twisted-pair wires. The highest applied frequency for the simultaneous energized PD test cells was 2000 Hz due to the current limitation of the HV amplifier.

In addition, the effect of frequency and air pressure on the PD inception voltage (PDIV) of the artificial PD sources as well as the detailed characteristics of the PD pulse waveforms were investigated experimentally. It was concluded that the both frequency and air pressure do affect the discharge mechanism. The value of the PDIV decreases with decreasing the air pressure whereas increasing the applied frequency causes a reduction in the PDIV. Therefore, the gap length between the energized conductors and the applied frequency as well as the insulation material in the design of insulation system for HV equipments operating in the electric power system of the aircraft must be carefully selected. It was observed that a drop in the air pressure results in increasing the risetime, falltime and pulse width of the PD pulse waveform whereas the slewrate decreases. Increasing the frequency

of the power source supply has much less effect on the PD pulse parameters and it was observed that PD pulses are generated at both positive and negative half voltage cycles at frequencies less than 1 kHz. This causes faster degradation of the insulation system due to the higher amplitude of the PD pulses at the positive half cycle. For frequencies higher than 1 kHz, the PD pulses were observed during negative half cycle under an applied voltage of 20% higher than PDIV.

5.1 Future Work

In this thesis, a PD detection algorithm was proposed which aims to detect PDs at excessive noisy environment and sub-atmospheric pressures. The proposed method can be implemented for on-line and off-line PD measurements. In addition, an algorithm was developed based on the time-domain features of PD pulse waveforms to separate and classify the concurrent PD sources. The measurement results demonstrate that both of the proposed algorithms are practical to be employed for monitoring the insulation condition in an aircraft power system. The potential research which could be continued to enrich this thesis are presented in the following:

- In this study, PD measurements were performed to conduct an investigation on the effect of air pressure and applied frequency on the PD pulse waveform characteristics at the room temperature. Due to the drop in the temperature with altitude, the effect of temperature could be investigated on the discharge mechanism.
- Since the percentage of air gas constituents changes with the altitude, the PD measurements could be performed on the air gas with the different percentage of the elements. Further, the effect of humidity on the discharge mechanism could be evaluated.
- The PD sources considered in this thesis, were needle-plane electrode and twisted-pair wires. Different PD sources such as PDs between motor winding and stator slot,

impregnated winding motors and various electrode arrangements could be employed to generate PD pulses of different nature.

- Sine voltage waveform were used for PD tests and performing separation and classification. In order to control the amount of power delivered to the actuators in the electric power system of the aircraft, pulse-width modulation (PWM) technique is used [7]. Hence, the impact of this repetitive voltage waveform on the PDIV and PRPD pattern could be evaluated. Under this applied voltage waveform, the polarity inversion of the voltage generates switching noises.
- The proposed PD detection method based on the wavelet and differential energy techniques, could be evaluated by generating PRPD patterns for various PD sources as well different levels of environmental noise.
- In order to generate features for the separation and classification of sources of PD, time-domain parameters of PD pulse parameters were utilized. Further, feature generation could be done by calculating frequency-domain parameters such as dominant frequency of the PD pulse.
- The proposed algorithms could be used in mixed methods. In this procedure, the parameters related to the PRPD patterns of the single source as well as multi-sources PDs could be used as the features space for the separation and classification of the PD sources of different nature.
- Different classifiers such as fuzzy logic, neural networks, and logistic regression could be used for the classification of concurrent PD sources and their reliability and accuracy rates could be compared with the proposed algorithm.

References

- [1] R. Rui and I. Cotton, "Impact of low pressure aerospace environment on machine winding insulation," in *2010 IEEE International Symposium on Electrical Insulation*, June 2010, pp. 1–5.
- [2] K. Emadi and M. Ehsani, "Aircraft power systems: technology, state of the art, and future trends," *IEEE Aerospace and Electronic Systems Magazine*, vol. 15, no. 1, pp. 28–32, Jan 2000.
- [3] T. Billard, C. Abadie, and T. Lebey, "Partial discharge testing in aeronautic environment on magnet wire and feeder cables," in *2016 IEEE Electrical Insulation Conference (EIC)*, June 2016, pp. 101–104.
- [4] D. Xiao, *Gas Discharge and Gas Insulation*, ser. Energy and Environment Research in China. Springer Berlin Heidelberg, 2015.
- [5] E. Kuffel, W. Zaengl, and J. Kuffel, *High Voltage Engineering: Fundamentals*, 2nd ed. Newnes, August 2000.
- [6] A. Trentin, P. Zanchetta, P. Wheeler, and J. Clare, "Power conversion for a novel ac/dc aircraft electrical distribution system," *IET Electrical Systems in Transportation*, vol. 4, no. 2, pp. 29–37, June 2014.
- [7] A. Eid, H. El-Kishky, M. Abdel-Salam, and M. T. El-Mohandes, "On power quality of variable-speed constant-frequency aircraft electric power systems," *IEEE Transactions on Power Delivery*, vol. 25, no. 1, pp. 55–65, Jan 2010.
- [8] *High-voltage test techniques - Partial discharge measurements*, IEC 60270 International Standard, Rev. 3, December 2000.
- [9] G. Stone, E. Boulter, I. Culbert, and H. Dhirani, *Electrical Insulation for Rotating Machines: Design, Evaluation, Aging, Testing, and Repair*, 1st ed. Wiley-IEEE Press, January 2014.
- [10] G. Stone, M. K. Stranges, and D. G. Dunn, "Common questions on partial discharge testing: A review of recent developments in IEEE and IEC standards for offline and online testing of motor and generator stator windings," *IEEE Industry Applications Magazine*, vol. 22, no. 1, pp. 14–19, jan 2016.

-
- [11] D. F. Grosjean, D. L. Schweickart, D. G. Kasten, S. A. Sebo, and X. Liu, "Development of procedures for partial discharge measurements at low pressures in air, argon and helium," *IEEE Transactions on Dielectrics and Electrical Insulation*, vol. 15, no. 6, pp. 1535–1543, December 2008.
- [12] A. Esfahani, S. Shahabi, G. Stone, and B. Kordi, "Investigation of corona partial discharge under variable frequency and air pressure," in *2018 Electrical Insulation Conference (EIC), San Antonio, TX, USA, 17 - 21 June 2018*. IEEE, 2018.
- [13] D. G. Kasten, X. Liu, S. A. Sebo, D. F. Grosjean, and D. L. Schweickart, "Partial discharge measurements in air and argon at low pressures with and without a dielectric barrier," *IEEE Transactions on Dielectrics and Electrical Insulation*, vol. 12, no. 2, pp. 362–373, April 2005.
- [14] E. Sili, F. Koliatene, and J. P. Cambronne, "Pressure and temperature effects on the paschen curve," in *2011 Annual Report Conference on Electrical Insulation and Dielectric Phenomena*, Oct 2011, pp. 464–467.
- [15] W. M. Ravindra Arora, "High voltage and electrical insulation engineering," in *High Voltage and Electrical Insulation Engineering*, 2011.
- [16] *Standard Test Method for Detection and Measurement of Partial Discharge (Corona) Pulses in Evaluation of Insulation Systems*, ASTM International ASTM D1868-13, Rev. 2, 2013.
- [17] F. Alrumayan, I. Cotton, and A. Nelms, "Partial discharge testing of aerospace electrical systems," *IEEE Transactions on Aerospace and Electronic Systems*, vol. 46, no. 2, pp. 848–863, April 2010.
- [18] Y. Raizer, V. Kisin, and J. Allen, *Gas Discharge Physics*. Springer Berlin Heidelberg, 2011.
- [19] E. Husain and R. S. Nema, "Surface discharge studies with uniform field electrodes at low pressures," *IEEE Transactions on Electrical Insulation*, vol. EI-16, no. 2, pp. 128–133, April 1981.
- [20] H. Okubo, S. Yuasa, K. Ota, N. Hayakawa, and M. Hikita, "Discharge characteristics under non-uniform electric field in he, ar and air at low pressures," *IEEE Transactions on Dielectrics and Electrical Insulation*, vol. 4, no. 4, pp. 450–455, Aug 1997.
- [21] H. Okubo, Y. Yamano, A. Ohashi, and K. Kato, "Vacuum discharge phenomena under non-uniform field conditions," in *Proceedings ISDEIV. 18th International Symposium on Discharges and Electrical Insulation in Vacuum (Cat. No.98CH36073)*, vol. 1, Aug 1998, pp. 93–100 vol.1.
-

-
- [22] E.-N. Li and J. M. K. MacAlpine, "Negative corona in air using a point/cup electrode system," *IEEE Transactions on Dielectrics and Electrical Insulation*, vol. 7, no. 6, pp. 752–757, Dec 2000.
- [23] D. L. Schweickart, D. F. Grosjean, D. G. Kasten, X. Liu, and S. A. Sebo, "Partial discharge measurements at low pressures with and without a dielectric barrier," in *The 17th Annual Meeting of the IEEE Lasers and Electro-Optics Society, 2004. LEOS 2004.*, Oct 2004, pp. 462–465.
- [24] M. Tabrizchi and F. Rouholahnejad, "Corona discharge ion mobility spectrometry at reduced pressures," *Review of Scientific Instruments*, vol. 75, no. 11, pp. 4656–4661, nov 2004.
- [25] —, "Comparing the effect of pressure and temperature on ion mobilities," *Journal of Physics D: Applied Physics*, vol. 38, no. 6, p. 857, 2005.
- [26] X. Liu, "Partial discharge detection and analysis in low pressure environments," Ph.D. dissertation, The Ohio State University, Department of Electrical and Computer Engineering, The Ohio State University, 2006.
- [27] X. Liu, D. G. Kasten, and S. A. Sebo, "Partial discharge measurements for a twisted pair of insulated conductors at low pressures in air, argon and helium," in *Conference Record of the 2006 IEEE International Symposium on Electrical Insulation*, June 2006, pp. 286–289.
- [28] C. Forssen and H. Edin, "Partial discharges in a cavity at variable applied frequency part 1: measurements," *IEEE Transactions on Dielectrics and Electrical Insulation*, vol. 15, no. 6, pp. 1601–1609, December 2008.
- [29] —, "Partial discharges in a cavity at variable applied frequency part 2: measurements and modeling," *IEEE Transactions on Dielectrics and Electrical Insulation*, vol. 15, no. 6, pp. 1610–1616, December 2008.
- [30] X. Bian, L. Wang, J. M. K. Macalpine, Z. Guan, J. Hui, and Y. Chen, "Positive corona inception voltages and corona currents for air at various pressures and humidities," *IEEE Transactions on Dielectrics and Electrical Insulation*, vol. 17, no. 1, pp. 63–70, February 2010.
- [31] X. Bian, X. Meng, L. Wang, J. M. K. Macalpine, Z. Guan, and J. Hui, "Negative corona inception voltages in rod-plane gaps at various air pressures and humidities," *IEEE Transactions on Dielectrics and Electrical Insulation*, vol. 18, no. 2, pp. 613–619, April 2011.
- [32] P. Sattari, G. S. P. Castle, and K. Adamiak, "A numerical model of trichel pulses in air; the effect of pressure," *Journal of Physics: Conference Series*, vol. 301, no. 1, p. 012058, 2011.
-

-
- [33] P. Sattari, C. F. Gallo, G. S. P. Castle, and K. Adamiak, "Trichel pulse characteristicsnegative corona discharge in air," *Journal of Physics D: Applied Physics*, vol. 44, no. 15, p. 155502, 2011.
- [34] S. J. He, J. Ha, Y. H. Han, Z. Q. Liu, and S. Q. Guo, "Trichel pulses in a negative corona discharge in air at low pressure," *Journal of Physics: Conference Series*, vol. 418, no. 1, p. 012091, 2013.
- [35] A. Cavallini, L. Versari, and L. Fornasari, "Feasibility of partial discharge detection in inverter-fed actuators used in aircrafts," in *2013 Annual Report Conference on Electrical Insulation and Dielectric Phenomena*, Oct 2013, pp. 1250–1253.
- [36] C. Emersic, C. Zhang, I. Cotton, R. Lowndes, S. Rowland, R. Freer, S. of Electrical, E. Engineering, and (EEE), "Degradation of printed circuit board coatings due to partial discharge," in *2015 Electrical Insulation Conference (EIC), Seattle, Washington, USA, 7 -10 June 2015*. IEEE, 2015.
- [37] C. Emersic, R. Lowndes, I. Cotton, S. Rowland, and R. Freer, "The effects of pressure and temperature on partial discharge degradation of silicone conformai coatings," *IEEE Transactions on Dielectrics and Electrical Insulation*, vol. 24, no. 5, pp. 2986–2994, oct 2017.
- [38] C. Abadie, , T. B. T. LEBEY, I. A. de Saint Exupry 2Laboratoire Laplace, and CNRS-UPS-INP, "Influence of pressure on partial discharge spectra," in *2016 Electrical Insulation Conference (EIC), Montral, Qc, Canada, 19 - 22 June 2016*. IEEE, 2016.
- [39] X. Li, X. Cui, T. Lu, D. Li, B. Chen, and Y. Fu, "Influence of air pressure on the detailed characteristics of corona current pulse due to positive corona discharge," *Physics of Plasmas*, vol. 23, no. 12, p. 123516, 2016.
- [40] T. Liu, Y. Xiao, Y. Lu, X. Huang, Q. Li, and Z. Wang, "Effect of voltage frequency on surface discharge characteristics and aging process," in *2017 IEEE Electrical Insulation Conference (EIC)*, June 2017, pp. 463–466.
- [41] G. Dong, T. Liu, M. Zhang, Q. Li, and Z. Wang, "Effect of voltage waveform on partial discharge characteristics and insulation life," in *2018 12th International Conference on the Properties and Applications of Dielectric Materials (ICPADM)*, May 2018, pp. 144–147.
- [42] Y. Zhou, Z. Zhou, L. Zhang, Y. Zhang, Y. Mo, and J. Sun, "Characterization and comprehension of corona partial discharge in air under power frequency to very low frequency voltage," *Plasma Science and Technology*, vol. 20, no. 5, p. 054016, 2018.
- [43] B. XingMing, Z. JunYu, Y. Wei, W. ShuWei, Q. Lei, L. XueBao, and L. HaiBing, "The role of low air pressure in the variation of negative corona-generated space charge in a rod to plane electrode," *High Voltage*, vol. 3, no. 2, pp. 126–132, 2018.
-

-
- [44] G. C. Stone, M. K. W. Stranges, and D. G. Dunn, "Recent developments in iec and iec standards for off-line and on-line partial discharge testing of motor and generator stator windings," in *2014 IEEE Petroleum and Chemical Industry Technical Conference (PCIC)*, Sept 2014, pp. 79–84.
- [45] R. Bartnikas, "Partial discharges. their mechanism, detection and measurement," *IEEE Transactions on Dielectrics and Electrical Insulation*, vol. 9, no. 5, pp. 763–808, Oct 2002.
- [46] I. Power and E. Society, "Ieee guide for the measurement of partial discharges in ac electric machinery," in *IEEE Guide for the Measurement of Partial Discharges in AC Electric Machinery*. IEEE, 2014.
- [47] T. Pinpart and M. D. Judd, "Experimental comparison of uhf sensor types for pd location applications," in *2009 IEEE Electrical Insulation Conference*, May 2009, pp. 26–30.
- [48] M. Hikita, H. Yamashita, T. Hoshino, T. Kato, N. Hayakawa, T. Ueda, and H. Okubo, "Electromagnetic noise spectrum caused by partial discharge in air at high voltage substations," *IEEE Transactions on Power Delivery*, vol. 13, no. 2, pp. 434–439, April 1998.
- [49] J. E. Timperley and J. M. Vallejo, "Condition assessment of electrical apparatus with emi diagnostics," *IEEE Transactions on Industry Applications*, vol. 53, no. 1, pp. 693–699, Jan 2017.
- [50] H. Janani, "Partial discharge source classification using pattern recognition algorithms," Ph.D. dissertation, University of Manitoba, Department of Electrical and Computer Engineering, University of Manitoba, 2016.
- [51] E. S. Committee, *Winding wires Test methods Part 5: Electrical properties*, IEC 60851-5 International Standard, Rev. 3, July 2008.
- [52] L. Hao, P. L. Lewin, and S. G. Swingler, "Improving detection sensitivity for partial discharge monitoring of high voltage equipment," *Measurement Science and Technology*, vol. 19, no. 5, p. 055707, 2008.
- [53] A. A. Bajwa, S. Habib, and M. Kamran, "An investigation into partial discharge pulse extraction methods," *International Journal of Electrical Power & Energy Systems*, vol. 73, pp. 964 – 982, 2015.
- [54] M. Ashtiani and S. Shahrtash, "Partial discharge pulse localization in excessive noisy data window," *IEEE Transactions on Dielectrics and Electrical Insulation*, vol. 22, no. 1, pp. 428–435, feb 2015.

-
- [55] A. Cavallini, L. Lusuardi, D. R. Meyer, and S. Machipeddy, "Modelling partial discharge inception in magnet wires at different altitudes," in *2016 IEEE Conference on Electrical Insulation and Dielectric Phenomena (CEIDP)*, Oct 2016, pp. 449–452.
- [56] K. Wang, R. Liao, L. Yang, J. Li, S. Grzybowski, and J. Hao, "Optimal features selected by nsga-ii for partial discharge pulses separation based on time-frequency representation and matrix decomposition," *IEEE Transactions on Dielectrics and Electrical Insulation*, vol. 20, no. 3, pp. 825–838, June 2013.
- [57] H. Janani, B. Kordi, and M. J. Jozani, "Classification of simultaneous multiple partial discharge sources based on probabilistic interpretation using a two-step logistic regression algorithm," *IEEE Transactions on Dielectrics and Electrical Insulation*, vol. 24, no. 1, pp. 54–65, Feb 2017.
- [58] K. Wang, J. Li, S. Zhang, R. Liao, F. Wu, L. Yang, J. Li, S. Grzybowski, and J. Yan, "A hybrid algorithm based on s transform and affinity propagation clustering for separation of two simultaneously artificial partial discharge sources," *IEEE Transactions on Dielectrics and Electrical Insulation*, vol. 22, no. 2, pp. 1042–1060, April 2015.
- [59] M. Cacciari, A. Contin, and G. C. Montanari, "Use of a mixed-weibull distribution for the identification of pd phenomena [rotating machines]," *IEEE Transactions on Dielectrics and Electrical Insulation*, vol. 2, no. 4, pp. 614–627, Aug 1995.
- [60] A. Cavallini, G. C. Montanari, A. Contin, and F. Pulletti, "A new approach to the diagnosis of solid insulation systems based on pd signal inference," *IEEE Electrical Insulation Magazine*, vol. 19, no. 2, pp. 23–30, March 2003.
- [61] A. Contin and S. Pastore, "Classification of partial discharge signals by means of auto-correlation function evaluation," in *Conference Record of the 2006 IEEE International Symposium on Electrical Insulation*, June 2006, pp. 302–303.
- [62] —, "Classification and separation of partial discharge signals by means of their auto-correlation function evaluation," *IEEE Transactions on Dielectrics and Electrical Insulation*, vol. 16, no. 6, pp. 1609–1622, December 2009.
- [63] A. Cavallini, G. C. Montanari, F. Puletti, and A. Contin, "A new methodology for the identification of pd in electrical apparatus: properties and applications," *IEEE Transactions on Dielectrics and Electrical Insulation*, vol. 12, no. 2, pp. 203–215, April 2005.
- [64] T. Pinpart and M. D. Judd, "Differentiating between partial discharge sources using envelope comparison of ultra-high-frequency signals," *IET Science, Measurement Technology*, vol. 4, no. 5, pp. 256–267, September 2010.
- [65] A. Baug, N. R. Choudhury, R. Ghosh, S. Dalai, and B. Chatterjee, "Identification of single and multiple partial discharge sources by optical method using mathematical
-

-
- morphology aided sparse representation classifier,” *IEEE Transactions on Dielectrics and Electrical Insulation*, vol. 24, no. 6, pp. 3703–3712, Dec 2017.
- [66] L. Hao, P. L. Lewin, J. A. Hunter, D. J. Swaffield, A. Contin, C. Walton, and M. Michel, “Discrimination of multiple pd sources using wavelet decomposition and principal component analysis,” *IEEE Transactions on Dielectrics and Electrical Insulation*, vol. 18, no. 5, pp. 1702–1711, October 2011.
- [67] J. A. Ardila-Rey, J. M. Martinez-Tarifa, G. Robles, and M. V. Rojas-Moreno, “Partial discharge and noise separation by means of spectral-power clustering techniques,” *IEEE Transactions on Dielectrics and Electrical Insulation*, vol. 20, no. 4, pp. 1436–1443, August 2013.
- [68] J. M. Martinez-Tarifa, J. A. Ardila-Rey, and G. Robles, “Automatic selection of frequency bands for the power ratios separation technique in partial discharge measurements: part i, fundamentals and noise rejection in simple test objects,” *IEEE Transactions on Dielectrics and Electrical Insulation*, vol. 22, no. 4, pp. 2284–2291, August 2015.
- [69] J. A. Ardila-Rey, J. M. Martinez-Tarifa, and G. Robles, “Automatic selection of frequency bands for the power ratios separation technique in partial discharge measurements: part ii, pd source recognition and applications,” *IEEE Transactions on Dielectrics and Electrical Insulation*, vol. 22, no. 4, pp. 2293–2301, August 2015.
- [70] F. Alvarez, J. Ortego, F. Garnacho, and M. A. Sanchez-Uran, “A clustering technique for partial discharge and noise sources identification in power cables by means of waveform parameters,” *IEEE Transactions on Dielectrics and Electrical Insulation*, vol. 23, no. 1, pp. 469–481, February 2016.
- [71] “IEEE guide for the statistical analysis of electrical insulation breakdown data,” *IEEE Std 930-2004 (Revision of IEEE Std 930-1987)*, pp. 1–41, 2005.
- [72] E. Gulski and A. Krivda, “Neural networks as a tool for recognition of partial discharges,” *IEEE Transactions on Electrical Insulation*, vol. 28, no. 6, pp. 984–1001, Dec 1993.
- [73] S. Poyhonen, M. Conti, A. Cavallini, G. C. Montanari, and F. Filippetti, “Insulation defect localization through partial discharge measurements and numerical classification,” in *2004 IEEE International Symposium on Industrial Electronics*, vol. 1, May 2004, pp. 417–422 vol. 1.
- [74] R. M. Sharkawy, R. S. Mangoubi, T. k. Abdel-Galil, M. M. A. Salama, and R. Bartnikas, “Svm classification of contaminating particles in liquid dielectrics using higher order statistics of electrical and acoustic pd measurements,” *IEEE Transactions on Dielectrics and Electrical Insulation*, vol. 14, no. 3, pp. 669–678, June 2007.
-

- [75] A. Contin, A. Cavallini, G. C. Montanari, G. Pasini, and F. Puletti, “Digital detection and fuzzy classification of partial discharge signals,” *IEEE Transactions on Dielectrics and Electrical Insulation*, vol. 9, no. 3, pp. 335–348, June 2002.
- [76] S. Theodoridis and K. Koutroumbas, “Pattern recognition,” in *Pattern Recognition (Fourth Edition)*, fourth edition ed., S. Theodoridis and K. Koutroumbas, Eds. Boston: Academic Press, 2009, pp. 151 – 260.

Appendix A

PRPD Patterns

The proposed detection method generates different patterns which can be useful in the investigation of PDs activity in MEA. In this appendix, obtained patterns for single PD source and multiple PD sources are shown at different air pressure levels and frequencies. It was mentioned that the frequency variation of the three-phase variable frequency AC (VFAC) system is between 360 and 900 Hz [7]. Therefore, the generated patterns for the two applied frequencies, 500 (for multiple PD sources) and 1000 Hz (for single PD source) are presented in this appendix.

A.1 Single Source PRPD Patterns

PRPD patterns related to twisted-pair wires and needle-plane electrode have been presented in this section.

Fig. A.1, Fig. A.3 and Fig. A.5 indicate PRPD patterns generated by needle-plane electrode under AC voltage frequency and different air pressure levels. Fig. A.2, Fig. A.4 and Fig. A.6 show PRPD patterns generated by twisted-pair wires under AC voltage frequency and different air pressure levels.

A.2 Multi Sources PRPD Patterns

PRPD patterns related to twisted-pair wires and needle-plane electrode as concurrent activated PD sources have been presented in this section. Fig A.7, Fig. A.8 and Fig. A.9 show DE, MDE and CD patterns generated by two simultaneous activated PD sources, respectively.

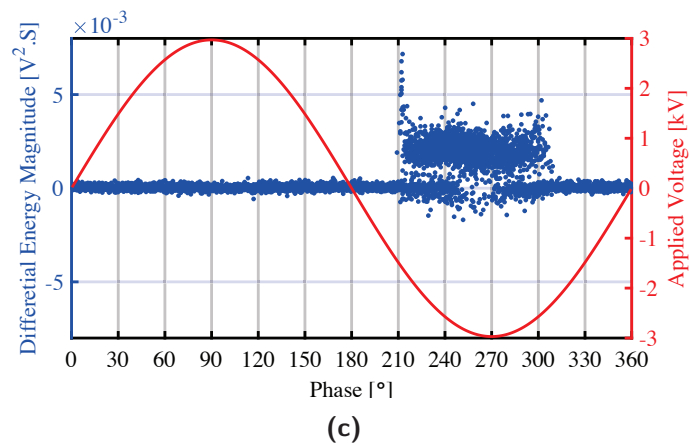
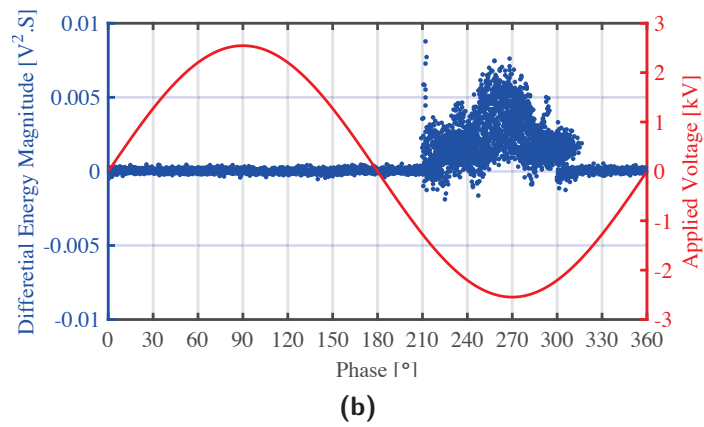
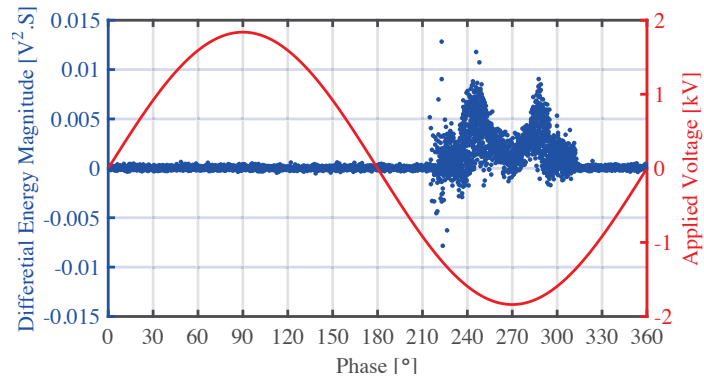
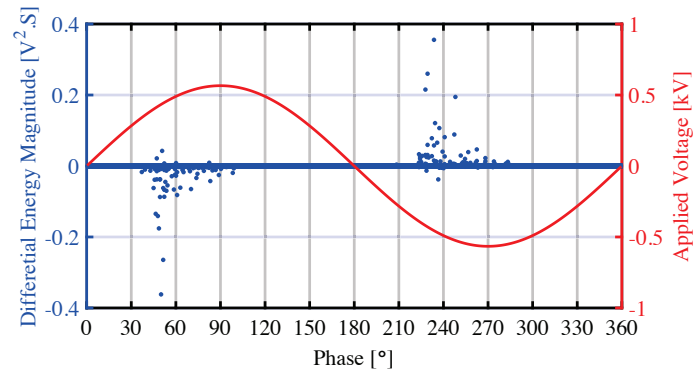
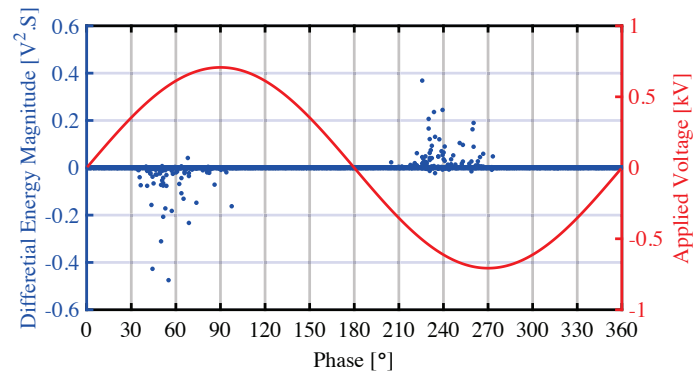


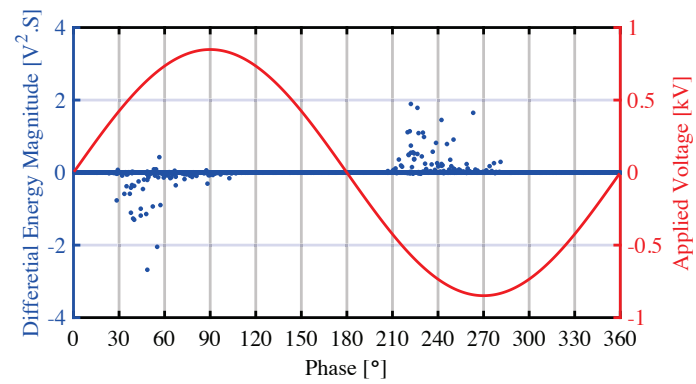
Fig. A.1: Differential Energy (DE) pattern for corona in air generated by needle-plane electrode under AC applied voltage frequency of 1kHz and air pressure levels of (a) 33 kPa (b) 67 kPa (c) 101 kPa.



(a)



(b)



(c)

Fig. A.2: Differential Energy (DE) pattern generated by twisted-pair wires under AC applied voltage frequency of 1kHz and air pressure levels of (a) 33 kPa (b) 67 kPa (c) 101 kPa.

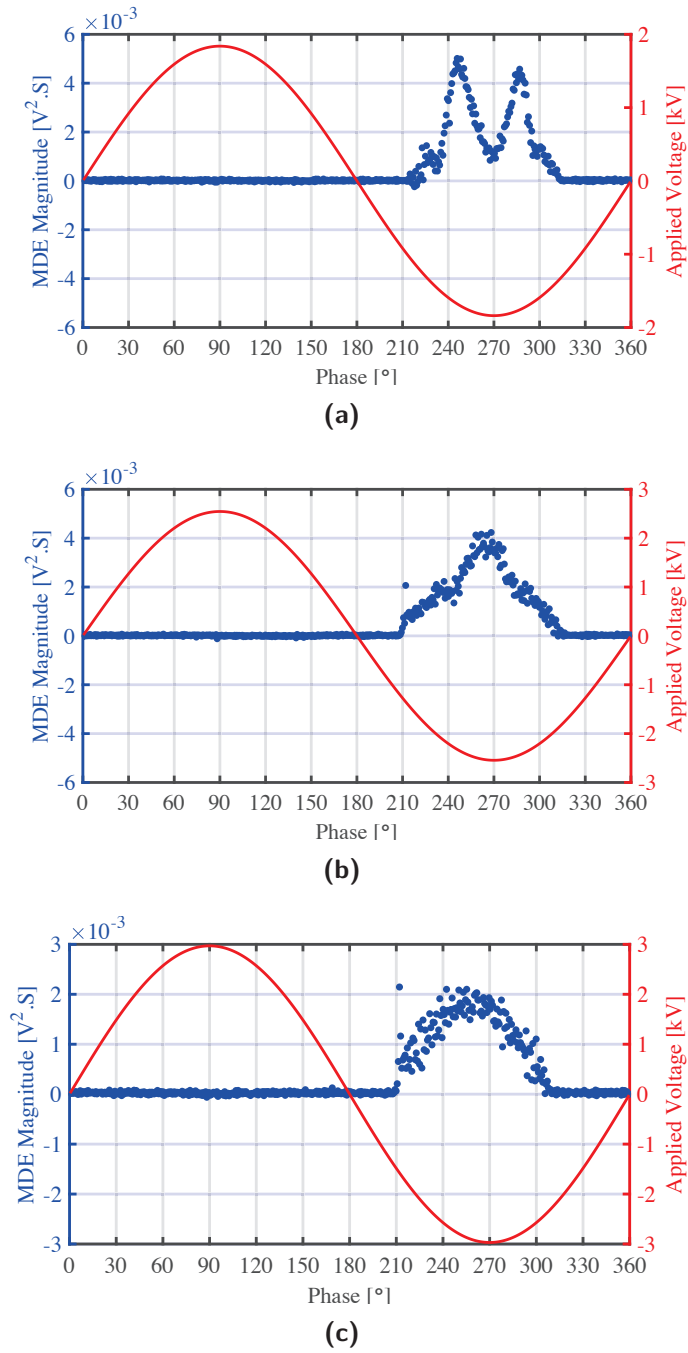
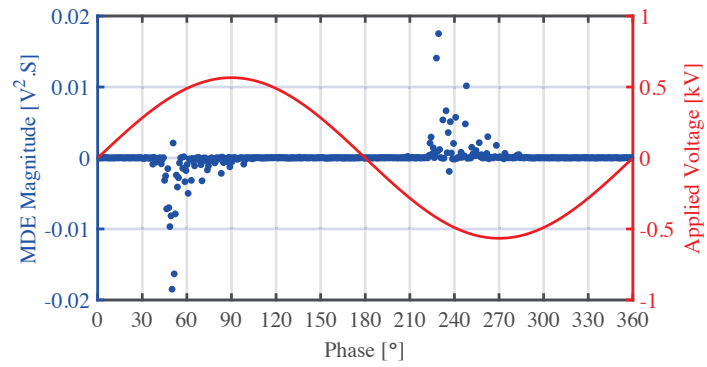
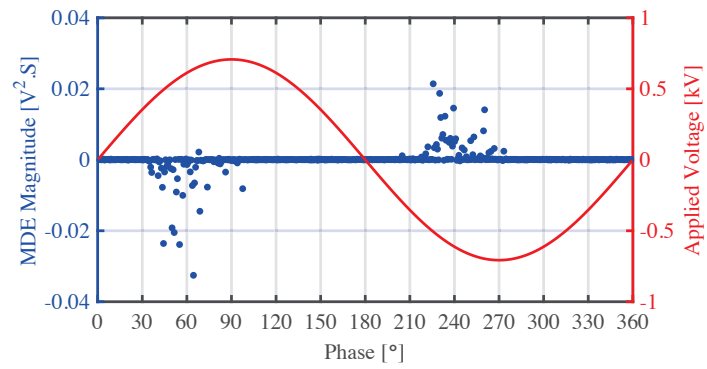


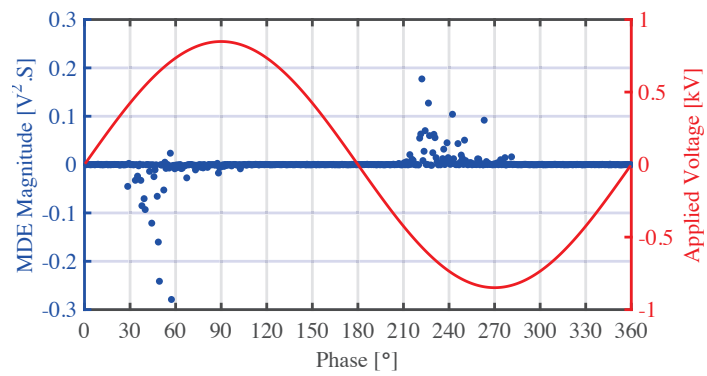
Fig. A.3: MDE pattern for corona in air generated by needle-plane electrode under AC applied voltage frequency of 1kHz and air pressure levels of (a) 33 kPa (b) 67 kPa (c) 101 kPa.



(a)



(b)



(c)

Fig. A.4: MDE pattern generated by twisted-pair wires under AC applied voltage frequency of 1kHz and air pressure levels of (a) 33 kPa (b) 67 kPa (c) 101 kPa.

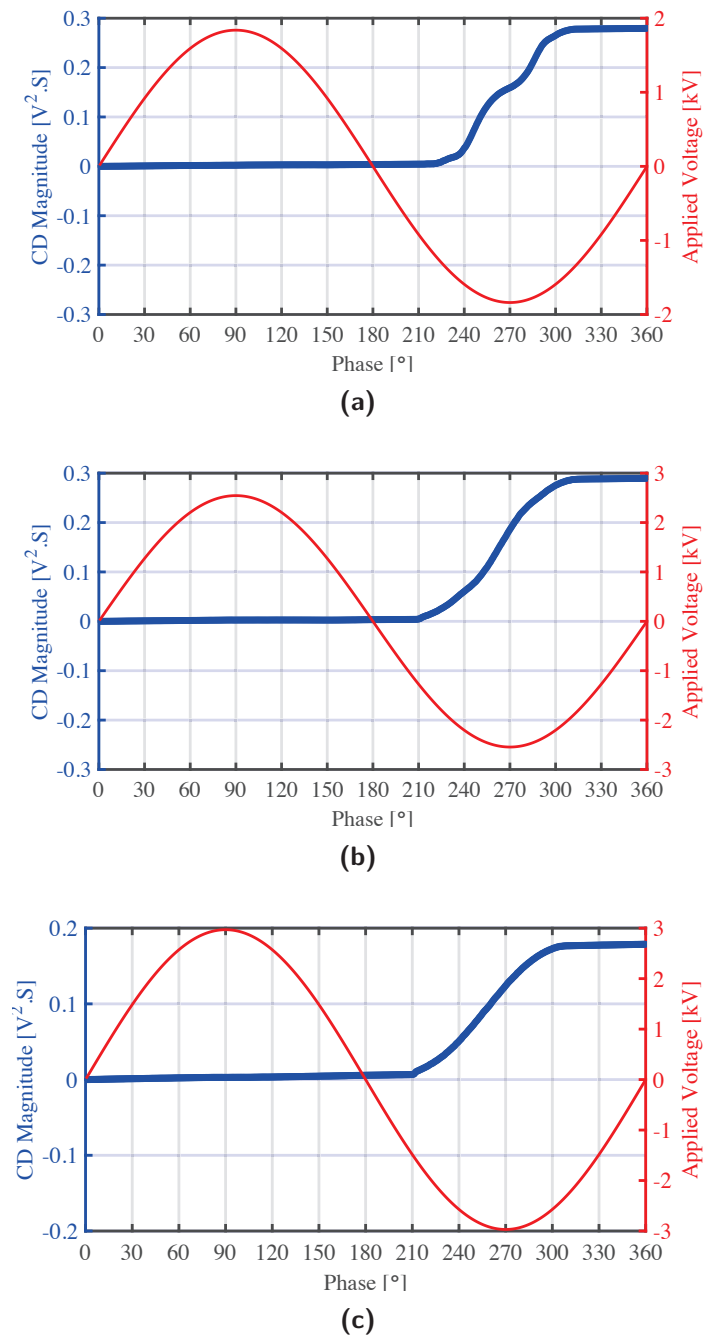
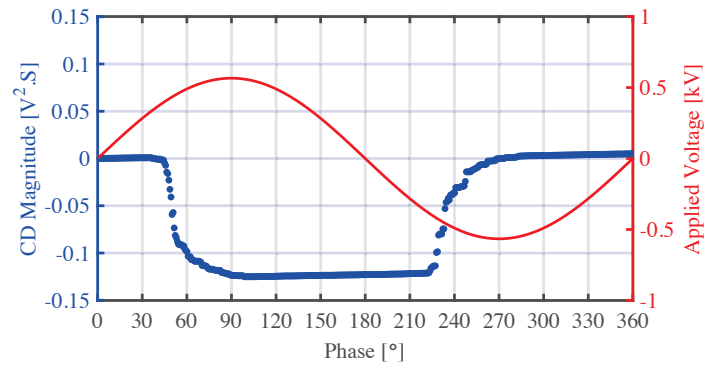
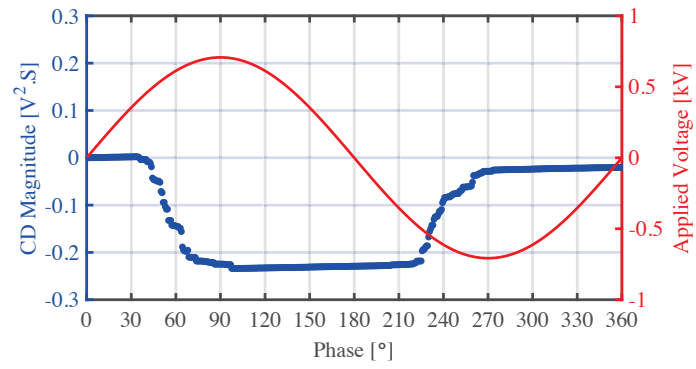


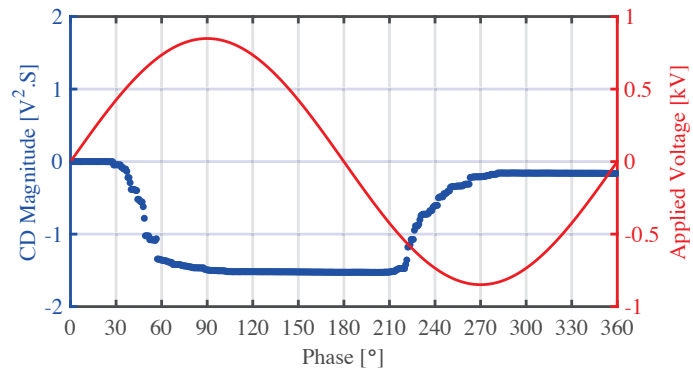
Fig. A.5: CD pattern for corona in air generated by needle-plane electrode under AC applied voltage frequency of 1kHz and air pressure levels of (a) 33 kPa (b) 67 kPa (c) 101 kPa.



(a)

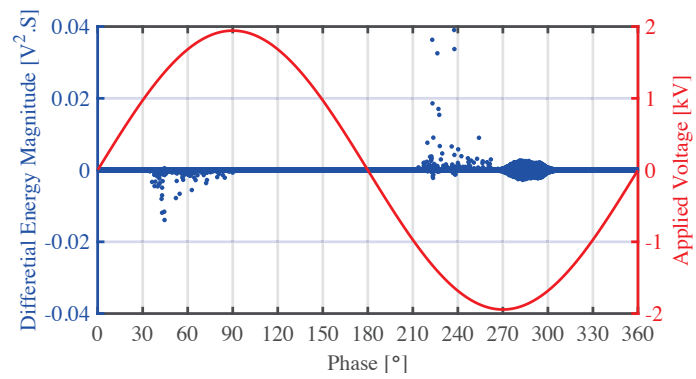


(b)

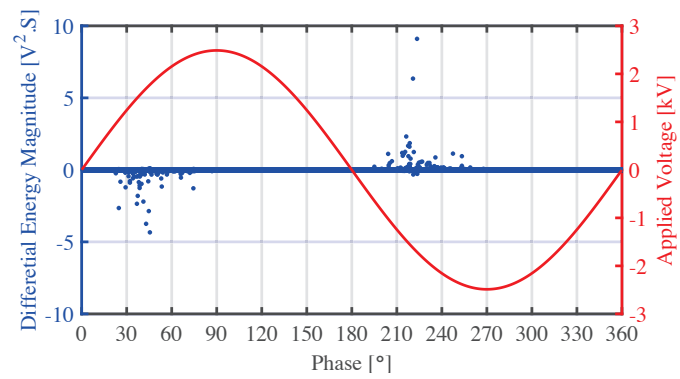


(c)

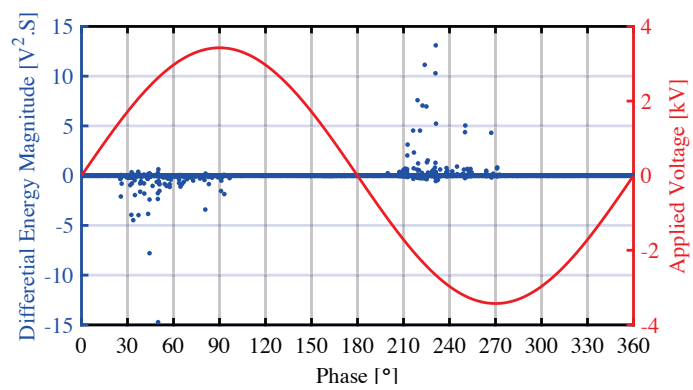
Fig. A.6: CD pattern generated by twisted-pair wires under AC applied voltage frequency of 1kHz and air pressure levels of (a) 33 kPa (b) 67 kPa (c) 101 kPa.



(a)



(b)



(c)

Fig. A.7: DE pattern generated by two simultaneously activated PD sources under AC applied voltage frequency of 500 Hz and air pressure levels of (a) 33 kPa (b) 67 kPa (c) 101 kPa.

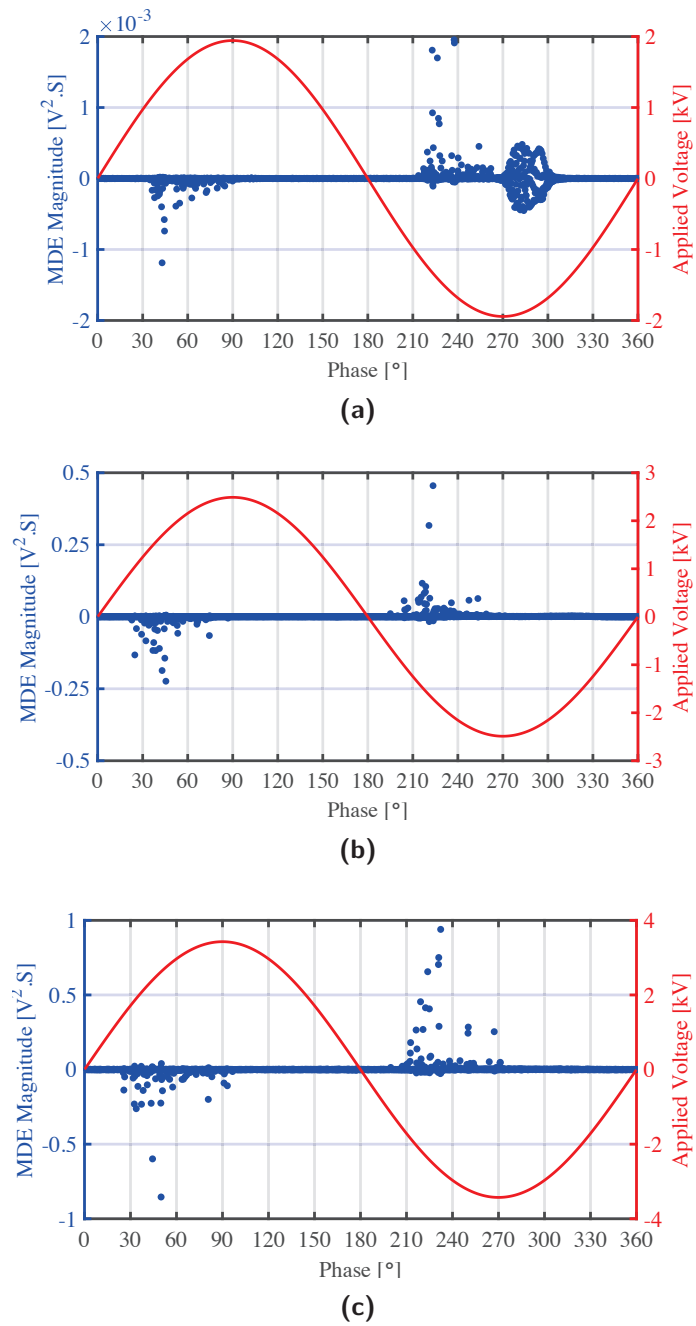
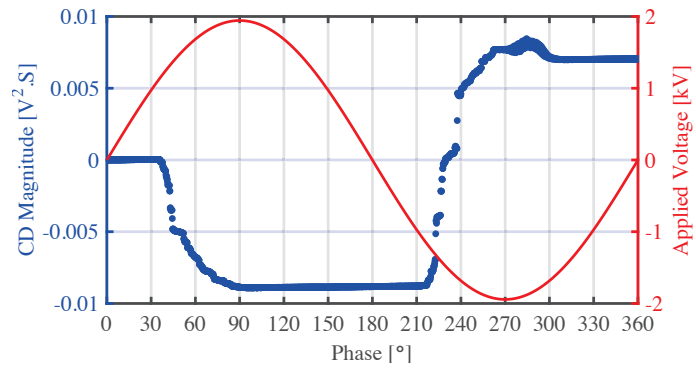
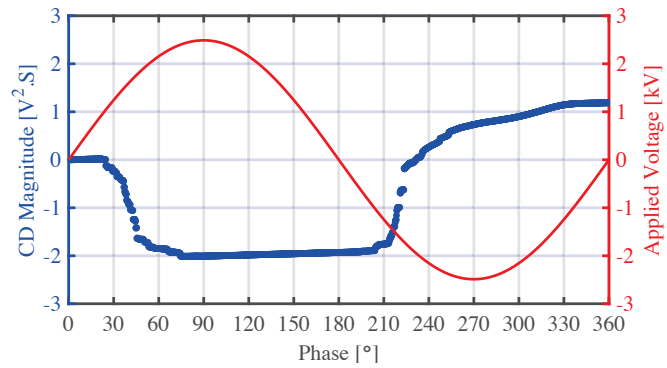


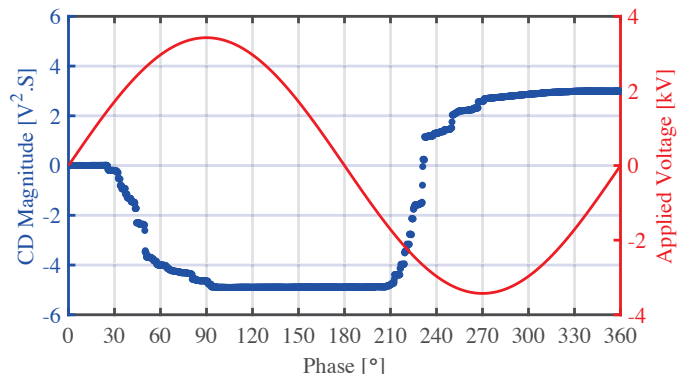
Fig. A.8: MDE pattern generated by two simultaneously activated PD sources under AC applied voltage frequency of 500 Hz and air pressure levels of (a) 33 kPa (b) 67 kPa (c) 101 kPa.



(a)



(b)



(c)

Fig. A.9: CD pattern generated by two simultaneously activated PD sources under AC applied voltage frequency of 500 Hz and air pressure levels of (a) 33 kPa (b) 67 kPa (c) 101 kPa.

Appendix B

Separation and Classification of Concurrent PD sources

B.1 Separation and Probabilistic analysis

In this section, the separation maps of multi PD sources system are presented. Also, the Weibull and Normal distribution related to the each feature distribution are shown. The results related to the AC applied voltage frequency of 500 Hz are presented.

Figs. B.1 and B.2 show the separation map of clusters related to the needle-plane electrode and twisted-pair wires as PD sources. The applied voltage frequency was 500 Hz under air pressure level of 33 kPa. Figs. B.7 and B.8 indicate the separation map of the clusters under atmospheric pressure of 101 kPa. Fig. B.3 to Fig. 4.12 show the Weibull and Normal distributions related to the distributions of the PD pulse waveform characteristics.

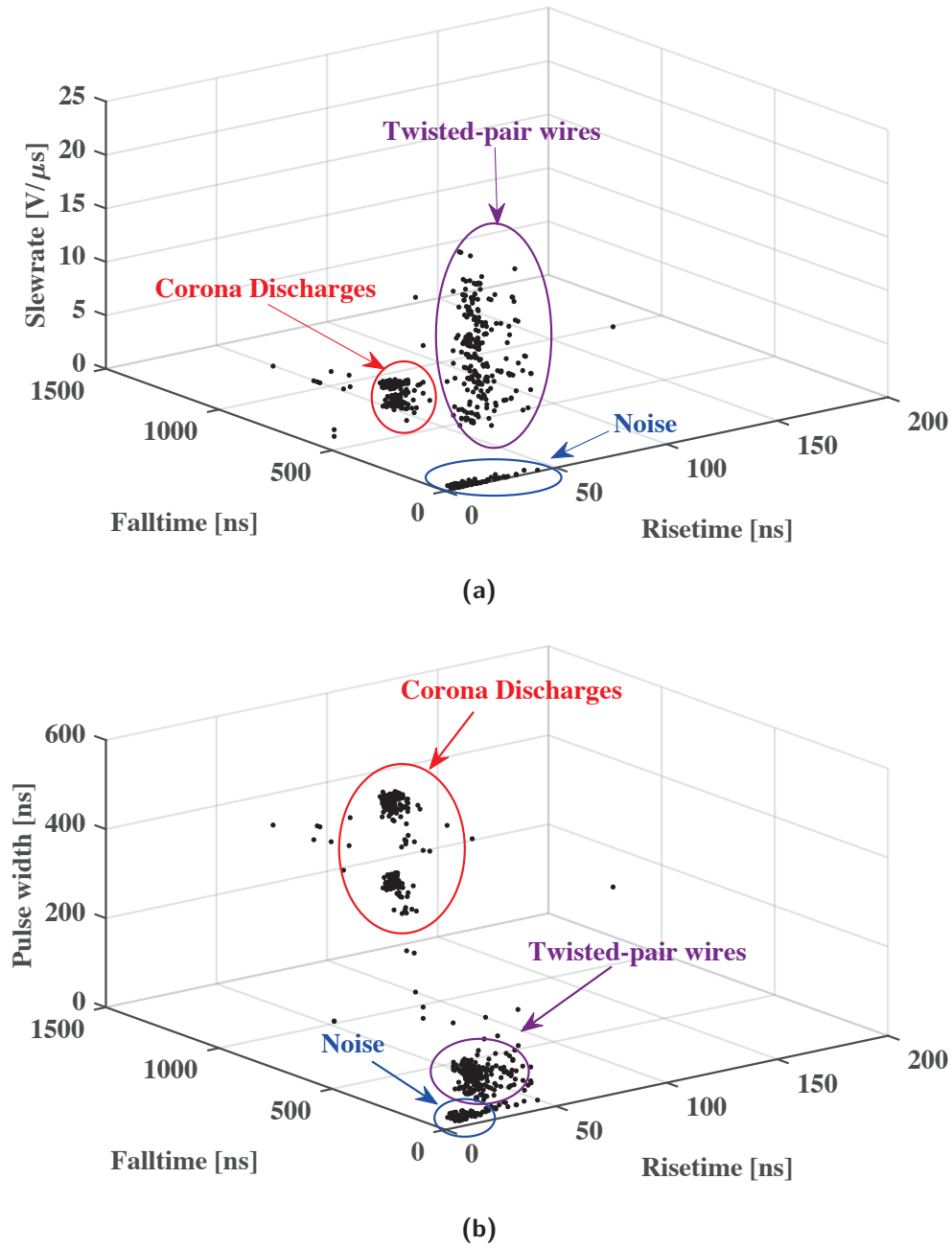
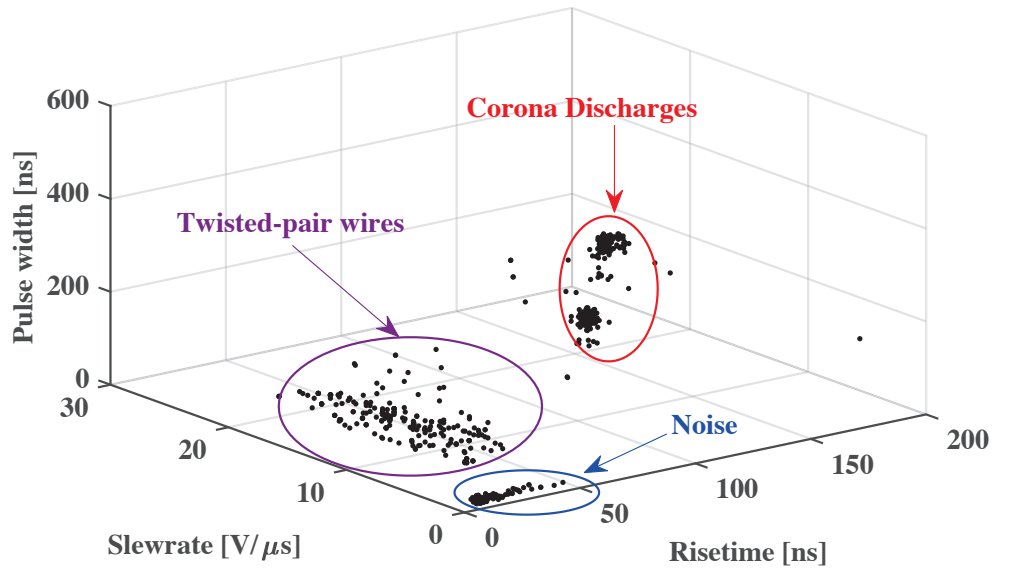
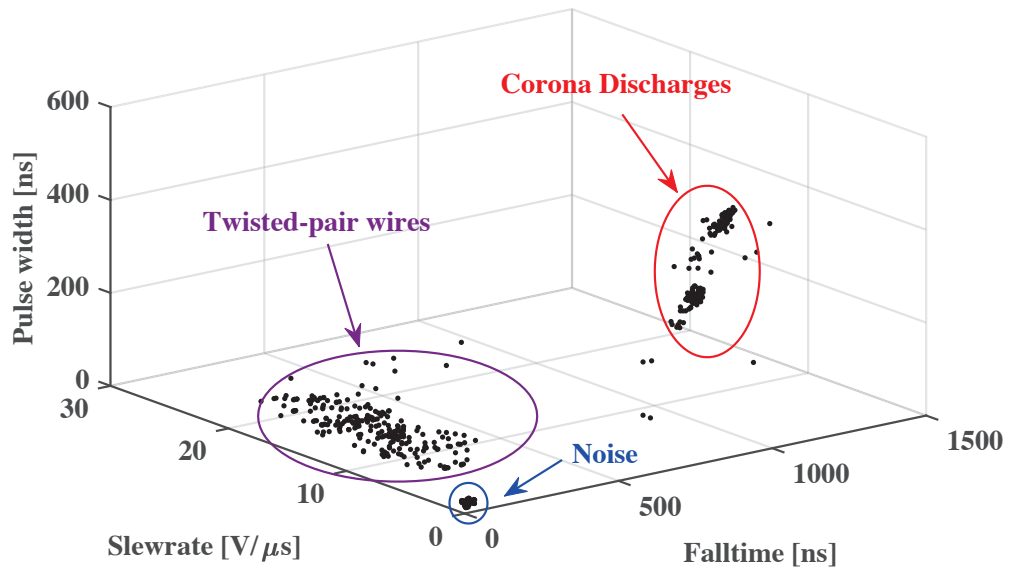


Fig. B.1: The separation map of PD sources under the applied frequency of 500 Hz and sub-atmospheric pressure of 33 kPa (a) (SR, FT,RT) (b) (PW, FT, RT)

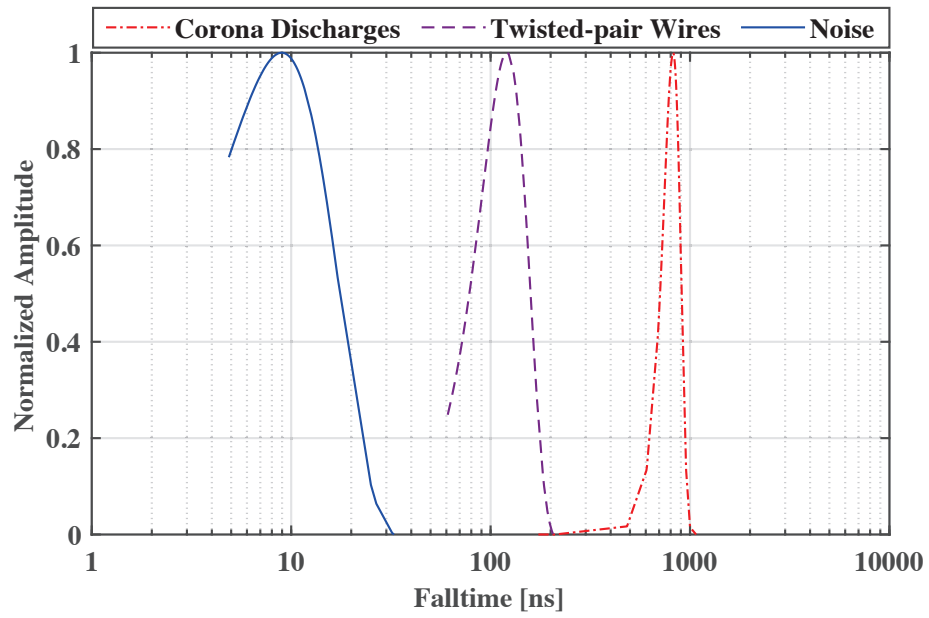


(a)

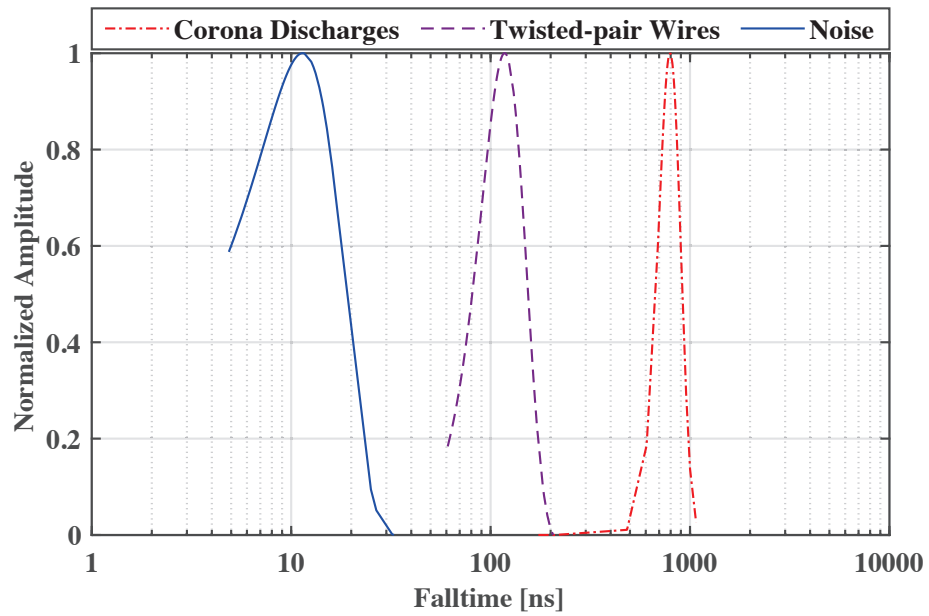


(b)

Fig. B.2: The separation map of PD sources under the applied frequency of 500 Hz and sub-atmospheric pressure of 33 kPa (a) (PW, SR, RT) (b) (PW, SR, FT)

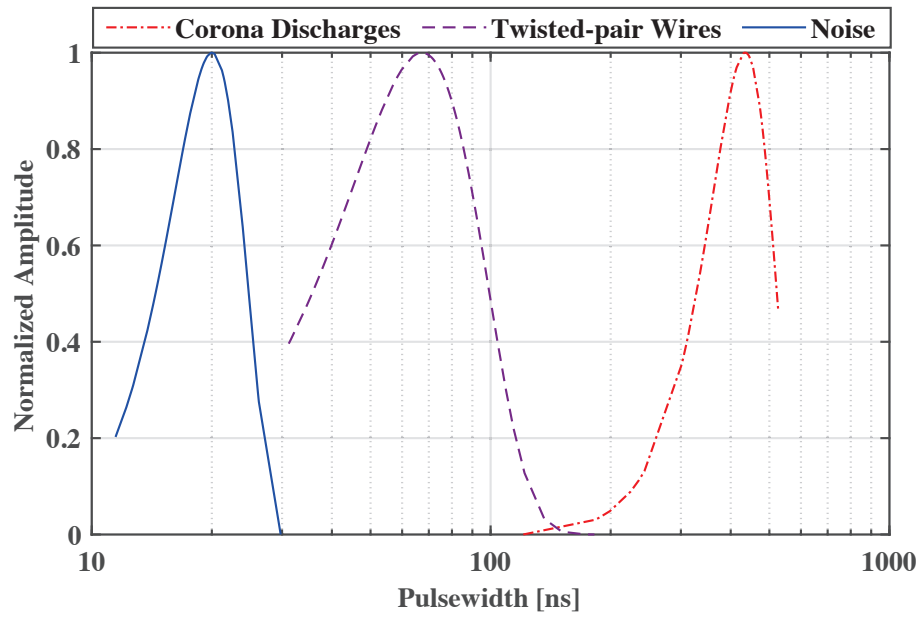


(a)

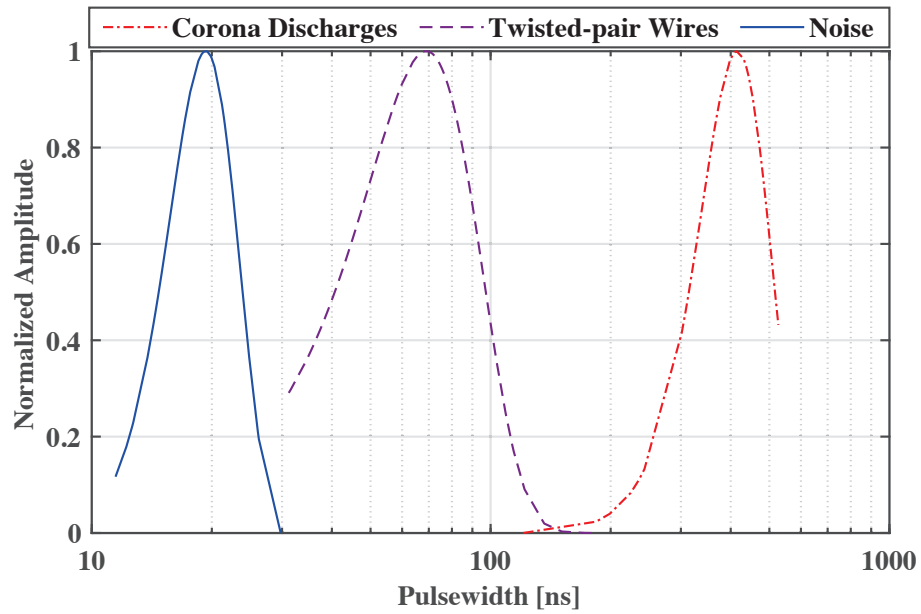


(b)

Fig. B.3: Weibull and Normal distribution of fall time for applied frequency of 500 Hz and air pressure level of 33 kPa (a) Weibull distribution (b) Normal distribution.

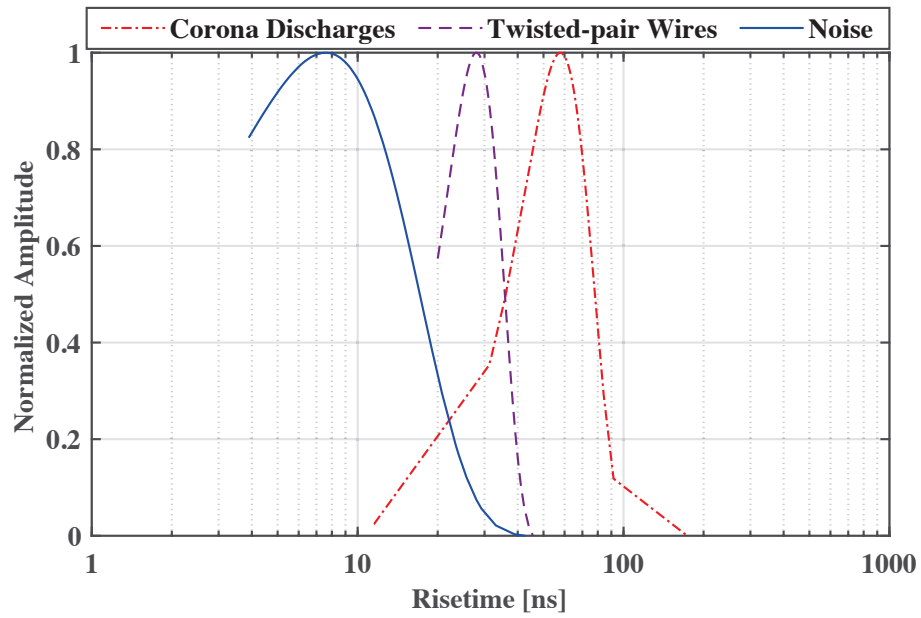


(a)

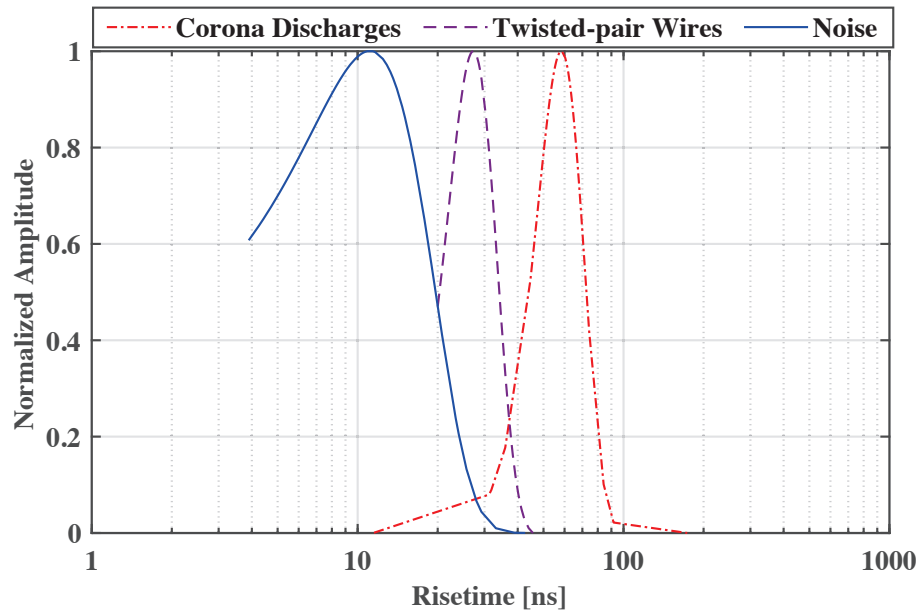


(b)

Fig. B.4: Weibull and Normal distribution of pulse width for applied frequency of 500 Hz and air pressure level of 33 kPa (a) Weibull distribution (b) Normal distribution.

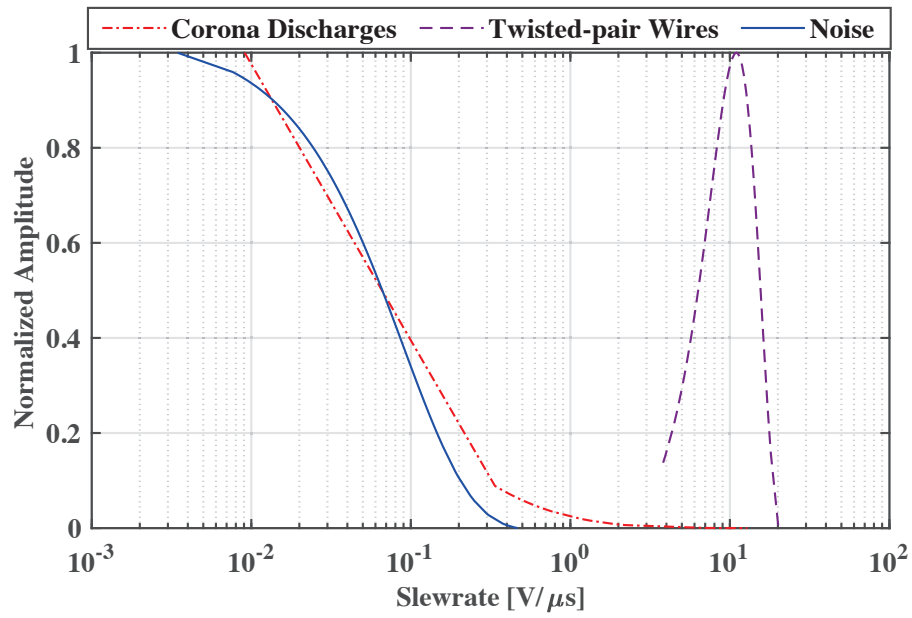


(a)

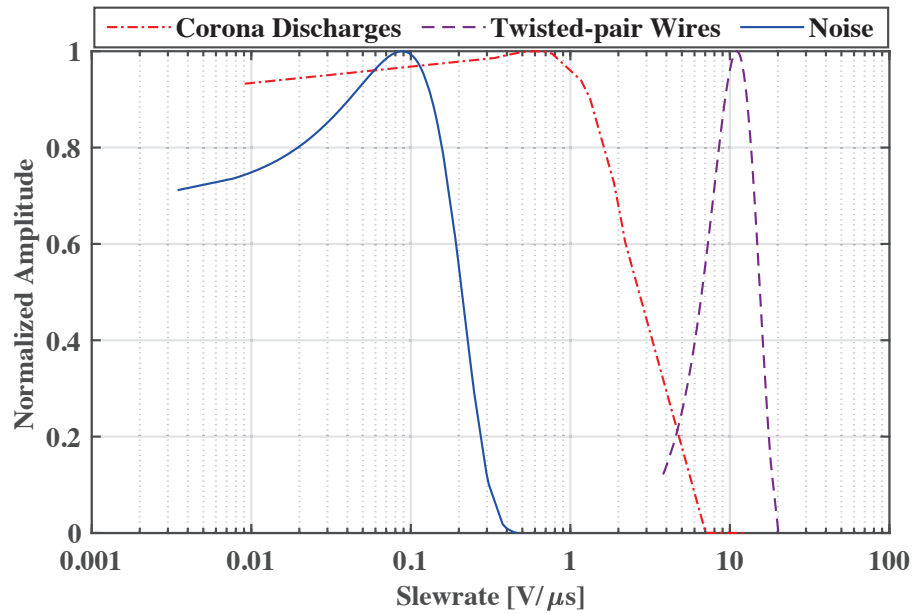


(b)

Fig. B.5: Weibull and Normal distribution of rise time for applied frequency of 500 Hz and air pressure level of 33 kPa (a) Weibull distribution (b) Normal distribution.



(a)



(b)

Fig. B.6: Weibull and Normal distribution of slew rate for applied frequency of 500 Hz and air pressure level of 33 kPa (a) Weibull distribution (b) Normal distribution.

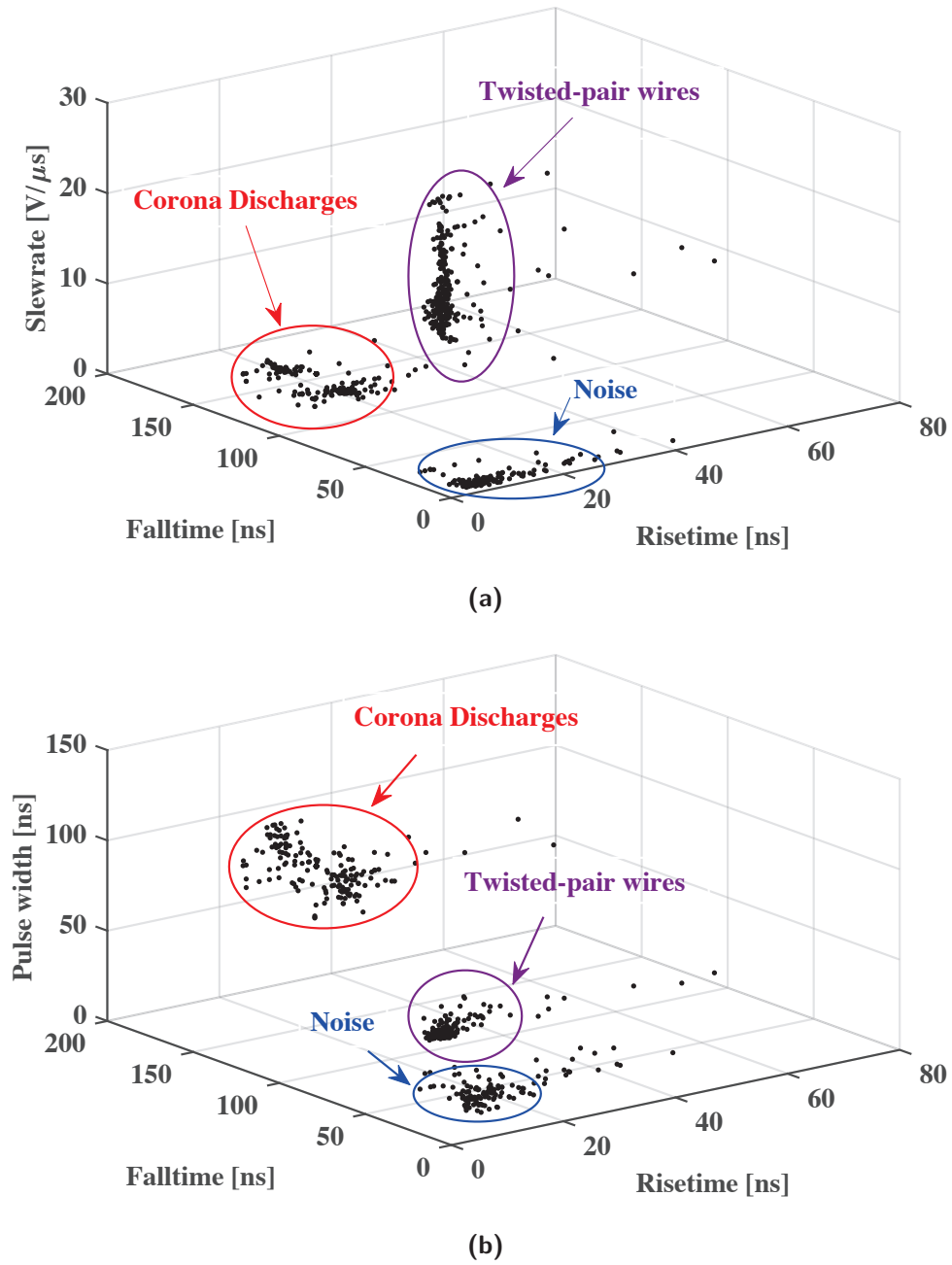
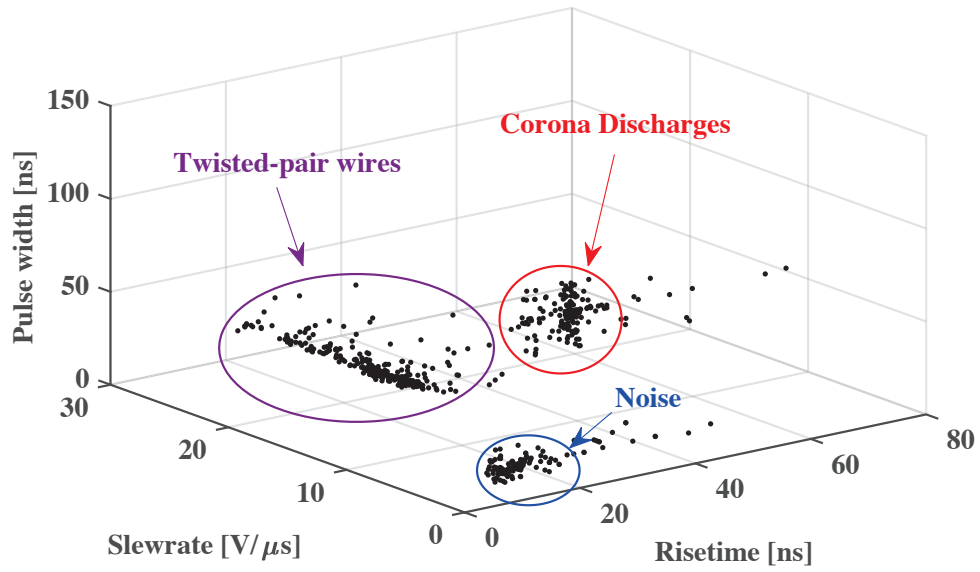
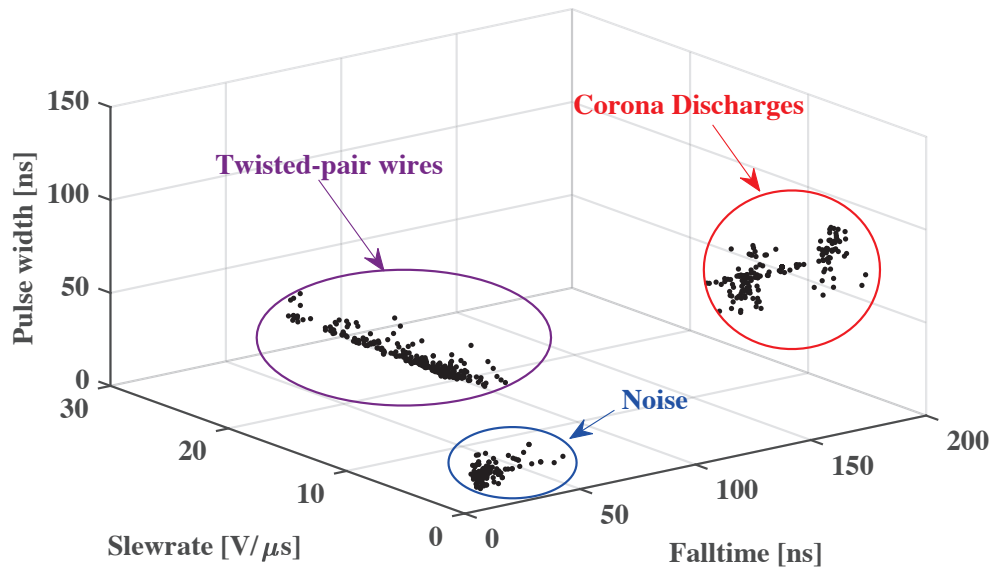


Fig. B.7: The separation map of PD sources under the applied frequency of 500 Hz and atmospheric pressure of 101 kPa (a) (SR, FT, RT) (b) (PW, FT, RT)

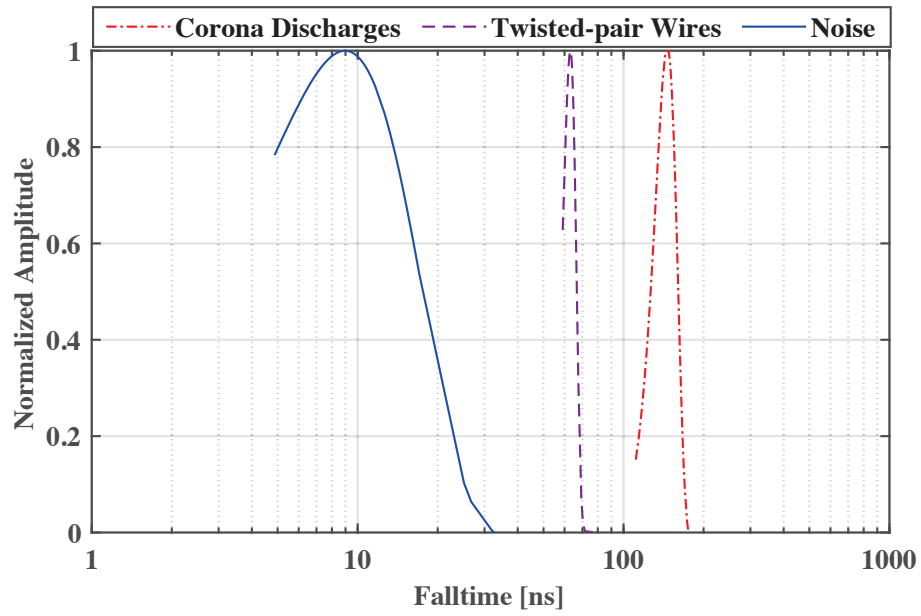


(a)

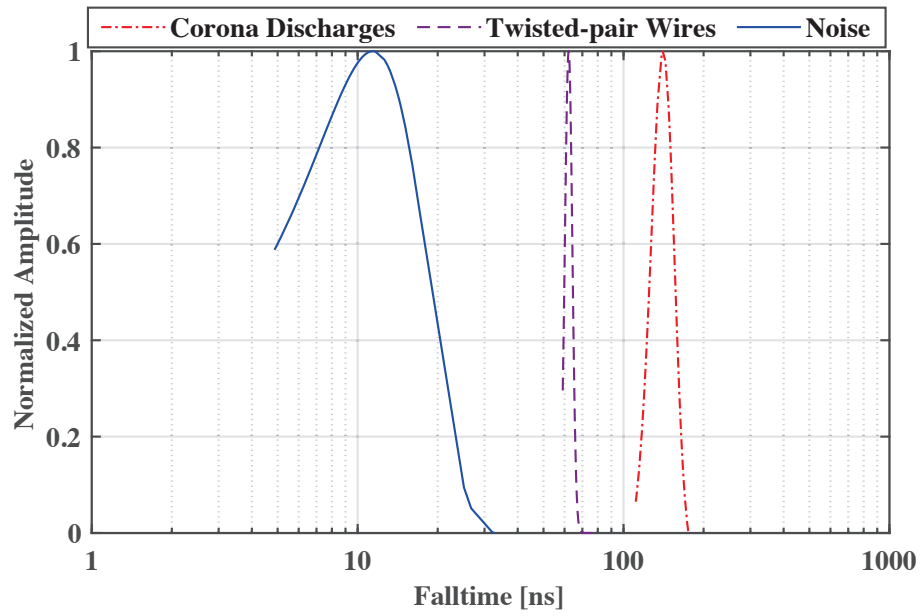


(b)

Fig. B.8: The separation map of PD sources under the applied frequency of 500 Hz and atmospheric pressure of 101 kPa (a) (PW, SR, RT) (b) (PW, SR, FT)

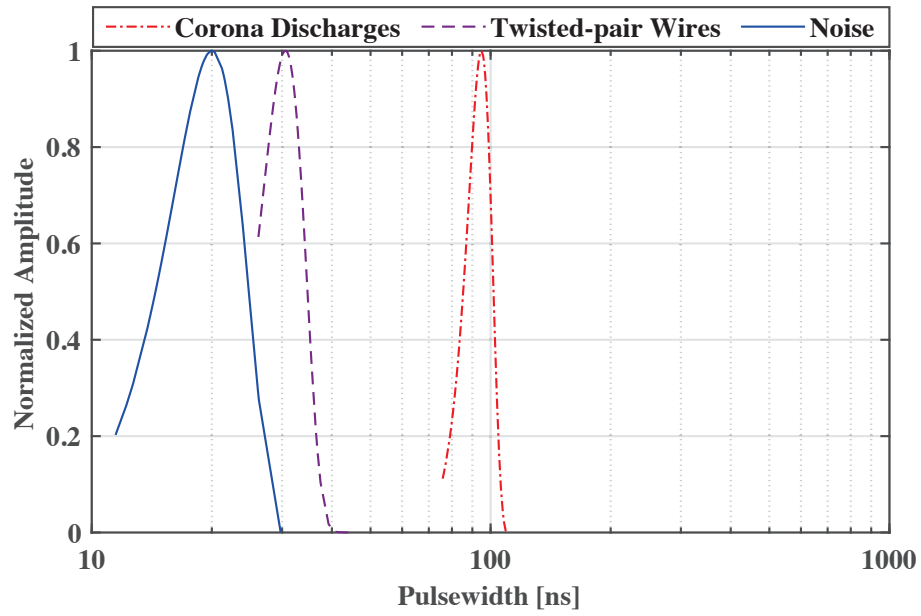


(a)

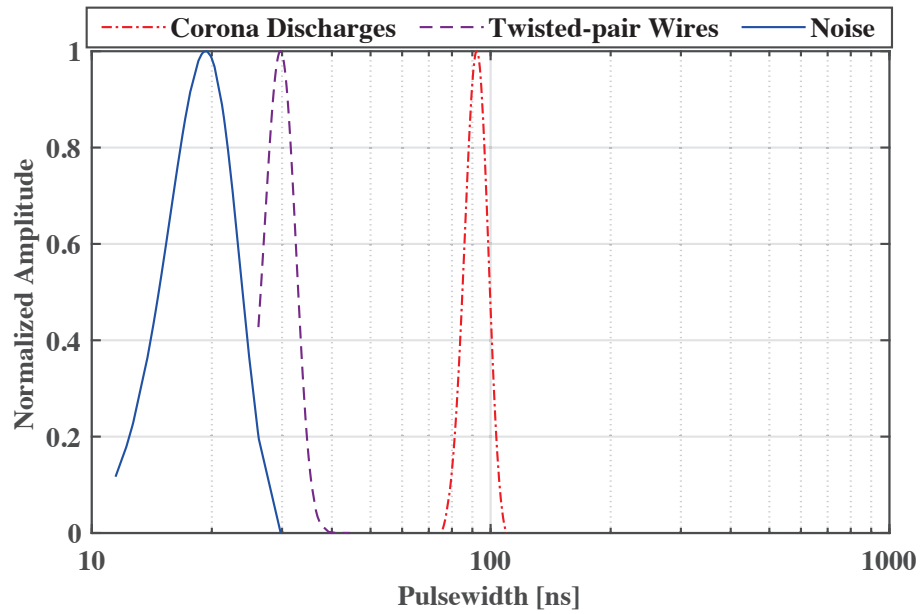


(b)

Fig. B.9: Weibull and Normal distribution of fall time for applied frequency of 500 Hz and air pressure level of 101 kPa (a) Weibull distribution (b) Normal distribution.

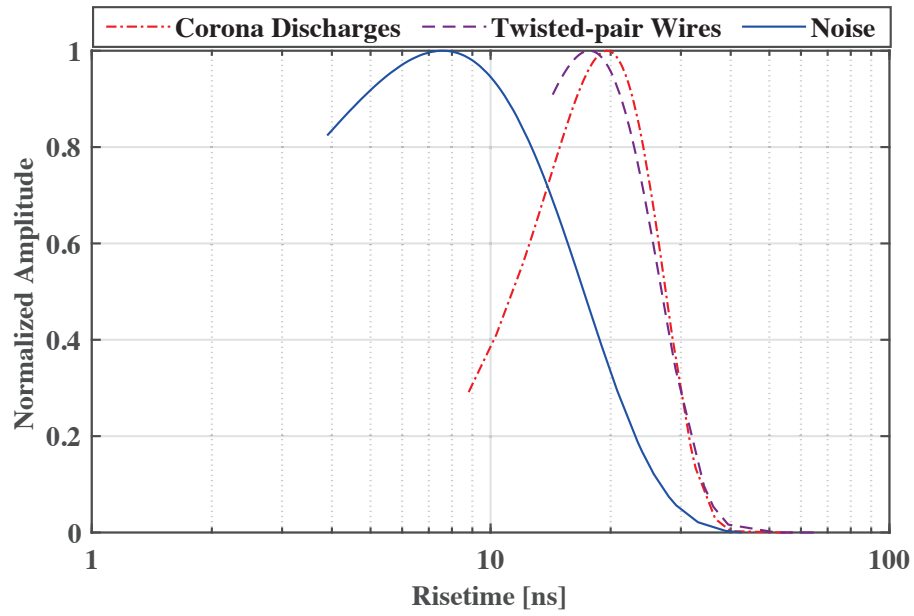


(a)

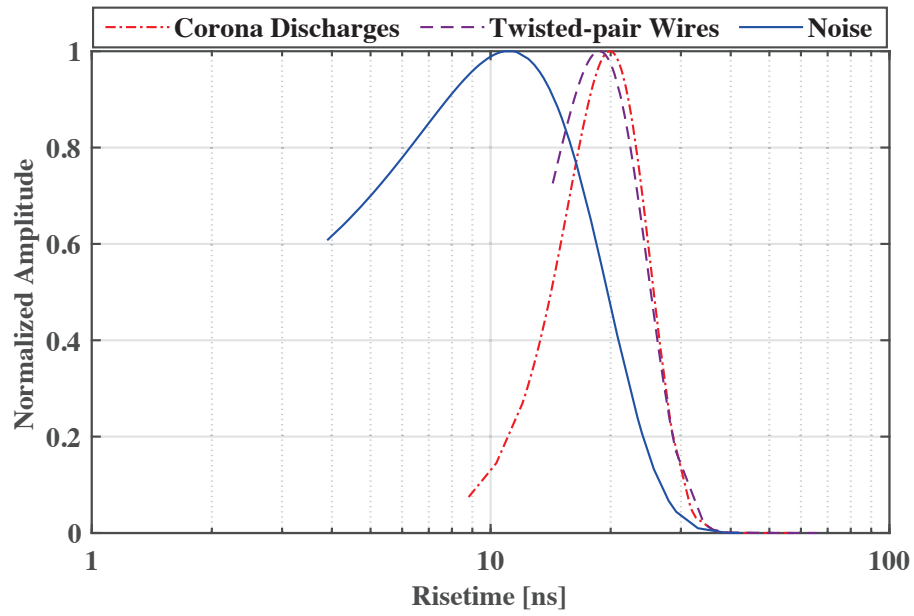


(b)

Fig. B.10: Weibull and Normal distribution of pulse width for applied frequency of 500 Hz and air pressure level of 101 kPa (a) Weibull distribution (b) Normal distribution.

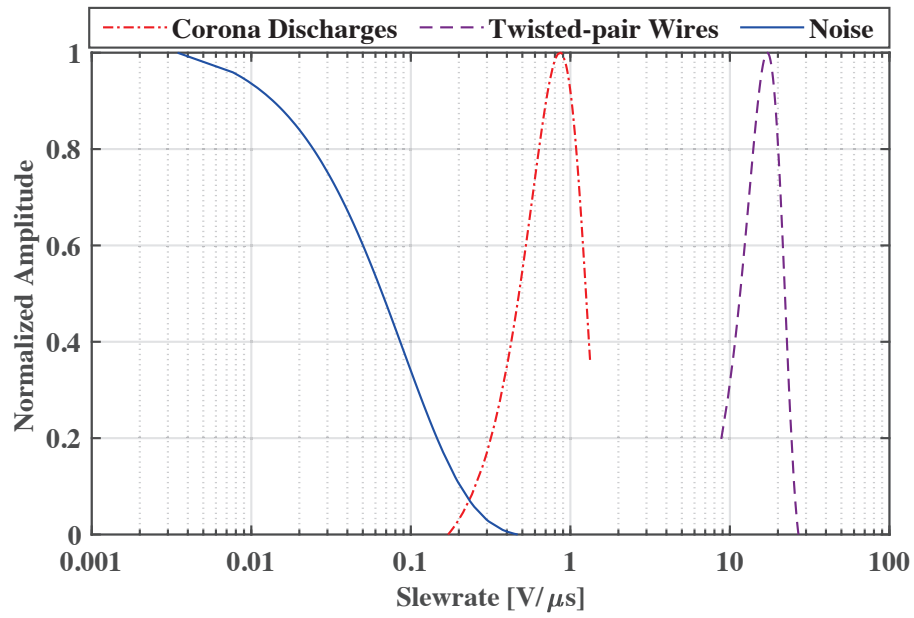


(a)

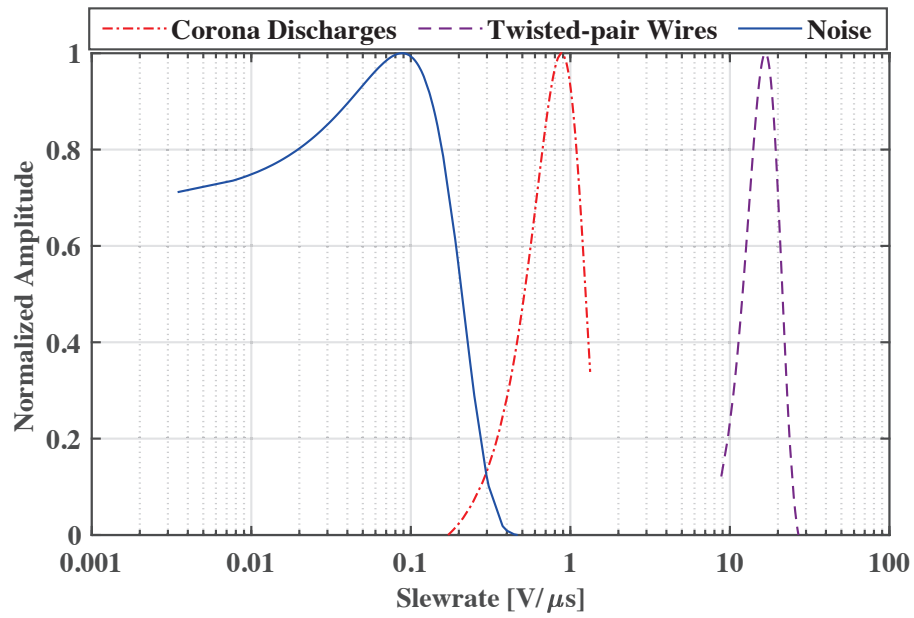


(b)

Fig. B.11: Weibull and Normal distribution of rise time for applied frequency of 500 Hz and air pressure level of 101 kPa (a) Weibull distribution (b) Normal distribution.



(a)



(b)

Fig. B.12: Weibull and Normal distribution of slew rate for applied frequency of 500 Hz and air pressure level of 101 kPa (a) Weibull distribution (b) Normal distribution.